CHALMERS

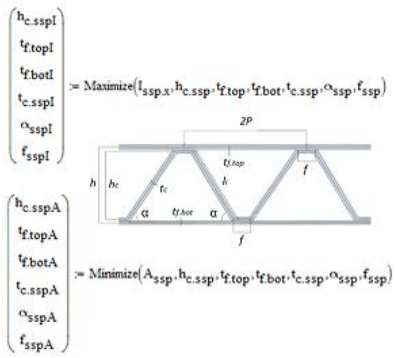

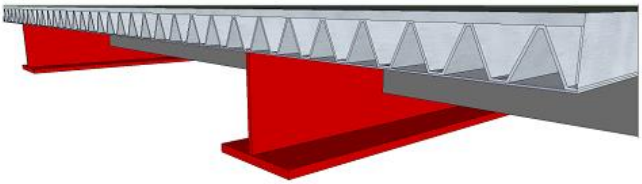

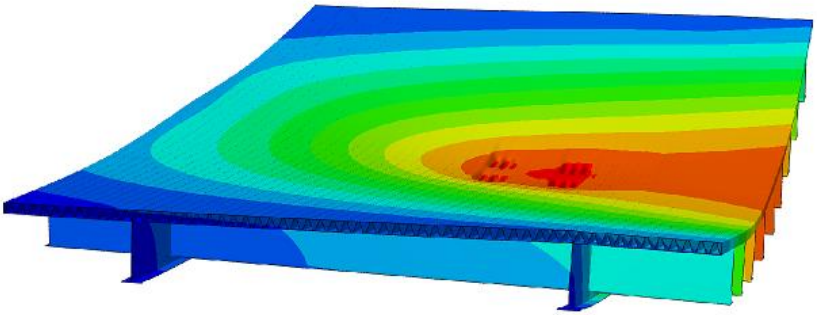

Innovative road bridges with steel sandwich decks

Optimization of the structural performance of a laser welded steel sandwich deck

Master of Science Thesis in the Master's Programme Structural Engineering and Building Performance Design

ENDRIT BENEUS
ISMAIL KOC

Department of Civil and Environmental Engineering
Division of Structural Engineering
Steel and Timber Structures
CHALMERS UNIVERSITY OF TECHNOLOGY
Göteborg, Sweden 2014

Master's Thesis 2014:95

MASTER'S THESIS 2014:95

Innovative road bridges with steel sandwich decks

Optimization of the structural performance of a laser welded steel sandwich deck

Master of Science Thesis in the Master's Programme Structural Engineering and Building Performance Design

ENDRIT BENEUS

ISMAIL KOC

Department of Civil and Environmental Engineering
Division of Structural Engineering
Steel and Timber Structures
CHALMERS UNIVERSITY OF TECHNOLOGY

Göteborg, Sweden 2014

Innovative road bridges with steel sandwich decks
Optimization of the structural performance of a laser welded steel sandwich deck

Master of Science Thesis in the Master's Programme Structural Engineering and Building Performance Design

ENDRIT BENEUS
ISMAIL KOC

Examensarbete / Institutionen för bygg- och miljöteknik,
Chalmers tekniska högskola 2014:95

Department of Civil and Environmental Engineering
Division of Structural Engineering
Steel and Timber Structures
Chalmers University of Technology
SE-412 96 Göteborg
Sweden
Telephone: + 46 (0)31-772 1000

Cover: Picture showing optimization routines, modelling of bridge in Abaqus/CAE and the final form of the bridge.

Chalmers reproservice / Department of Civil and Environmental Engineering
Göteborg, Sweden 2014

Innovative road bridges with steel sandwich decks

Optimization of the structural performance of a laser welded steel sandwich deck

Master of Science Thesis in the Master's Programme Structural Engineering and Building Performance Design

ENDRIT BENEUS

ISMAIL KOC

Department of Civil and Environmental Engineering
Division of Structural Engineering
Steel and Timber *Structures*
Chalmers University of Technology

ABSTRACT

The demand for lighter steel bridges is always sought after. Manufacturers are always searching for new solutions to decrease the weight of bridges and to improve the service life without sacrificing bearing capacity. Possible improvements which are covered in this thesis are replacing the conventional orthotropic steel deck with a steel sandwich deck for improved weight and performance.

Orthotropic steel decks were a good answer to steel bridges when the concept was first discovered. It provided a satisfactory solution to the bending and torsional stiffness of the deck. Nonetheless, the deck is exposed to fatigue cracks in welded details and to compensate for this phenomenon the thickness of the deck plate was increased adding to the weight of the structure.

A new deck concept which has been developed over recent years is that of the steel sandwich panel (SSP) deck. A SSP deck is composed of two thin face plates separated by a corrugated core which results in high relative stiffness to weight ratio. The SSP concept can reach a weight reduction of up to 50% of conventional steel profiles, have improved fatigue resistance due to the connections being laser welded, and save on construction time due to production being automated.

In this thesis a thorough literature study was conducted to observe the uses and benefits of SSPs in load bearing structures. Thereafter, two optimization studies were performed where the dimensional parameters of a SSP deck were optimized in relation to an existing orthotropic deck. The first optimization increased the bending stiffness of the deck without increasing the weight and the second optimization reduced the weight of the deck without sacrificing bending stiffness.

Three bridges were then modelled in Abaqus/CAE, two with the optimized decks and the other with the orthotropic deck. The response of the models under traffic loads was investigated and compared to each other. Bridges with SSP decks showed exceptional structural performance than the orthotropic bridge.

Finally parameters of the bridge with the lighter SSP deck were further improved to utilize the different structural elements to their full potential. This was done with weight reduction in mind and results showed that bridges with SSP decks have improved structural performance and significant weight reduction than bridges with conventional decks.

Key words: Steel sandwich panels, bridge decks, optimization, laser welding

Innovativa vägbroar med stålsandwichdäck

Optimering av strukturella prestanda hos ett stålsandwichdäck

Examensarbete inom Structural Engineering and Building Performance Design

ENDRIT BENEUS

ISMAIL KOC

Institutionen för bygg- och miljöteknik

Avdelningen för Konstruktionsteknik

Chalmers tekniska högskola

SAMMANFATTNING

Lättare konstruktionslösningar för stålbroar är alltid eftertraktade. Tillverkarna söker konstant efter nya lösningar för att minska vikten på broar och för att förbättra livslängden utan att försämra bärigheten. Möjliga förbättringar som presenteras i denna uppsats är att ersätta konventionella ortotropiska ståldäck med ett stålsandwichdäck för bättre vikt och prestanda.

Ortotropiska däck av stål var en bra lösning för stålbroar initialt. Det gav en tillfredsställande böj- och vridstyvhet av däcket. Dock har det visat sig att däcket är utsatt för utmattningsproblem i svetsade detaljer. För att kompensera för detta fenomen har tjockleken på däckplattan ökats, vilken ökade vikten av strukturen.

Ett nytt däck koncept som har utvecklats under de senaste åren är stålsandwichpanel (SSP) däck. Ett SSP däck består av två tunna ytplåtar som åtskiljs av en korrugerad kärna, vilket resulterar i hög styvhet till vikt-förhållande. SSP-konceptet kan nå en viktminskning på upp till 50% av konventionella stålprofiler, det har förbättrad utmattningshållfasthet på grund av svetsarna som är lasersvetsade, och det kan minska byggtiden på grund av att produktionen automatiseras.

I denna uppsats har en grundlig litteraturstudie genomförts för att studera användningsområden och fördelar med SSP i bärande konstruktioner. Därefter har två optimeringsstudier utförts där de geometriska parametrarna hos en SSP däck har optimerats i jämförelse med ett befintligt ortotropiskt däck. Den första optimeringen ökade böj styvheten av däcket utan att öka vikten och den andra optimeringen minskade vikten på däcket utan att reducera böj styvhet.

Tre broar har modellerats i Abaqus/CAE, två med de optimerade däcken och den tredje med det ortotropiska däcket. Resultaten av trafikbelastning undersöktes och jämfördes med varandra. Broar med ett SSP däck visade överlägsen strukturell prestanda jämfört med den ortotropiska bron.

Slutligen, geometrin av bron med det lättare SSP däck var ytterligare förbättrat för att utnyttja materialet till fullo. Detta gjordes med viktminskning i åtanke och resultatet visade att broar med SSP däck kan ha förbättrad strukturell prestanda och betydande viktminskning jämfört med broar med konventionella däck.

Nyckelord: Stålsandwichpaneler, brobanor, optimering, lasersvetsning

Contents

Preface

This master thesis deals with the application of steel sandwich panels in bridge decks. The work was carried out at the Division of Structural Engineering, Civil and Environmental Engineering Department, Chalmers University of Technology. The thesis was carried out between January and June 2014.

We would like to thank our supervisor, Associate Professor Mohammad Al-Emrani, who guided and supported us throughout this process. We would like to thank Dr. Kristoffer Ekholm and Peter Nilsson for their involvement and help throughout this project. We would like to thank our class mates for their support and encouragement. Finally we would like to thank our friends and family who always believed and supported us throughout this project.

Göteborg June 2014

Endrit Benéus

Ismail Koc

Notations

Roman upper case letters

A_c, A_f	Area, per unit width, perpendicular to corrugation axis, of the corrugated core section and the face plate sheet, respectively, [m]
D_x, D_y	Bending stiffness for a corrugated steel sandwich panel profile, per unit width, associated with bending caused around x-, and y-axes, respectively [Nm]
D_{xy}	Torsional stiffness for a corrugated steel sandwich panel profile [Nm]
G_{xy}	Horizontal shear stiffness of a corrugated steel sandwich panel [Nm]
D_{Qy}, D_{Qx}	Transverse shear stiffness, per unit width, of a corrugated steel sandwich panel, in the y- and x-direction, respectively [Nm]
E_c, E_f	Modulus of elasticity of the core and face sheet material, respectively, [Pa]
E_x, E_y	Axial stiffness in x-, and y-directions, respectively [N/m]
G_c, G_f	Shear modulus of elasticity of the core material and face sheet material, respectively [Pa]
S	Non-dimensional coefficient in formula for D_{Qy}
Q_k	Axle loads indicator [N]
G	Self-weight of the bridge [N/m^2]
B	Weight of the asphalt covering [N/m^2]
$G_{kj,sup}$	Permanent loads acting on the bridge [N/m^2]
ψ_0	Reduction factor for TS and UDL
L	Length of bridge [m]

Roman lower case letters

$2p$	Corrugation pitch, [m]
f	Length of the corrugated flat segment, [m]
h	Height of sandwich profile, measured from the middle of the face sheets, [m]
h_c	Height of the core, measured from the centre lines, [m]
l_c	Length of one corrugation leg measured along the centre line, [m]
t_c, t_f	Thickness of the corrugated-core and face sheet, respectively, [m]

t_c, t_p	Thickness of the orthotropic core and top sheet, respectively, [m]
l_i	Inclined length of the core leg (SSP) and of the ribs (Ortho) [m]
l_p	Length between the centres of two ribs in the orthotropic deck [m]
$l_{h,stiff}$	Length of the horizontal part of the ribs in the orthotropic deck [m]
f_y	Yielding strength of the material, [MPa]
q_k	Uniform distributed load indicator [N/m^2]
w_1	Width of the lane [m]
u_{max}, u_{mg}, u_{sg}	Maximum deflection, deflection in main and transverse girder, respectively [mm]

Greek lower case letters

α	Corrugation angle
ν_c, ν_f	Poisson's ratio of the core and face sheet material, respectively
λ	Buckling load factor, (eigenvalue)
ε	Strength ratio for the cross-sectional class
α_Q, α_q	Adjustment factors
σ_x, σ_y	Axial stresses in the x- and y-direction respectively, [Pa]
σ_{max}	Maximum value of the axial stresses, [Pa]
σ_{vM}	Von Misses stresses [Pa]
σ_c	Stress for weld category [Pa]
b	Length of half of the bridge width, [m]
b_{eff}	Effective width, [m]

Abbreviations

HAZ	Heat Affected Zone
HLAW	Hybrid Laser Arc Welding
GMAW	Gas Metal Arc Welding
SPS	Sandwich Plate System
SSP	Steel Sandwich Panel
SLS	Serviceability Limit State
ULS	Ultimate Limit State
FEM	Finite Element Method

LM1, LM3	Load Model 1, 3
TS	Tandem System
UDL	Uniformly Distributed Loads
LASCOR	LASer welded corrugated CORe

1 Introduction

1.1 Background

The construction of steel decks in bridges has not changed much over the past 40 years. The deck structure that is mostly used today is an orthotropic steel deck. It is composed of a face plate with open or close ribs which act as stiffeners. The closed ribs are considerably more resistant to torsional forces than open ribs and are therefore used more often in steel bridge deck construction (Wolchuck, 1963). The main disadvantage of the orthotropic deck is its fatigue performance and construction time since the welding is often conducted manually. Because of its many welding details, the orthotropic deck is prone to large stress concentration at these details, causing fatigue cracking in the welds. As a result orthotropic steel decks have a relatively short service life, before they need to be maintained or replaced.

To counteract the problem with fatigue failure, weight, and construction time, designers have come up with a new design of replacing orthotropic steel decks. The proposal is to use a steel sandwich panel (SSP) deck which has considerable advantages in fatigue and construction time than the orthotropic one. Originally designed for use in the marine and aviation industry, the SSP is also making its way into the civil engineering industry.

A sandwich panel is composed of three layers, two face sheets attached to a core. The core of the sandwich panel can have different configurations, each with its unique advantages and disadvantages. The plate is supposed to carry the bending moments while the core is supposed to resist only shear forces. Such a construction form has distinct advantages over conventional structural sections, because it promises high stiffness and strength to weight ratio and it has better distribution of loads leading to less stress raisers in the welded details.

The concept of the SSP has been used for some time now, however until now the production of SSP decks has been quite limited because of difficulties in welding. An optimal method of welding together SSPs is laser welding, which uses a high powered laser to weld together materials with relative ease. Until recently laser technology was undeveloped and therefore hindering the production and use of steel sandwich panels. A new welding concept called hybrid laser arc welding or HLAW is a state of the art method of welding steel plates together quickly and efficiently. HLAW improves on laser welding in that it combines laser welding and gas metal arc welding or GMAW into one for increased efficiency and weld quality.

New breakthroughs in laser welding technology have made the use of SSPs much more convenient in different industrial sectors especially in the bridge deck construction.

1.2 Project Aim

The aim of this master thesis was to arrive at an optimized SSP deck configuration from the point of view of structural performance and material reduction. Furthermore, conduct a thorough production review with regards to limitations and possibilities.

1.3 Method

The master thesis was started with a thorough literature study in the subject of orthotropic steel decks and the steel sandwich panel (SSP). Concepts like history, cross-section configuration, applications, and previously conducted research were covered in the literature study for both panel designs.

A thorough production review was conducted on the SSP to truly understand the process and different factors involved in producing a SSP. Concepts that were covered in the review were material characteristics, welding methods, and the process itself.

An optimization analysis was performed on the SSP deck using available analytical solutions. The analysis was based on an existing orthotropic bridge deck and the SSP was optimized to have the same area per unit width as the orthotropic panel with maximized bending stiffness. Another optimization was performed where the bending stiffness was kept the same while the area of the SSP was minimized. The optimization analysis was conducted with Mathcad software.

To have an overview of the structural performance of the SSP deck, a FEM analysis of three bridge models two with the optimized decks and the other with the existing deck was performed using the Abaqus/CAE software. Results obtained from the analysis were effective flange width, local and global stresses in ULS, deflections in SLS, fatigue stresses, and a buckling analysis.

Finally the bridge with the lighter deck was further optimized with regards to maximum utilization of the structural elements and to decrease the weight even further. This was conducted in Abaqus/CAE.

1.4 Outline

The introduction chapter which describes the thesis and its purpose is followed by chapter two which covers the literature study. The literature study was performed mainly on the orthotropic steel deck and the SSP covering some key facts about the two designs.

The following chapter three covers a detailed production review of SSP. Concepts in production that were studied were the material possibilities that can be used to build a sandwich deck, different welding methods that can possibly be used to weld together SSPs, and the production process itself which covers the process from manufacturing to the mounting of SSPs at the work site.

In chapter four the optimization study of the steel sandwich deck was covered. Analytical elastic constants were derived by using the Reissner-Mindlin plate theory. These constants were then used to obtain optimal geometrical parameters that give the best bending stiffness or the least weight within certain constraints.

In chapter five three bridge models two with SSP decks and one with an orthotropic deck was further analysed with the help of Abaqus/CAE. Stresses, deflection, shear lag effect, buckling analysis, and a fatigue analysis was performed in this chapter. Finally an attempt to decrease the weight of the bridge with the lighter deck was performed while still having sufficient bearing capacity.

In chapter six a discussion is carried out on aspects of the study that could have been analysed further or differently.

Chapter seven is the conclusion chapter where insight is given and suggestions for future research are expressed.

1.5 Limitations

The sandwich plate system (SPS) where you have an elastomer material as the core of the sandwich panel with two face steel plates glued to it, was briefly mentioned, but not considered in this thesis.

Steel sandwich panels come in different core configurations. The corrugated V-core model was the only model studied in this report due to its superior performance compared to other core models and its ease of fabrication.

Focus has mainly been placed on the structural behaviour of the SSP deck and not the whole bridge superstructure, for example, transverse and longitudinal stiffeners were taken from the original bridge and not designed by us.

Panel to panel connections are mentioned briefly in the text where it is specified how these connections can influence the bridge structure. Further study in these joints is not undertaken, however the need for improved connections is regarded as very important.

The original (bascule) orthotropic bridge is simplified from being fixed at one end and cantilever in the other end to both ends being simply supported. The reasoning was that when the bridge is closed it can be considered as simply supported which also simplifies the calculations.

2 Literature Study

When studying steel bridge designs, one can see that the deck of almost all steel bridges consist of an orthotropic deck system. The deck is supposed to be lightweight and durable; however there are disadvantages to using this type of deck mainly in relation to fatigue. The alternative is by replacing the traditional orthotropic deck with a steel sandwich panel. In this chapter a literature study was conducted on the orthotropic steel deck and on the steel sandwich panel.

2.1 Orthotropic steel decks

Orthotropic bridge decks consist of different parts that work together to complete the overall structure of the deck resulting in a lightweight and durable structure. These parts are put together as a network of longitudinal stiffeners, transversal stiffeners, and the deck plate itself.

Orthotropic plate decks come in two variations, decks with open ribs and decks with closed ribs, see Figure 2.1. The difference between the two is their resistance to torsion, with decks with closed ribs being considerably more resistant to torsion than decks with open ribs. The ribs are continuous elements passing through and welded to the floor beam. The floor beam can be a fully welded detail or include a void between the floor-beam web and the rib's bottom making it a partially welded detail.

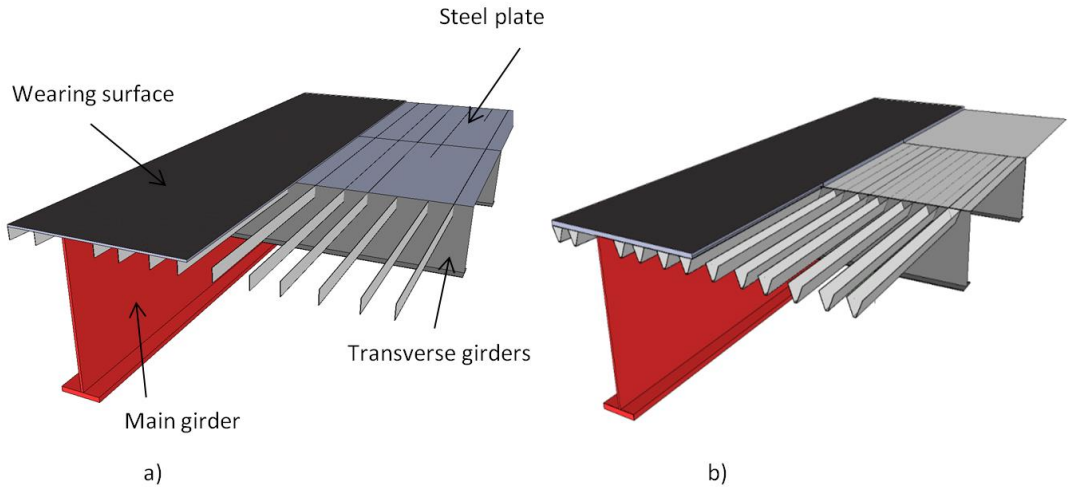

Figure 2.1 Orthotropic deck with (a) open ribs (b) closed ribs.

Orthotropic plate decks are very sensitive to fatigue failures due to the build-up of stress concentrations on the many welded joints, specifically in the rib-to-deck joints, see Figure 2.2. This detail is crucial in determining the fatigue strength of a bridge, especially in highway bridges where the concentrated traffic loads from heavy vehicles cause extremely high load cycles. Furthermore, the increase of traffic year by year is causing the design life of steel bridges to be shorter than what they are designed for.

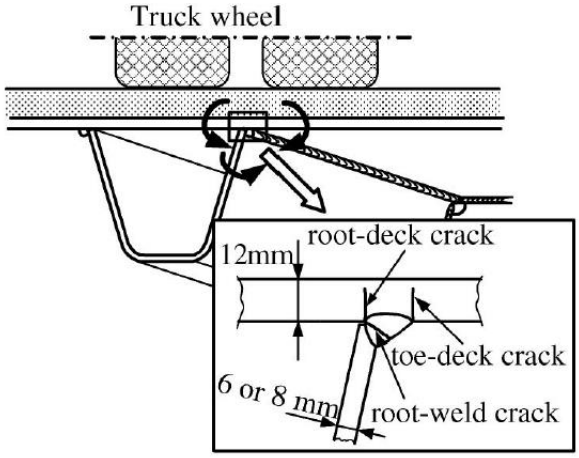

Figure 2.2 Fatigue cracks in rib-to-deck welded joint of an orthotropic steel deck. (Ya, et al., 2011)

Researchers have tried optimising the deck profile to minimise fatigue failure. A study proposed a new detail in which the deck plate is 1.5 times thicker and the closed ribs are 1.5 times larger than those used in standard orthotropic bridge decks (Mizuguchi, 2004). Ono et al. (2009) have experimented with steel fibre reinforced concrete to retrofit/repair existing orthotropic steel decks. Others like Ya & Yamada (2008) and Xiao et al. (2008) have shown that by increasing the thickness of the deck plate (~16mm) might improve the fatigue durability of the rib-to-deck joints.

These improvements have one thing in common in that they improve on the existing orthotropic deck and often making it more durable to fatigue, but also increasing the weight of the deck. In this study focus will be on replacing the existing orthotropic deck all together with a steel sandwich panel (SSP) which has considerable benefits in regards to fatigue strength and also being light weight.

2.1.1 History of orthotropic steel decks

In the 1930´s steel plate deck bridge system, known as the "battle deck floor", was introduced by the American Institute of steel Construction in an attempt to reduce the deadweight of highway bridges. In this system, which was used mostly on movable bridges and for replacement of the floor in old bridge structures, a steel plate deck was welded to the longitudinal I-beam stringers, supported by or framed into transverse floor beams as shown Figure 2.3 (Wolchuck, 1963).

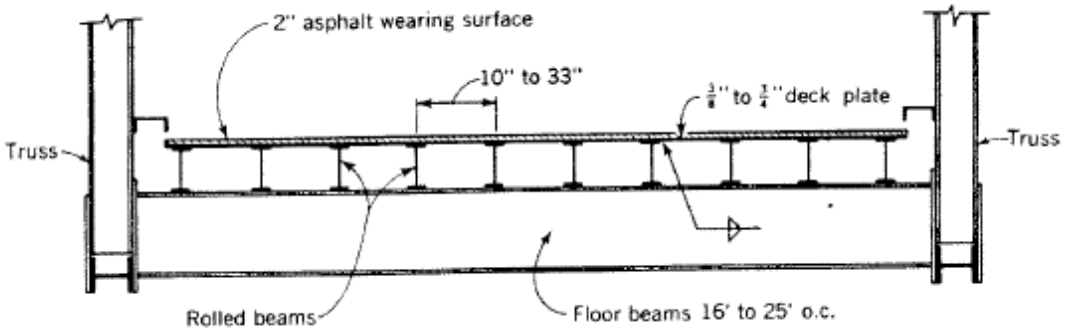

Figure 2.3 Typical "battle deck floor" bridge cross section (Wolchuck, 1963)

The battle deck floor construction failed as an alternative design because it did not participate in the stresses of the individual stringers as part of their top flanges, nor did it contribute to the rigidity and strength of the main carrying members of the bridge. However, an insight was gained through all the experiments performed on the battle deck floors, showing that the strength of a flat steel plate loaded by a wheel is much greater than predicted.

During this time, German engineers were experimenting with lightweight steel bridge decks of cellular construction. These decks consisted of longitudinal and transverse stiffeners welded to a thin steel plate. The large amount of welding which had to be performed manually forced the designers to increase the spacing of the stiffeners. As a result the deck was subjected to high local deflections, which in turn caused cracking in the asphalt wearing surface.

It wasn't until the end of WWII where many bridges needed to be built in Germany that the design of the steel orthotropic deck was implemented and improved as time went by. More than 1000 steel bridges were built with orthotropic decks since WWII and even more structures making use of orthotropic panels were built in sectors like civil, machine, air and space engineering (Fryba & Urushadze, 2011).

2.2 Steel sandwich panel (SSP)

A steel sandwich panel is composed of two thin, stiff and strong sheets of dense material separated by a core which results in high relative stiffness, strength and inherent energy absorbing capacity. The face plates are in pure tension or compression carrying the global bending moment, whereas the core is used to resist shear forces.

The key advantages of SSPs are that they are 30 – 50% lighter than other conventional steel profiles saving on material costs and production time. SSPs have a high strength to weight ratio, act as a single plate due to its shearing strength and it has improved fatigue resistance and corrosion life. These advantages significantly increase the design life of the SSP deck.

2.2.1 History of SSP

Development of the steel sandwich panels came as a result of a need for lighter and stronger structures for moving vehicles, such as ships, cars, busses, etc. The idea was to make use of new materials or develop new designs. Thus the idea of composite

materials and sandwich structures was developed to make structures and vehicles lighter and have a high strength to weight ratio.

Proposals for the construction of sandwich panels were already being made during the 1950s, but limitations with welding technology halted the progress for some time. It was cheaper to build sandwich panels in comparison to materials used, but the welding procedure was expensive and not efficient. One welding procedure which would solve this problem was by means of laser welding see Section 3.2.3, however at the time the machinery to efficiently laser weld was not developed, therefore the idea was abandoned until a more economical and efficient solution became available.

The first laser welded sandwich panels were being developed and tested in 1980s by the United States Navy for use in their ships. Later between the late 1980s and the early 1990s Europe took over the lead of research of sandwich panels with key research sites in Britain, Germany and Finland.

Since then large amounts of research has been conducted on SSPs to improve and optimise its current design for desired applications. Today many European manufacturers have adopted the use of steel sandwich to create lightweight decks and stairs in cruise ships, lightweight balconies, and even flooring for a multi-level sports arena.

2.2.2 Core configurations

The core profile can be produced into different profiles each with its unique strengths and weaknesses. Some of the core profiles are shown in Figure 2.4 and further described below.

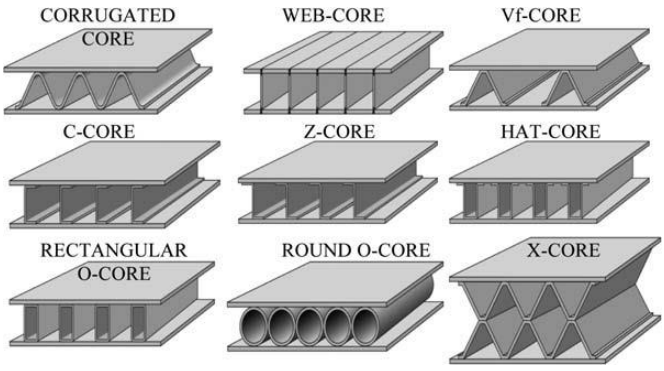

Figure 2.4 Variations of core profiles of SSPs (Romanoff & Varsta, 2006)

Each core design has their specific performances when compared to each other and its worth mentioning that the structural performance is improved when the core is about the same weight as the two plates (Säynäjäkangas & Taulavuori, 2004). The X-core for example has a very good capacity to absorb energy. The O-core has a high nominal stiffness, but adds to the weight of the structure. The C- and Z-core have high bending and shear stiffness in the direction of the core, however both stiffness properties are relatively weak in the transverse direction.

The corrugated core and Vf-core are similar designs. The overall stiffness of the corrugated core in the longitudinal and transversal direction is superior to other

configurations and therefore it is often the desired design for manufactures (Alwan & Järve, 2012).

Truss-core profiles similar to Figure 2.5 are principally different than the corrugated core in a way that the vertical web elements are directly welded to the top and bottom plates instead of being a folded plate. The advantages of such a configuration besides being lighter are that it has higher shear strength than the corrugated core. The resulting moment from the corrugated core causes local deflection of the face plates. This local deflection is minimal in the truss-core profile since the core is only subjected to compression and tension forces, see Figure 2.6. The only drawback with the truss-core is its difficulty to fabricate in steel and as a result many manufactures choose to use steel corrugated core profiles. Truss profiles can be easily manufactured in aluminium through a process called aluminium extrusion.

Figure 2.5 Geometry of a triangular truss core sandwich panel

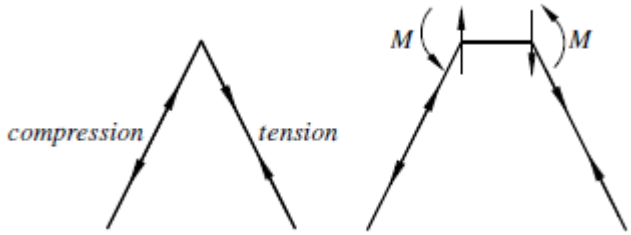

Figure 2.6 Force transfer in the truss-core profile (left) and corrugated core profile (right) (Alwan & Järve, 2012)

The web-core profile is limited in use because their response to dynamic loading causing fatigue damage is still unexplained. The stress levels in this type of configuration are often dependent on the stiffness of the T-joint, the connection of the I-beam to the plate. If the connection is laser welded, the weld is often thinner than the plates it connects to, thus making it considerably more flexible than a fillet-welded T-joint. The increased flexibility reduces the shear stiffness of the web in the plane orthogonal to the plate direction and thus resulting in increased deflection.

2.2.3 Applications of SSP

Corrugated-core sandwich panels, due to their exceptionally high flexural stiffness-to-weight ratio are commonly used in aviation, aerospace, marine industry and civil engineering. Due to their capacity to absorb energy and resistance to absorb static and

dynamic loads, SSPs are of special interest for potential use in bridges for deck replacement.

Some practical applications of SSPs in ships are for structural elements of ship hull and ramps, flat surface like decks, walls, and side shells, see Figure 2.7.

Figure 2.7 *Internal walls made of SSP (left), internal ramp of a Ro-Ro ship made of SSP* (Kozak J. , 2009)

An important project showing the benefits of a corrugated sandwich panel was conducted for the US Navy in the mid-1980s. They needed to reduce the weight and lower the centre of gravity for their ships to improve the performance at a reasonable cost. The result was a SSP called LASCOR (LASer-welded corrugated-CORe). The LASCOR panels provided enhanced strength, protection and corrosion resistance since stainless steel material was used. Hybrid-laser arc welding was used to minimise thermal distortions. The project was a success with a weight reduction of 40% compared to conventional panels, however the costs per square foot were higher and at the time no company was able to cost-effectively produce laser welded SSPs (Abbott, et al., 2007).

2.2.3.1 Sandwich plate system (SPS)

The application of SSPs in steel bridge decks has not yet been developed to a degree where it is practical to use for manufacturers. Sandwich bridge decks have been built with a similar system called the sandwich plate system (SPS), which consists of two steel plates bonded to a solid elastomer core, see Figure 2.8. The advantages of the elastomer core are; it prevents the steel plate from buckling, intermediate stiffeners are not required, dimensions can be adjusted to the structural load required, and it has low stiffness to weight ratio compared to concrete decks.

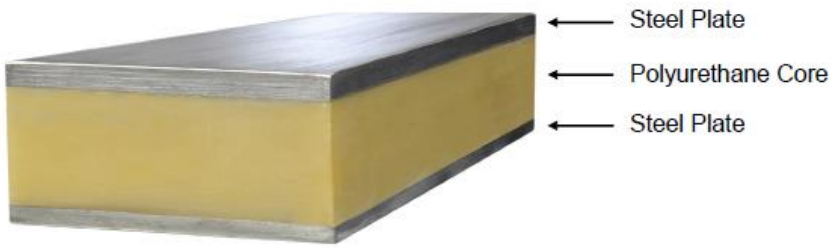

Figure 2.8 Sandwich Plate System (SPS) (Harris, 2007)

SPS was developed by Intelligent Engineering over the past decade and was mainly used in the marine industry for replacement of deteriorating ship decks. The potential for this type of deck was soon realised in the civil engineering industry, mainly for bridge deck building. In 2003 the Shenley Bridge was constructed in Saint-Martin, Québe, Canada utilising a SPS deck, see Figure 2.9.

Further study will not be conducted in the subject of SPS because it is inferior to the SSP. Some of these inferiorities are, the durability of the elastomer core material is questionable in long term performance and steel sandwich panels have a higher strength and better structural performance than the sandwich plate system (Alwan & Järve, 2012). Furthermore, it will be beneficial to continue with the study of the steel sandwich panel since there is lack of existing data on the behaviour of the steel sandwich panels for bridge design.

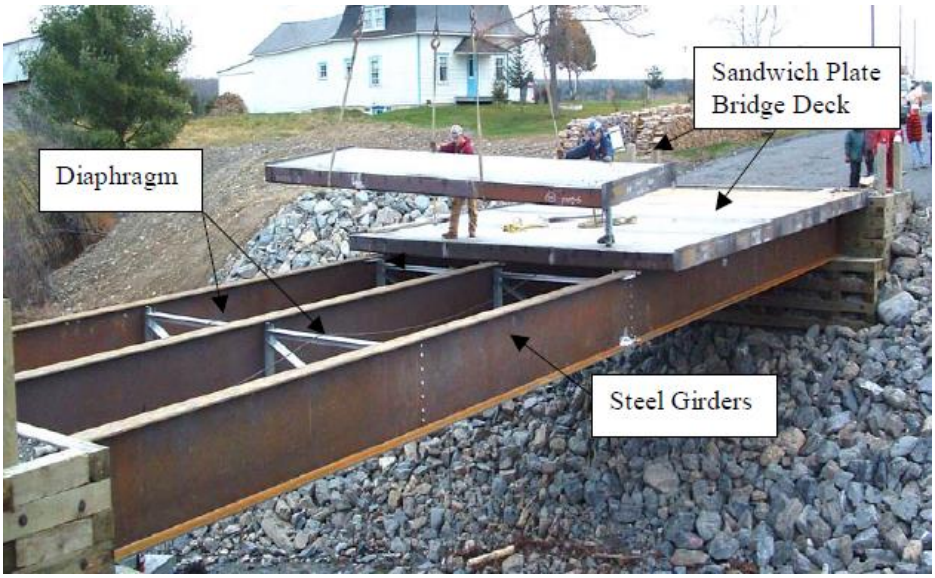

Figure 2.9 The Shenley Bridge (Harris, 2007)

2.2.4 Conducted research

Large amounts of research have been conducted on steel sandwich panels. Some relevant studies which show the benefits of a SSP as a replacement for conventional steel panels are listed below.

A study conducted by Pentti Kujala and Alan Klanac at Helsinki University of technology has shown the savings both in costs and weight of using a SSP instead of

the traditional orthotropic plate. The case study that was conducted was based on replacing a traditionally constructed car-deck on a ship with a much lighter web-core SSP. Three models were compared to each other see Figure 2.10. Variant A was an optimised alternative to the original deck, Variant B was a sandwich-grillage car-deck, a sandwich panelled car-deck with grillage supporting structures and variant C was a sandwich panelled car-deck with C girders on perimeters.

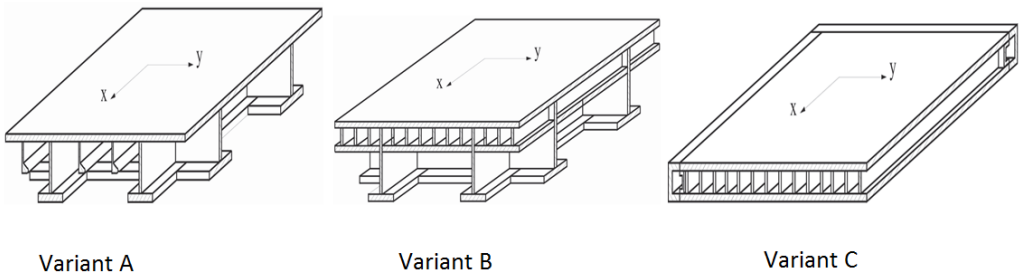

Figure 2.10 Three concepts that of a car-deck in a ship (Kujala & Klanac, 2005)

Results from the study indicated that variant C was the most promising design in regards to costs and weight. Variant B and C were about the same weight per square meter, but variant C was somewhat cheaper to produce than variant B. No noticeable improvements were noticed in variant A. However, it was not far off from the other two variants.

Another study conducted by Romanoff, J. et al. (2011) compared the strength of corroded web-core and corrugated-core sandwich panels. Results showed that the reduction of strength was greater for the web-core than the corrugated-core profile. They also concluded that by filling the core with polyurethane (PU) foam, it would slow down the corrosion process. Likewise, in another study conducted by Frank et al. (2012) indicated that the PU foam contained in the core partially carries the external loading and contributes to the decrease of shear stresses and deformation of the steel structure, which in turn leads to smaller deflections and bending moments in the panel joint.

Biagi & Bart-Smith (2012) have studied the in-plane loading response of a corrugated sandwich panel, see Figure 2.11 and concluded that they compare favourably with competing designs, while minimising weight at the same time. The study was thought as necessary for the corrugated SSP to achieve widespread use in next generation multifunctional applications.

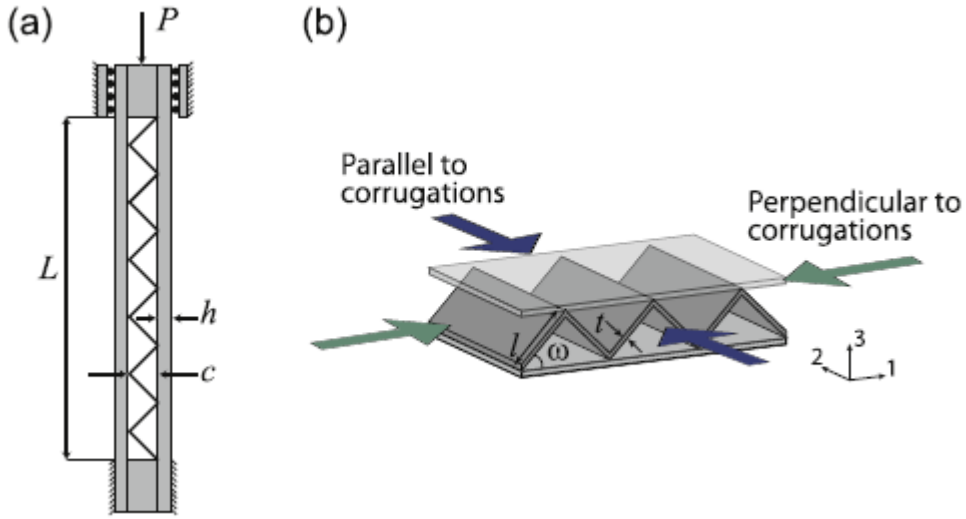

Figure 2.11 *(a) corrugated core column compressed perpendicular to the corrugation. (b) in-plane loading direction for a corrugated core sandwich structure* (Biagi & Bart-Smith, 2012)

Considerable optimization studies have been conducted on steel sandwich panels with different core configuration, especially corrugated core profiles, see Figure 2.12. Alwan and Järve (2012) calculated that with increased ratio of h_c/t_c the panel will experience a decreased stiffness as a result of a thinner core. They also calculated the relationship of the angle of the corrugation pitch divided by the core height p/h_c and showed that with increased values of the ratio the stiffness of the sandwich panel decreases. This is due to the decreasing amount of corrugation for a given plate width. Chang et al. (2005) calculated optimal ratios of some geometric parameters and concluded that t_c should be equal to t_f, if t_f decreases while t_c is kept the same the stiffness of the plate decreases. The corrugation angle α should be between 45° and 70°, if the corrugation angle is too high the bending stiffness will marginally increase, whereas the shear stiffness will greatly decrease. The ratios of h_c/t_c should be around 20 and p/h_c should be between 1 and 1.2 to avoid negative moments in the direction perpendicular to the corrugation.

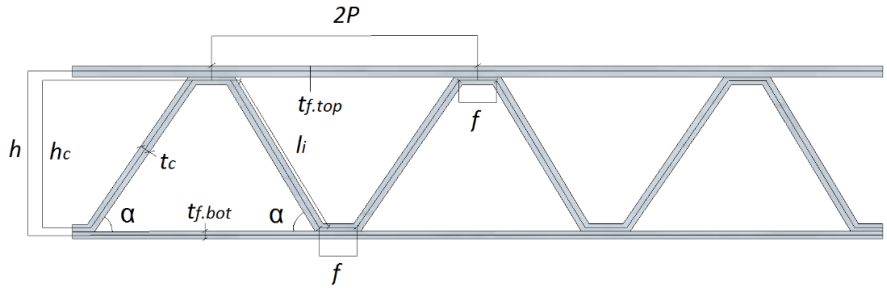

Figure 2.12 *A corrugated core profile*

This research has only broadened the knowledge on the behaviour of steel sandwich panels under different conditions. Hence, it has helped engineers make smarter decisions in the application of SSPs.

2.2.5 Fatigue review

The term fatigue is used to describe the weakened state of a material, including steel, when subjected to repeated strains. The material will eventually crack and if the loading continues the cracks will grow leading to fatigue failure. In large load bearing structures, including steel bridges, fatigue damage often occurs in welded joints and discontinuities where the structure is prone to high stress concentrations.

The service life of a SSP bridge deck is strongly dependent on the fatigue strength of a weld profile and the fatigue properties of the welded material. The fatigue performance of the weld profile is strongly dependent on its geometry and weld quality. If the weld has high irregularities then it is prone to high stress concentrations which can cause fatigue cracking in the weld, thus decreasing the fatigue life.

Welding methods like hybrid laser arc welding (HLAW) improve on the weld geometry making it more symmetrical with decreased irregularities. Caccese et al. (2006) showed that laser welded profiles had significantly better fatigue life than conventionally welded profiles when subjected to shear and tensile forces. The tests were conducted on cruciform welded profiles, see Figure 2.13, and the results were compared to historical data provided by Munse et al. (1983) and also data on conventional welded cruciform specimens made of the same material provided by Kihl (2002).

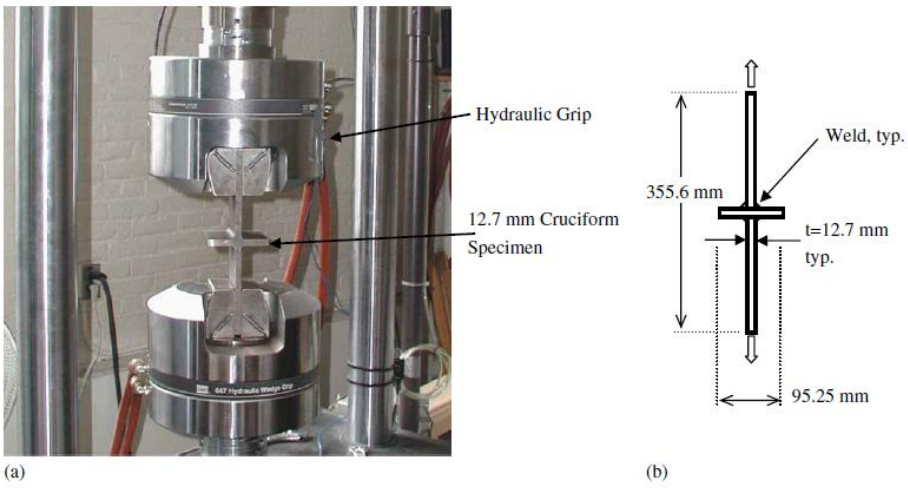

Figure 2.13 a) picture of the cruciform test specimen and the test setup b) geometrical dimensions of the test specimen (Caccese et al., 2006)

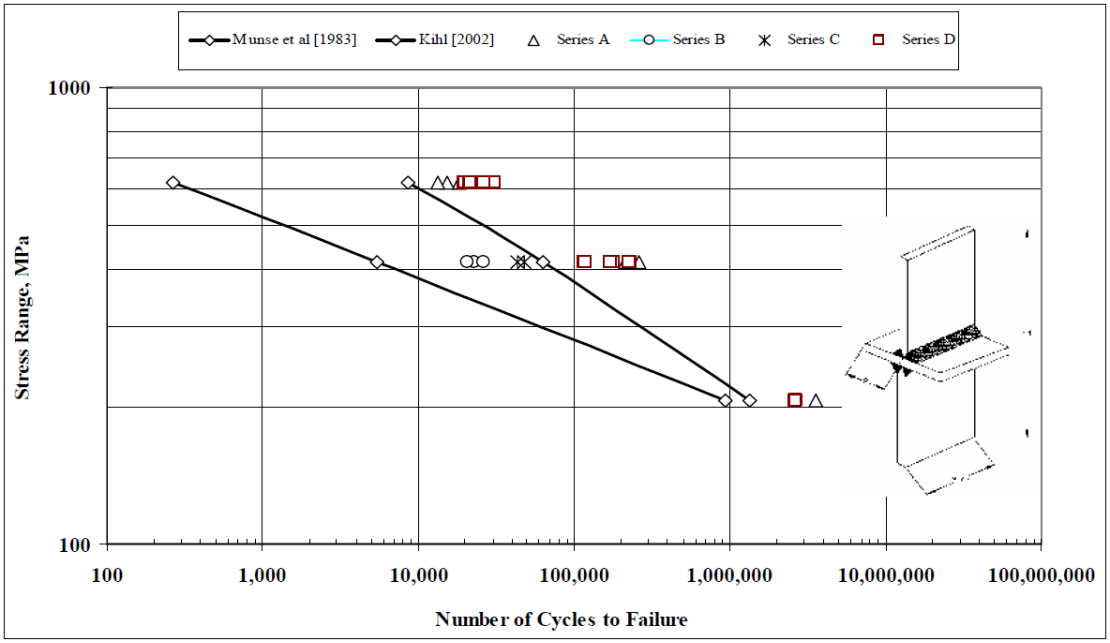

Figure 2.14 *S-N curve obtained from the fatigue-test study performed on cruciform profile weld profile* (Abbott et al., 2007)

In Figure 2.14 series A – C are used as a baseline for comparison while series D is the final production detail of the fillet weld. As it is shown from series D, that laser welded profiles have better fatigue life than conventional welded profiles.

Another study performed by Kozak (2005) discusses the fatigue strength of an all steel sandwich panel with vertical webs. Laser welding was used to join the plates to the core and according to the experiments performed laser welding showed promising results in fatigue strength. Experiments were performed on I-core panels with different configurations and boundary conditions to study the fatigue failures that can occur. It was concluded that for all sandwich panels fatigue cracking can occur in the following ways:

Type 1: Fatigue crack in the laser welded toe in the top plate, in the direction parallel to the web, as a result of the tensile stresses caused by global bending.

Type 2: Fatigue crack in the laser welded toe in the top plate, in the direction transverse to the web, as a result of the tensile stresses caused by global bending.

Type 3: Fatigue crack in top plate caused by local bending or buckling.

Type 4: Fatigue crack in the laser welded contact area of the web and the plates due to transverse bending.

Type 5: Fatigue crack in the laser welded contact area of the web and the plates due to longitudinal shear.

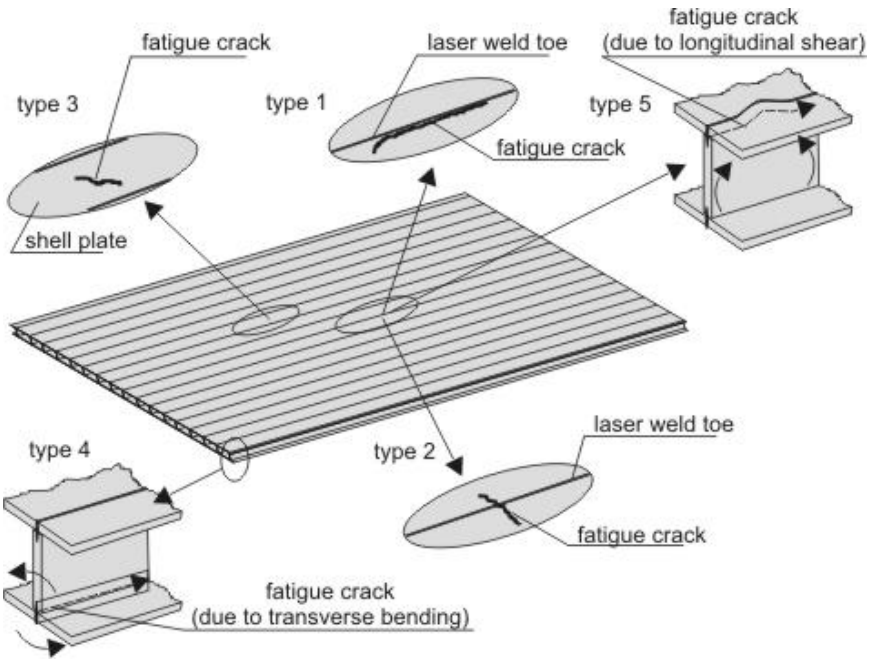

Figure 2.15 Figure showing possible fatigue cracks that can occur on an I-core sandwich panel due to loading Kozak (2005)

Bright & Smith (2004) performed fatigue tests on a laser welded sandwich bridge deck with an I-core configuration. One test was a web bending test that might occur under offset wheel loads and the other was a deck bending test under direct wheel loads. The results from the two experiments were promising and showed that laser welds compare favourably to conventional welding methods. It was observed that in the web bending test fatigue failure occurred in the parent metal of the web and not the weld.

In the deck bending test, the shear capacity of the laser welds was the design criteria. Tests were conducted on profiles with both two and four welds per flange and failure of the deck was defined to occur when fatigue cracks first appeared on both sides of any individual laser weld, see Figure 2.16a. The stress on the deck plate at the outer edge of the laser weld was measured for each load exerted on the deck and the results of all the fatigue tests were compared with mean S-N curves for weld classes published in BS 54001. The results were recorded graphically in Figure 2.16b and it can be seen that mean values from the 2-weld flange resembles closely a Class C curve. A stress value of 120MPa on the deck plate is recorded for 5 million load cycles.

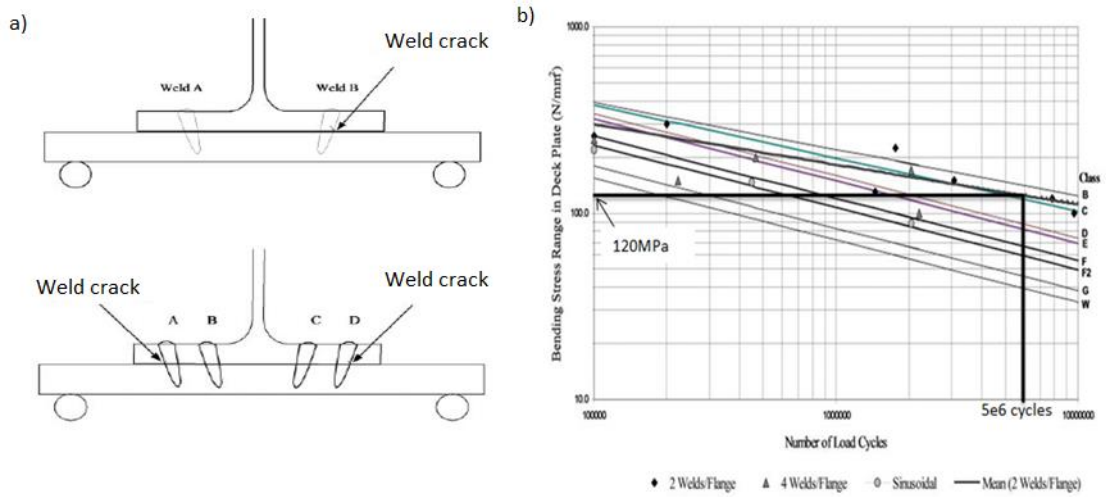

Figure 2.16 *a) Cross section of a I-core sandwich panel showing the amount of laser welds and the crack initiation on the weld b) Comparison of deck bending test results with mean S-N curves for weld classes published in BS 54001* (Bright & Smith, 2004)

It was concluded in the report that laser welds have satisfactory shear resistance and perform better than conventional welds. Furthermore, results indicated that SSP design with laser welded joints has exceptional fatigue performance.

3 Production review

The production of steel sandwich panels (SSP) is much more convenient and affordable with todays' technology. The advancements in laser welding technology and better steel grades have made the production of SSPs a competitive alternative to the traditional methods. Even though SSPs are replacing conventional steel plates, they are not yet being developed for large load bearing structures like bridges. The most common applications of SSPs are built for example; elevator floors, ship decks, walls, outlining's of vehicles, etc. These are all small load bearing structures compared to bridges. A company in Finland called Kenno Tech specializes only in steel sandwich panels, but again at small scales.

3.1 Material

A variety of metal alloys can be used to produce steel sandwich panels, for example, stainless steel, conventional structural steel, aluminium and titanium alloys. In this study stainless steel and carbon steel will be studied further since their use is much more common in large load bearing structures.

One of the principle advantages of stainless steel is its corrosion resistance. This is particularly important when the deck of the bridge will be exposed to de-icing salts, salt water, or high concentration of chlorides in the air. This characteristic of the stainless steel makes it much more durable then carbon steel, which increases the service life of the bridge. The design strength, ductility, toughness, welding and fatigue resistance of stainless steel compares favourably to carbon steel.

With these benefits in using stainless steel as an alternative for a bridge deck, the production and application in bridges is still limited. Firstly, the initial costs involved are much higher for stainless steel than for carbon steel. It can be argued that the increased service life of the bridge would compensate for the high initial costs. A study conducted by Ramböll in 2002 was based on doing a cost analysis on a highway bridge in Sweden build with carbon steel or duplex stainless steel (Collin & Lundmark, 2002). The analysis showed that the bridge would cost more if built with stainless steel. The maintenance costs were not covered in this study and stainless steel will most likely never see any market share until manufacturers start considering maintenance costs in the analysis. Secondly, there is a gap in design practice in building with stainless steel because of lack of standardized codes on the behaviour of the material under heavy loads. These restrictions are preventing stainless steel to be more commonly used in bridge structures.

3.2 Welding

Welding of steel sandwich panels can be achieved through different processes like spot welding, gas metal-arc welding, laser welding, and a combination of the last two called hybrid laser-arc welding or HLAW.

3.2.1 Spot welding

Spot welding is the process of joining two metal surfaces by welding at particular spots, see Figure 3.1. Two copper electrodes generate a current on a specific spot

between two plates. The metal that is being welded offers resistance which generates large amounts of heat which in turn starts to melt the metal and form the weld.

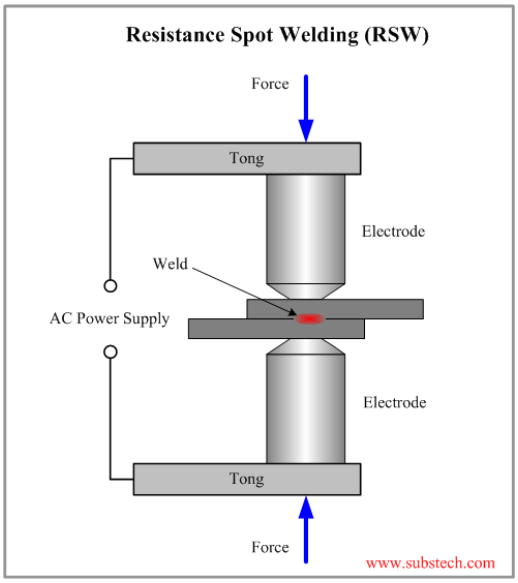

Figure 3.1 Typical spot welding of two plates (www.substech.com)

The advantages of spot welding are, the process can be automated which is quick and efficient, no need for filler metals, high production rates, and efficient energy use. The disadvantages of spot welding are the weld strength is significantly lower than other types of welding. This is because the plates are welded together at specific spots and not throughout the whole connection. Also silver and copper are difficult to spot weld because of their high thermal conductivity, which limits the use of spot welding for a broader material range. Spot welding is widely used in the automobile industry where automated robots perform several hundred spot welds per day.

In steel bridge decks the fatigue resistance of the weld is extremely important since very often fatigue failure of the weld is the design criteria. Therefore, it is not advantageous to use spot welding in an orthotropic or steel sandwich panel because of its apparent weakness to other welding methods.

3.2.2 Gas metal-arc welding (GMAW)

Gas Metal Arc Welding (GMAW) is a welding process where an electrode wire is continuously fed from an automatic wire feeder through a conduit and welding gun to the base metal, where a weld pool is created, see Figure 3.2 (Hoffman, et al., 2011). The welding process can be semi-automatic if a welder is controlling the direction of the weld and speed or fully automatic if a machine is controlling the direction and speed of the weld.

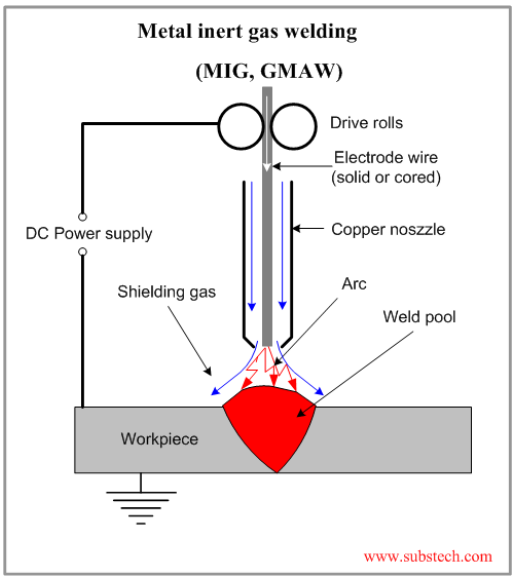

Figure 3.2 Gas Metal Arc Welding (GMAW) (www.substech.com)

Advantages of gas metal arc welding are high welding speeds, no slag removal required, affordable and high weld quality. The key disadvantages are that the equipment is quite complex and welding cannot be used in the vertical or overhead position because of the high heat input and because of the weld puddles fluidity. This is particularly a problem in welding together steel sandwich panels since the connecting details are complex for gas metal arc welding to work. GMAW has been widely used in welding together steel orthotropic bridge decks. The process is often semi-automatic which can lead to distortions in the weld. These distortions cause stress concentrations when loaded which might result in fatigue failure of the weld.

3.2.3 Laser welding

Laser welding is a relatively new and effective technique for welding together a wide variety of metals and alloys. Advantages of laser welding are ease of process automation, high welding speed, high productivity, increase process reliability, low distortion of the finished part and no requirement for filler metal (Caccese, et al., 2006). Laser welding has the potential to achieve excellent static and dynamic load resistance as well as a good fatigue life.

Laser welding is ideal for welding hard to reach connections similar to a steel sandwich panel as shown in Figure 3.3. The face sheet is metallically bonded directly to the core of SSP resulting in a continuous and reliable connection that can be expected to have many years of service. Laser welding improves on the welds geometric profile which is the main factor in determining fatigue life of the weld.

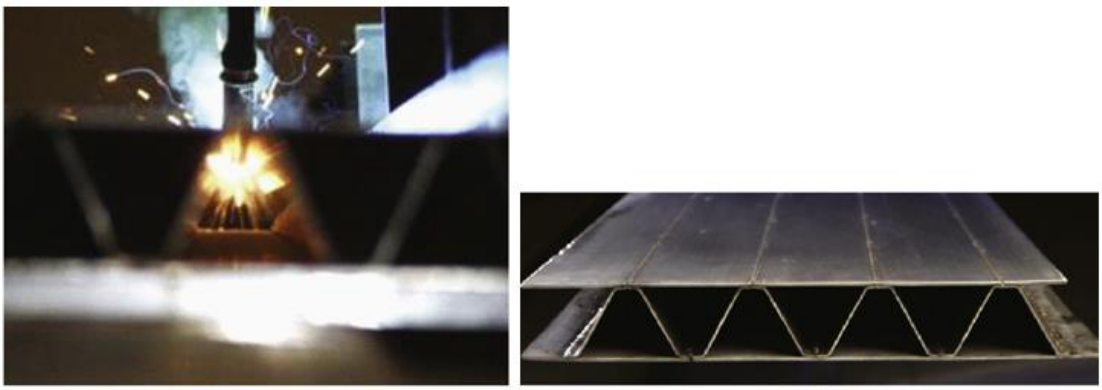

Figure 3.3: a) Laser stake welding of the core to the face-plate, (b) post production laser welded sandwich panel (Poirier, Vel, & Caccese, 2013)

Another key advantage of laser welding is that it occurs at much greater speeds than conventional welding, up to 5 to 10 times faster (Abbott, et al, 2007). High welding speeds not only saves time and money, but also leads to less heat input resulting in a small heat affected zone (HAZ), which in turn provides less distortions and hence improves the fatigue life (Alwan & Järve, 2012).

It is noteworthy to mention that penetration depth is dependent on welding speed with slower welds penetrating deeper, thus resulting in a stronger weld. Though too slow penetration can cause 'burn-throughs' which would weaken the weld, see Figure 3.4. There are no standards for penetration depth so the maximum penetration without burn-throughs should be used (Bright & Smith, 2004).

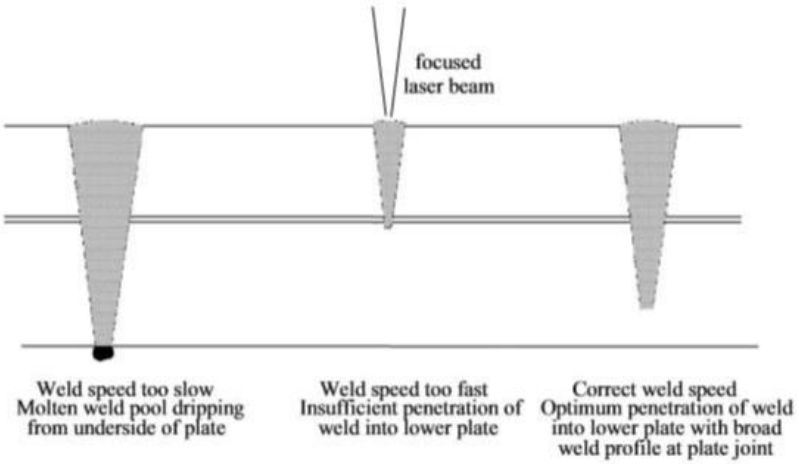

Figure 3.4 Laser stake welds showing the effects of weld speed (Bright & Smith, 2004)

3.2.4 Hybrid laser-arc welding (HLAW)

Hybrid laser-arc welding is a relatively new technique to welding. It improves on laser welding by combining it with gas metal arc welding (GMAW), see Figure 3.5.

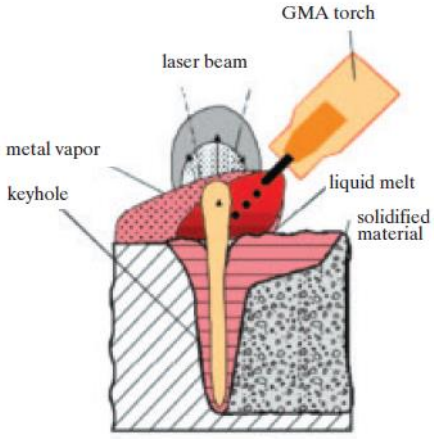

Figure 3.5 *Hybrid laser arc welding* (Defalco, 2007)

The laser component offers deep weld penetration and small heat affected zone (HAZ), while the GMAW component improves impurities, joint-root openings, root opening filling and contouring, and enhances control of the weld metallurgy (Defalco, 2007).

3.2.4.1 Applications of HLAW

Applications of HLAW are vast. One of its uses is to weld together T-profiles for use in ships and structural steel construction like bridges. HLAW improves on the weld profile by decreasing fillet size and the low distortion reduces the need for post-weld straightening. In orthotropic steel decks the connection of the top plate to the trough stiffener is vital. According to design codes the penetration of the weld has to reach at least 80% and with HLAW it can achieve 100% penetration, see Figure 3.6.

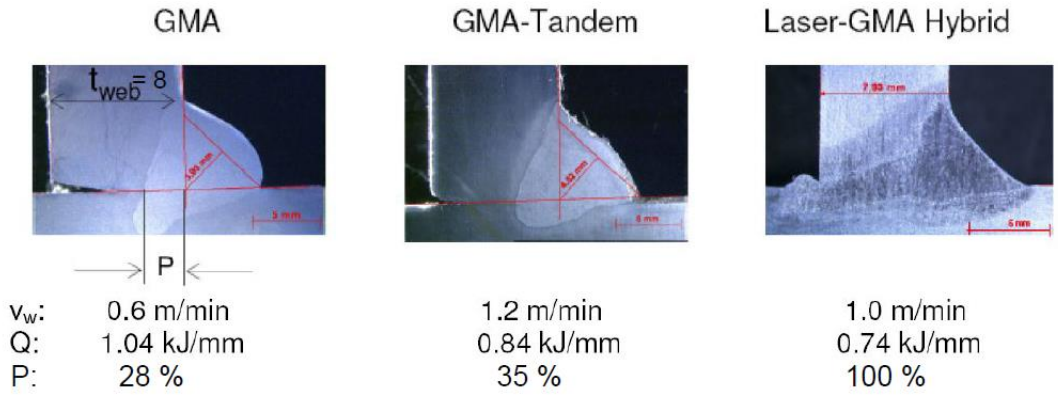

Figure 3.6 *Welding of a T-profile with three different welding methods. A T-profile using, GMAW with 28% weld penetration (left), GMA-Tandem with 35% penetration (middle), HLAW with 100% weld penetration right)* (Egerland, et al., 2013)

Hybrid laser welding is useful when it comes to welding together steel sandwich panels, see Figure 3.7. As mentioned in section 2.2 SSPs bring major advantages to conventional steel structures, however it has not been widely used because of difficulties in welding together such a configuration. Similar to laser welding the top

plate is metallically bonded to the core of the sandwich panel with sharp precision and great quality of the weld. With HLAW, manufactures can weld together thinner plates than what would be possible with other welding methods, which is why HLAW is practical for welding of SSPs since the face plates are usually very thin. Also with fully automated equipment large sections can be made at relative ease with precision weld quality control.

Figure 3.7 HLAW on a steel sandwich panel (SSP) (Defalco, 2007)

3.2.4.2 Commercial use of HLAW

With its entire benefits hybrid laser welding should be widely used in the market today, however that is not the case. In an email interview with Alexander Kaplan, professor at the University of Luleå in Sweden, which specialises in the research of laser and hybrid laser welding, said that the use of the two methods is not practiced on a regular basis. He said that even though interest is high within Swedish companies, laser welding and HLAW is rarely implemented. There are about 100 high effect lasers installed in Sweden for laser welding and none for HLAW. He went on further to say that in the whole world there are about 100 installations of HLAW with about 40 of them being in Germany.

Kaplan commented on the investment costs as well and said, when investing in HLAW the main investment is usually the laser generator, which would cost around 500 000 Swedish kronor per kw laser effect. Compared to the initial costs of other welding methods the price of HLAW is much higher. This was confirmed by Dr. Herbert Staufer at Fronius International GmBH which also added that one has to also take into account the investment costs of the robot which can be quite costly and of the safety cabin since safety is important when working with lasers.

A study conducted by the U.S. Department of Transportation in 2013 on the application of SSPs for tank car shell impact protection compared the costs of different welding procedures and concluded that HLAW which was highly superior to all other processes considered, was highly sophisticated and not readily available for routine manufacturing. The initial equipment costs were also very high compared to other processes.

There is a relation between weld penetration depth and the power of the laser used that most companies make a use of. Figure 3.8 shows the direct correlation between depth of penetration and laser power that the company ESAB uses for its laser

welding. For a speed of 1m/min the depth of penetration in mm is ~1.1 multiplied by [kW]. The relationship is linear so one can extrapolate in the case where higher power lasers are needed.

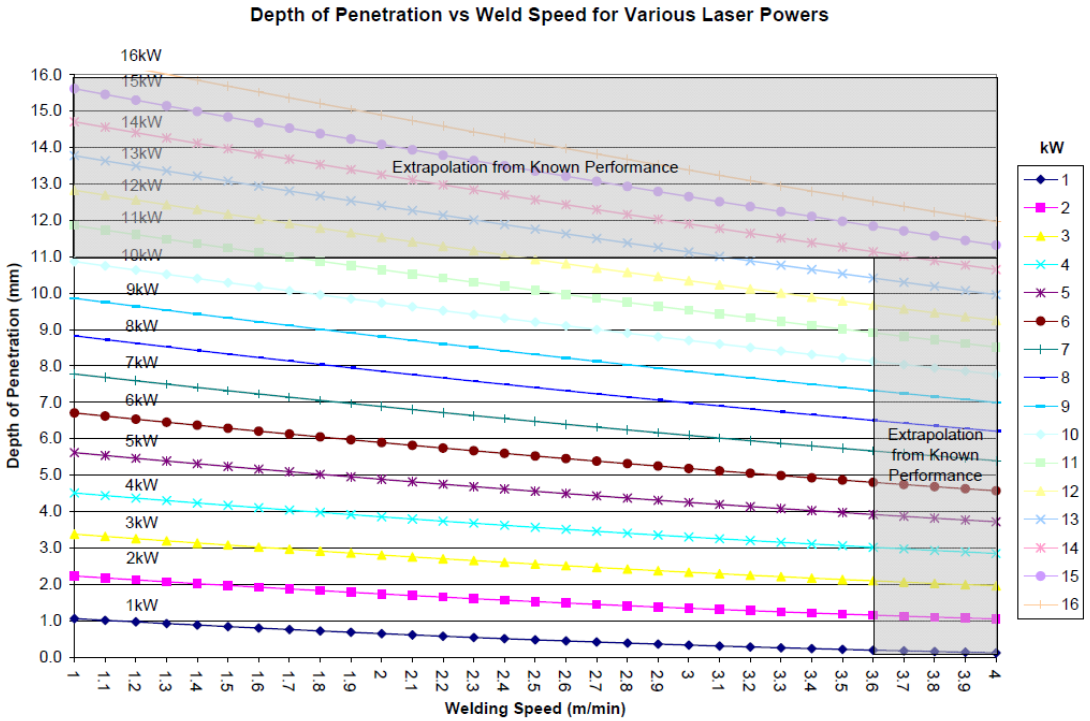

Figure 3.8 *Depth of penetration vs. weld speed for various laser powers* (ESAB , 2010)

Dr. Staufer at Fronius said that their company uses at highest a 10kW laser in welding together steel elements and added that any laser with a power output over 10kW would be very costly. If the material being weld is thicker than what a 10kW laser can weld in one pass than they simply run it in multiple passes. Of course that would take time which in turn would increase costs. Lars-Erik Stridh at ESAB has calculated the costs of running a hybrid laser with a laser power of 10kW and a 500 Amp power of GMAW to be around 1950 Swedish kronor per hour for one station. With this setup manufactures can reach welding speeds averaging at about 2.0 – 2.3 m/min with a utilization ratio of 60% in the station.

Even though HLAW is readily available in the market, most companies are not making good use of it for reasons that it's costly and complex. Also there is the phenomenon that it's difficult to change from an established method of welding to a new technology for most companies. New welding methods mean new possibilities and risks, and the industry wants before all security and avoid risks as much as possible, with other words to be conservative. Furthermore, there is very low knowledge and experience in the failure mechanics of hybrid laser welding; hence most companies prefer to continue with the established method. These factors and more hinder the transition from established welding methods to HLAW for most companies (Kaplan, 2014).

3.3 Production process

Production of steel sandwich panels is performed differently for different configurations. In this section, only the production process of the corrugated-core sandwich panel will be covered.

As mentioned above Kenno Tech specialises in the production of all steel sandwich panels for applications like plate heat exchangers, ballistic protection, and others. Even though their production of SSPs is mostly suited for small application when compared to bridges, the production process is principally the same.

Steel sandwich panels have yet to be developed for large load bearing structures like bridge decks. Therefore, the production process of the core and the plates was studied separately to have an idea what manufactures can produce today. According to EN 10029 the production of steel plates can be produced with a maximum thickness of 0.25 meters, a width of 3 meters and a length of 20 meters. The company Rukki can bend 20mm steel plates to a desired shape. This information would be particularly useful for the bending of the core to the sandwich panel, to see which thickness manufactures are able to bend. For the welding of the plates to the core, a 14mm thick plate can be laser welded with relative ease and a plate as thin as 1mm can be welded to another thanks to the precision of laser welding, see Figure 3.8. Thicker plates can be laser welded to the core if a higher powered laser is used or otherwise run the laser in several passes.

These dimensions are very generous in developing SSP bridge decks, which means that manufacturers have a relative freedom in dimensions when designing the panel for optimal strength or minimized weight or both.

For the production of corrugated sandwich panel, first the core is laser welded to one of the face sheets. The laser welding is carried out from the inside of the panel, meaning that the laser beam first melts the part of the core plate and then the face sheet. The other face sheet is now placed on top of the corrugated core and welded from outside, melting first the face sheet then the core sheet, see Figure 3.9. This is beneficial especially when manufacturing large size panels for example bridge decks, which might be somewhat heavy to turn around so they can be welded, but with this technique the need to reposition the panel parts are avoided.

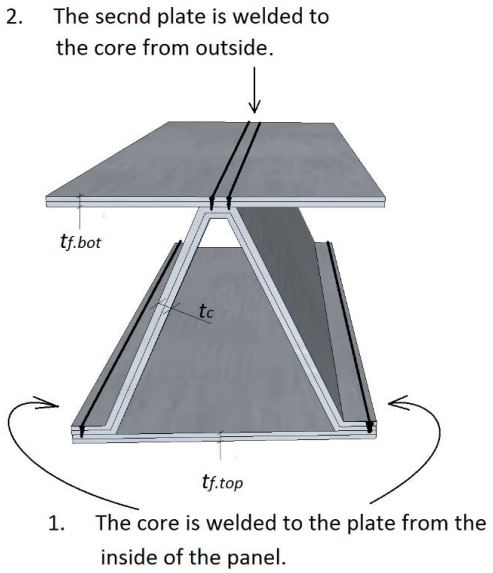

Figure 3.9 Illustration of the mounting process of the corrugated panel

3.3.1 Transportation

Steel sandwich panels can be prefabricated at a factory location and then transported to the work site where they will be mounted. This leads to a fast and efficient building process saving time and money. According to the Swedish Department of Transportation, goods can be transported with a maximum length of 23 meters, width of 2.6 meters, height of 4.5 meters and a maximum weight of 60 ton. These dimensions are more than generous for producing panels for a bridge deck which can be transported by means of automobiles. Because SSPs are supposed to be light weight, transportation is convenient and usually safe.

3.3.2 Joints

The joints between the steel panels or between panels and the steel superstructure are of outmost importance for the structure to function as a whole. One of the most important connections is the panel to panel connection in the longitudinal and transversal direction, see Figure 3.10.

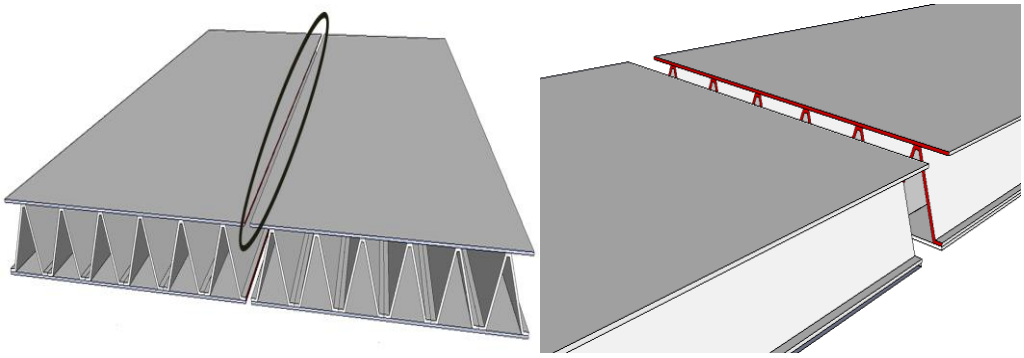

Figure 3.10 Panel to panel connection in the longitudinal (left) and transversal direction (right) of a SSP.

Panels are often connected on site forming the entire deck of the bridge and have to be able to carry the traffic loads acting on them. A common problem that arises in connections of steel decks today is poor fatigue performance. The joint is often prone to local stress raisers resulting from the in site welding which is usually done manually, often resulting in uneven welds.

4 Structural performance

The primary function of a bridge deck is to carry the traffic loads and distribute them to the steel superstructure without excessive and irreversible deformations. The deck is usually continuous along the longitudinal and transverse direction of the bridge span. In many cases the bridge deck is made composite with the longitudinal load bearing members. In composite action the deck serves as the top flange of the composite section and can be utilised for strength and stiffness. The main requirements the deck should fulfil are sufficient transverse bending stiffness and shear rigidity to satisfy deflection limits (Mara, 2014).

In the case of the steel sandwich panels the cross-sectional geometry is a critical factor in determining the strength of the SSP deck, due to the fact that different configurations have varying strength properties as mentioned in section 2.2.2. Other factors that influence the strength of the SSP deck are material properties, method of manufacture, and type of welding used.

4.1 Elastic constants

The elastic constants for a corrugated sandwich panel are given in the sections below. They are based on the research conducted by Charles Libove and Ralph E. Hubka in 1951.

By applying the Reissner-Mindlin plate theory the 3D sandwich panel can be transformed to an equivalent 2D panel which gives certain elastic constants that describe the physical behaviour of the sandwich panel, see Figure 4.1. The constants are the bending stiffness D_x and D_y, the torsional stiffness D_{xy}, axial stiffness E_x and E_y, horizontal shear stiffness G_{xy}, and transverse shear stiffness D_{Qy} and D_{Qx}.

With the help of these constants the sandwich panel can be optimized with regard to stiffness or area by changing certain geometrical parameters. Optimization analysis of the steel sandwich panel is covered in section 4.2.

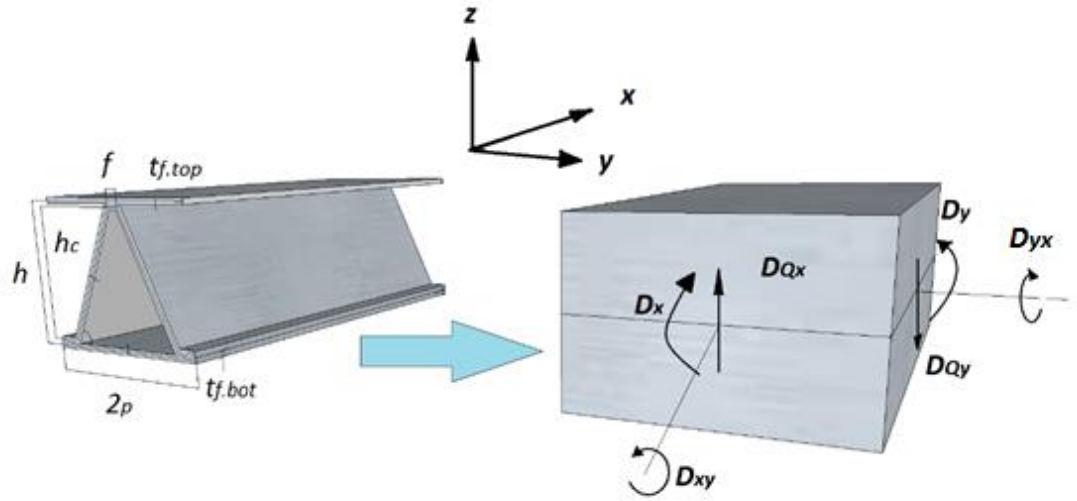

Figure 4.1 A section of a corrugated sandwich panel with dimensions (left) and equivalent elastic constants of a 2D-plate (right)

4.1.1 Bending and torsional stiffness

The bending and torsional stiffness for a corrugated steel sandwich panel are given below:

$$D_x = E_c I_c + E_f I_f \tag{4-1}$$

$$D_y = \frac{E_f I_f}{1 - \nu_f^2 (1 - \frac{E_f I_f}{D_x})} \tag{4-2}$$

$$D_{xy} = 2 G_f I_f \tag{4-3}$$

where:

$I_f = \frac{1}{2} t_f h^2$

E_c Modulus of elasticity of the core material, [Pa]

E_f Modulus of elasticity of face sheet material, [Pa]

ν_f Poisson's ratio of face sheet material

I_c Moment of inertia, per unit width, of corrugated cross-sectional area, [m^3]

I_f Moment of inertia, per unit width, of face sheet cross-sectional area, [m^3]

G_f Shear modulus of elasticity of face sheet material, [Pa]

4.1.2 Axial stiffness

The axial stiffness for a corrugated steel sandwich panel is given below:

$$E_x = E_c A_c + E_f A_f \tag{4-4}$$

$$E_y = \frac{E_f A_f}{1 - \nu^2 (1 - \frac{E_f A_f}{E_x})} \tag{4-5}$$

where:

$A_f = 2 t_f$

A_c Area, per unit width, of corrugation cross section perpendicular to corrugation axis, [m]

A_f Area, per unit width, of face plate sheet cross section perpendicular to corrugation axis, [m]

t_f Thickness of the face sheet, [m]

4.1.3 Shear stiffness

4.1.3.1 Horizontal shear stiffness

The horizontal shear stiffness is given for a corrugated core sandwich panel is given below:

$$G_{xy} = \frac{G_c t_c^2}{A_c} + 2G_c t_f \tag{4-6}$$

G_c Shear modulus of elasticity of core material, [Pa]

t_c Thickness of corrugated-core sheet, [m]

4.1.3.2 Transverse shear stiffness

The transverse shear stiffness in planes perpendicular to the corrugation axis is given below:

$$D_{Qy} = Sh\left(\frac{E_c}{1-\nu_c^2}\right)\left(\frac{t_c}{h_c}\right)^3 \tag{4-7}$$

h_c Depth of corrugation, measured vertically from centre line of crest to centre line at trough, [m]

ν_c Poisson's ratio of core material

S Non-dimensional coefficient depending upon shape of corrugation, relative proportions of sandwich cross section, and the material properties of the component parts

The transverse shear stiffness in planes parallel to the corrugation axis is given below

$$D_{Qx} = \frac{G_c t_c^2}{A_c}\left(\frac{h}{p}\right)^2 \tag{4-8}$$

where:

$$A_c = \frac{l_c t_c}{p}$$

A_c Area, per unit width, of the corrugation cross-section, [m]

l_c Length of one corrugation leg measured along the centre line, [m]

p Half of the corrugation pitch, [m]

Verification of the above elastic constants was conducted by Alwan and Järve (2012), where the constants were converted into orthotropic material properties, by analytical formulas obtained from Lok & Cheng (1999). The conversion was necessary in order to assign material properties to a 2D plate for modelling in Abaqus/CAE. The 3D equivalent SSP plate and the 2D orthotropic plate had the same load and boundary conditions. The deflection was measured and there was a 1.8% discrepancy between the two models, which is very little.

4.2 Optimization routines of a corrugated SSP

In the optimization study an existing orthotropic steel deck with fixed dimensions Figure 4.2 was compared with a similar size steel sandwich panel Figure 4.3 to understand how the geometry of the cross-section influences the structural performance of the panel. The cross-sectional area of the panels was taken per unit width and the calculations were performed in MathCad, see APPENDIX A.

The orthotropic deck was taken from an existing bridge located in Lyrestad, Sweden. The bridge is a bascule bridge which crosses the Göta Channel. It is a freeway bridge composed of two lanes. In order to save time with the calculations some simplifications were made on the deck. First the deck was taken to be as simply supported on the edges, while in reality it's simply supported on one side and on the other side the rotating mechanism is located with the counter weight. Also the length of the deck was taken to be a little longer than the original so that transversal girders would have an even distribution along the deck.

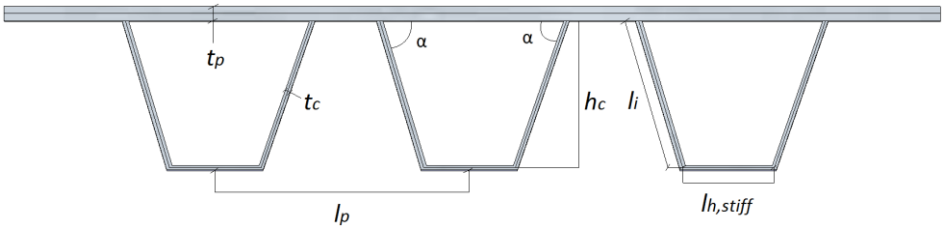

Figure 4.2 Orthotropic steel deck cross section

Table 4.1 Orthotropic deck dimensions

Dimensions	**Ortho [mm]**
t_p	16 mm
t_c	12 mm
l_p	0.5 mm
α	63 deg
h_c	179 mm
l_i	200 mm
$l_{h,stiff}$	171 mm

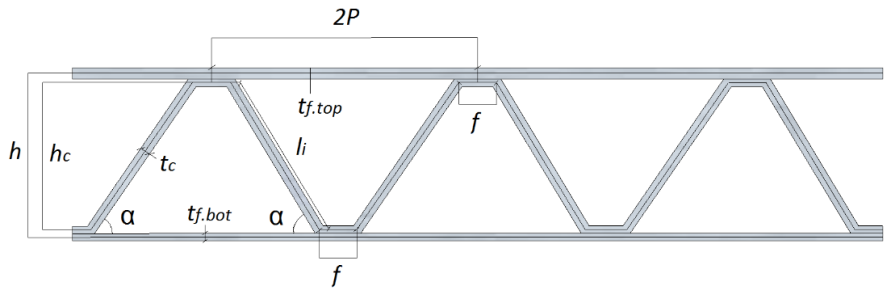

Figure 4.3 Steel sandwich panel cross section

Two optimization studies were performed on the SSP. First the geometrical dimensions were optimized to obtain the best possible bending stiffness D_x in the stiffer longitudinal direction of the SSP, while keeping the area of the cross section the same as to the area of the orthotropic deck. On the second optimization the stiffness of the SSP was kept the same as the stiffness of the orthotropic deck while minimizing the cross-sectional area of the SSP as much as possible. For the sake of simplification the optimization where the bending stiffness is maximized will be called Max D_x and for the optimization where the cross-sectional area is minimized will be called Min A.

The two optimization studies will give an insight on improvements that can be achieved with the SSP and savings in production and labour costs that can be reached by using a SSP deck instead of an orthotropic deck.

To accurately optimize the SSP deck the geometrical parameters listed below had to be set as variables. The programming was written in order to obtain the best possible combination of the geometric variables which gives the best possible bending stiffness or the lowest area within given restraints.

h_c	Height of corrugation
$t_{f.top}, t_{f.bot}$	Thickness of the top and bottom plate
t_c	Thickness of corrugated plate
α	Angle of corrugation
f	Length of the horizontal corrugated segment

4.2.1 Constraints

In order to perform the optimization analysis certain constraints needed to be defined. The restraints were based on norms from Eurocode and earlier optimization studies performed on a steel sandwich panel.

The first constraint that was implemented was the maximum width to thickness ratios for compression parts. According to EN 1993-1-9 (1993) the ratio is characterized according to cross-sectional classes and in this case the cross-sectional class three is used, which has to be designed assuming elastic stress distribution. The relationships that were set as constraints in this case are given below.

$$\frac{l_i}{t_c} \leq 42\varepsilon \qquad \frac{l}{t_{f.top}} \leq 42\varepsilon \qquad \frac{l}{t_{f.bot}} \leq 42\varepsilon$$

where

$\varepsilon = \sqrt{\frac{235MPa}{f_y}}$ Strength ratio for cross-section class 3

f_y Yielding strength of the material, [MPa]

The second constraint was the angle of corrugation. According to (Chang, et al., 2005) the angle of corrugation should be within 45 to 70 degrees. It was concluded in the study that with an increasing corrugation angle the shear stiffness decreases drastically, therefore the angle was kept within reasonable values.

The third constraint was keeping the cross-sectional area of the SSP smaller or equal to the area of the orthotropic deck. Also the moment of inertia of the SSP has to be larger or equal to the moment of inertia of the orthotropic plate.

The fourth constraint was to keep the local deflection of the top plate within $l/400$ according to TRVFS (2011:12) with l being the corrugation opening as shown in Figure 4.3.

The fifth constraint was to take into account the fatigue strength of the laser welded joints. In order for the joints to withstand the fatigue stresses caused by loads acting on the SSP deck, the stresses in the joints need to be less than the stress value obtained from the detail category given in EN 1993-1-9 (1993). There is no detail category in Eurocode for the laser weld detail connection that is used in a SSP thus 71MPa is taken as a reference value since it's a reasonable stress value used for toe cracking of the weld. Load Model 3 was used for the fatigue loads acting on the deck which is described in detail in section 5.6.

Finally the length of the horizontal corrugated segment f was set to be as small as possible to minimize the resulting moments and shear forces which cause local deflection in the face plate.

4.2.2 Results of the optimization study

The geometrical parameters obtained from each optimization performed on the SSP deck are given below in Table 4.2. Each bridge deck is further analysed in Chapter 5 with the help of a finite element analysis in Abaqus/CAE.

Table 4.2 Geometrical parameters for the two optimization studies performed on the SSP in

Variables	**Max D_x**	**Min A**
h_c	225 mm	184.1 mm
$t_{f.top}$	7.8 mm	6.5 mm
$t_{f.bot}$	7.1 mm	5.7 mm
t_c	7.2 mm	5.9 mm
α	65 deg	67 deg
f	35 mm	35 mm

In Table 4.3 the bending stiffness D_x and D_y, torsional stiffness D_{xy}, and the cross sectional area is given for the existing orthotropic and the SSP deck after the optimization. The stiffness in the direction parallel to the corrugation for the SSP was 82% larger than that of the orthotropic deck for optimization Max D_x. For optimization Min A, a 23% decrease in the area per unit width of the cross section of the SSP was obtained, which also means a decrease in the total weight by the same margins.

Table 4.3 Bending-, torsional stiffness and area for the SSP and orthotropic deck

	Max D_x				**Min A**			
	D_x [Nm]	**D_y [Nm]**	**D_{xy} [Nm]**	**Area [m^2/m]**	**D_x [Nm]**	**D_y [Nm]**	**D_{xy} [Nm]**	**Area [m^2/m]**
SSP	6.407e7	4.884e7	3.671e7	0.03	3.531e7	2.664e7	2e7	*0.024*
Ortho	3.531e7	1.186e7	2.046e7	0.03	3.531e7	1.186e7	2.046e7	*0.03*
Ratio	**82%**	**312%**	**79%**	**0%**	**0%**	**125%**	**0%**	**-23%**

With a significant increase in stiffness of the SSP deck, considerable improvements can be achieved. Some of the possible improvements are material savings in that the transverse girders can be rearranged so that the distance between them is larger hence decreasing the amount of girders needed. The dimensions of the main girder can possibly be decreased if stresses in ULS are found to be quite low. Materials savings are also achieved in the deck itself when the stiffness is kept the same while the weight is decreased. Further analysis needs to be conducted on the local and global behaviour of the SSP deck before final results can be recorded.

5 FEM analysis and results

The optimization analysis has given us an insight on the structural performance of the SSP in relation to bending stiffness. In order for the deck to genuinely be considered as a viable option for a bridge deck other analyses need to be performed.

A global analysis of the whole bridge structure will be performed in Abaqus/CAE. The results that will be analysed are the stresses in ULS, global and local deflection in SLS, loads including fatigue loads, and the effective width to account for shear lag. A linear buckling analysis will also be conducted on the whole bridge structure to determine critical buckling modes and buckling factor, λ, also known as eigenvalue.

5.1 Modelling of the bridge

For the FEM analysis, the program Abaqus/CAE was used to model the bridge. A total of three models were created, two models with the SSP deck one for each optimisation study and a model of the bridge with the orthotropic deck. The deck, transversal girders, and main girders in the models are made of linear elastic steel material, with a modulus of elasticity of 210GPa and Poisson's ratio of 0.3.

In order to properly compare the structural performance of the three bridges, they need to have the same structure height. Therefore the dimensions of the main and transverse girders for the bridge models with the SSP deck are modified so the total height of the two bridges with the SSP deck are the same as the original orthotropic bridge, see Figure 5.1.

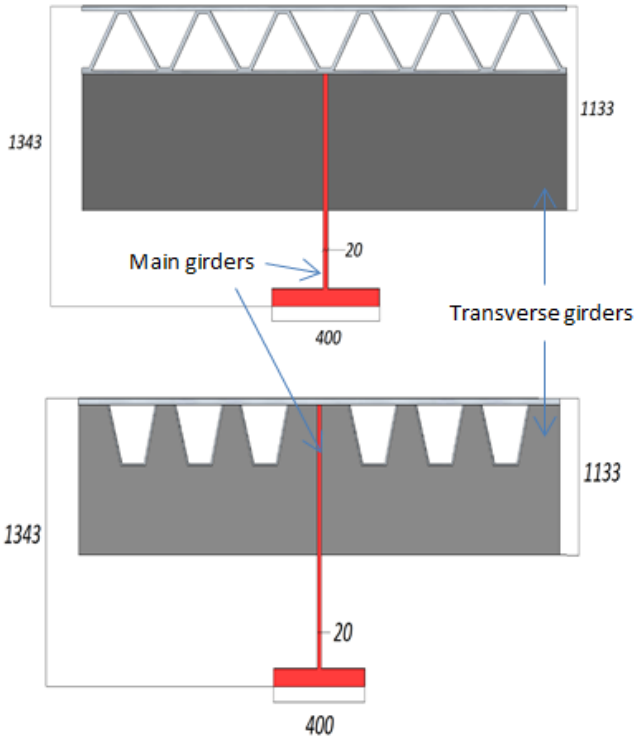

Figure 5.1 Illustration of the cross section of the bridge with the SSP deck (above) and the bridge with the orthotropic deck (below).

3D deformable shell elements were used to create the sandwich deck and the girders. Shell elements allow for out-of-plane loading in contrast to 2D solid elements where the loading is confined to the plane of the elements. Shell elements are also used to model structures when one dimension, in this case the thickness, is significantly smaller than the other dimensions. The thickness of the members was defined in the section properties.

After the assembly of the different parts, the model needed to be meshed. The type of mesh that is often chosen is dependent on the type of the analysis. For this analysis a mesh with quadrilateral elements was chosen. The results from the analysis are highly dependent on the size of the mesh, thus a convergence study was performed on the model. The convergence was performed in the area where the wheel load was located since that is where the local stresses are highest. The mesh size was changed until the difference between the maximum values of von Misses stresses was less than 10%. As shown in Table 5.1, the difference between the maximum stresses obtained for a mesh size of 20 and 8 are less than 10%, therefore, it is ok to use a mesh size of 8 at the areas where the wheel load will act on. A mesh size of 35 was used on the rest of deck since the smallest element will be the length of the corrugated flat segment f which has a measurement of 35mm. Transversal and main girders had an even larger mesh since the elements were larger.

Loads acting on the bridge were placed in the middle of the longitudinal span of the bridge to obtain the largest deflection possible.

Table 5.1 Values of the maximum von Misses stresses and how they vary with the mesh size.

	Mesh size 35	**Mesh size 20**	**Mesh size 8**
σ_{max} [MPa]	167	194	213
Change in %		14 %	8.9 % < 10 % OK!

5.2 Loads acting on the bridge

The loads acting on the bridge were defined from Eurocode 1: Part 2 (2003). Load Model 1 (LM1) was used for the load analysis which consists of two partial systems, see Table 5.2. These loads are double-axle concentrated loads (tandem system TS) with each axle having the following weight $\alpha_Q Q_k$ and uniformly distributed loads (UDL) having the following weight per square meter of notional lane $\alpha_q q_k$, where α_Q and α_q are adjustment factors according to the Swedish Transport Administration (TRVFS, 2011:12) given in Table 5.3.

Table 5.2 *Load Model 1 (LM1) showing all the characteristic values of the concentrated loads and uniformly distributed loads.* (SS-EN 1991-2, 2003)

Location	**Tandem system *TS***	***UDL* system**
	Axle loads Q_{ik} (kN)	**q_{ik} (kN/m^2)**
Lane number 1	300	9
Lane number 2	200	2.5
Lane number 3	100	2.5
Other Lanes	0	2.5
Remaining area (q_{rk})	0	2.5

Table 5.3 *Adjustment factors for traffic loads* (TRVFS, 2011:12)

α_{Q1}	0.9
α_{Q2}	0.9
α_{Q3}	0
α_{q1}	0.7
α_{qi}	1.0 for i > 1
α_{qr}	1.0

The number of notional lanes that the bridge in question can have and the load cases used are calculated according to Eurocode standards and are given in APPENDIX B. The bridge can have a total of four lanes, each with a width of 3m. The loads acting on the bridge are two pairs of concentrated loads Q_{1k}, Q_{2k}which are caused by the tires of the vehicles. Each concentrated load has an accompanying uniformly distributed load q_{1k}, q_{2k}. In addition q_{3k}, q_{4k}, q_{rk} are other uniformly distributed loads for lanes three, four, and the remaining area respectively and are all equal according to Table 5.2. Other loads that were considered were the self-weight of the bridge *G* and the weight of the asphalt covering *B.*

The wheel loads have a contact area of 400x400mm^2, however the contribution from the asphalt cover increases the contact area of the wheel load acting on the deck. The asphalt cover distributes the load in a 45° angle to the steel deck and with a thickness of 100mm the contact area of the wheel load is increased to 600x600mm^2 as shown in figure Figure 5.2.

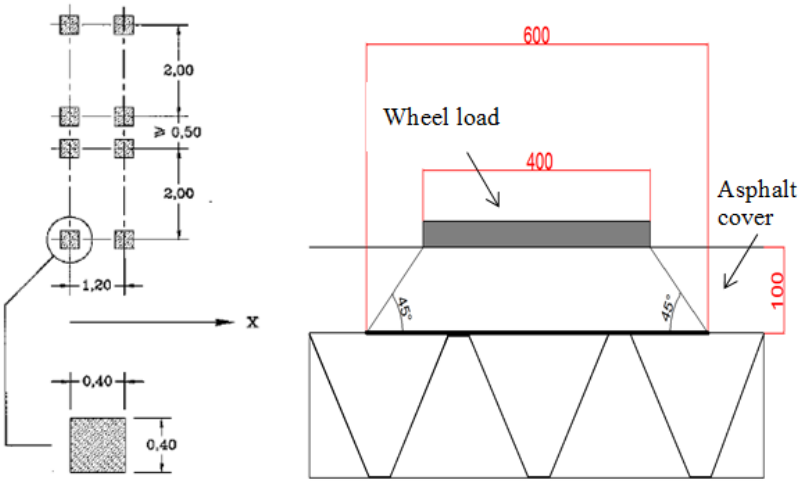

Figure 5.2 *Axle and wheel dimensions of an automobile (left) and contact area of wheel with contribution from asphalt cover (right)* (SS-EN 1991-2, 2003)

Three load cases were considered in the analyses that were thought to give the largest global stresses and deflection according to literature from previous studies, see Figure 5.3.

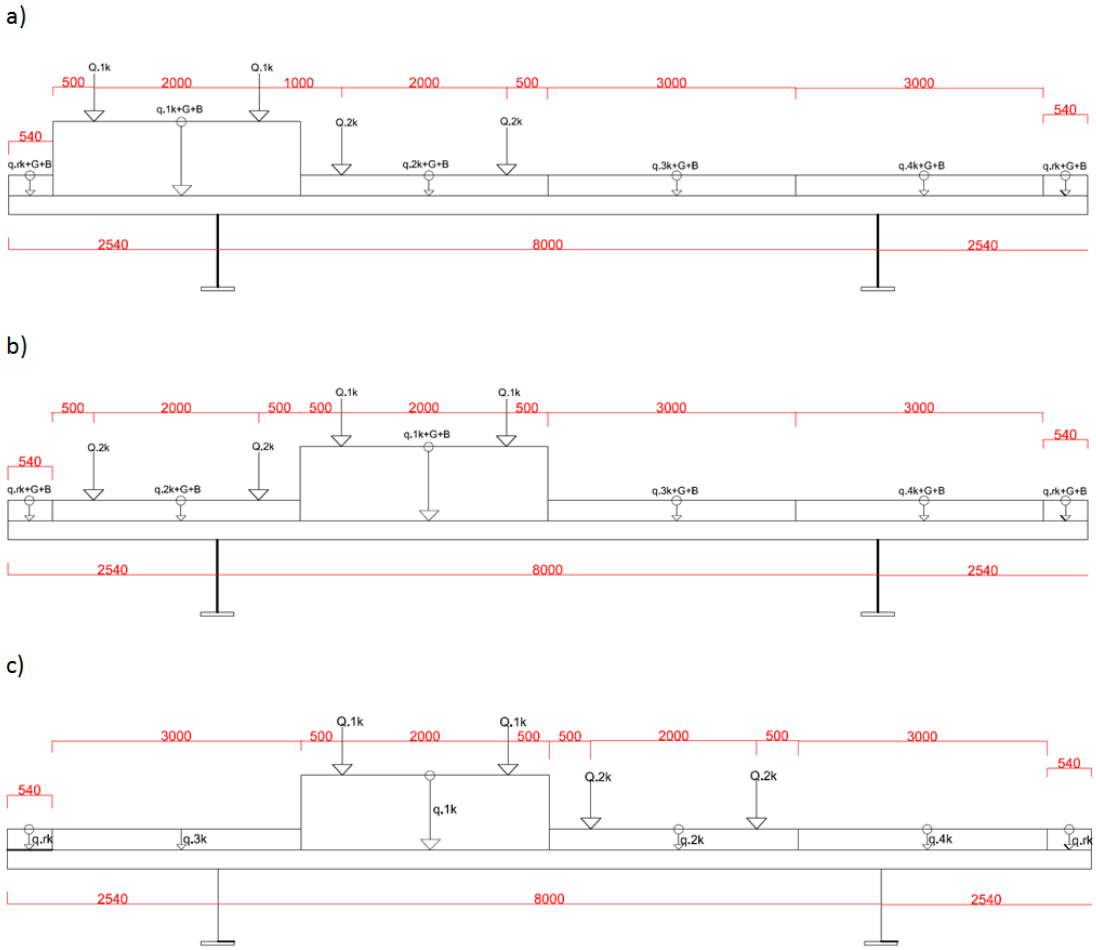

Figure 5.3 *a) load case one b) load case two c) load case three*

In order to obtain the largest influence of the loads acting on the bridge a load combination was conducted in ULS and SLS according to Table 5.4 below. In SLS the numerical values are omitted. The value $G_{kj,sup}$ symbolizes all the permanent loads acting on the bridge, in this case the self-weight of the bridge and the weight of the asphalt covering. The value of ψ_0 factor is recommended to be set to 0.75 for TS loads and 0.40 for UDL loads for road bridges according to (SS-EN 1990/A1:2005, 2006). All the possible load combinations of the three load cases are given in APPENDIX B and later writen in Abaqus/CAE.

Table 5.4 Design values for loads (TRVFS, 2011:12)

Persistent and transient cases	**Permanent loads**		**Variable main load**	**Concurrent variable loads**	
	Unfavourable	**Favourable**		**Largest load**	**Other loads**
6.10a	$1.35G_{kj,sup}$	$1.00G_{kj,inf}$		When load is unfavourable: $1.5\psi_{0,1}Q_{k,1}$ When load is favourable: 0	When load is unfavourable: $1.5\psi_{0,i}Q_{k,1}$ When load is favourable: 0
6.10b	$0.89 * 1.35G_{kj,sup}$	$1.00G_{kj,inf}$	When load is unfavourable: $1.5Q_{k,1}$ When load is favourable: 0		When load is unfavourable: $1.5\psi_{0,i}Q_{k,1}$ When load is favourable: 0

5.2.1 Horizontal loads

The horizontal loads that act on the bridge were modelled in Abaqus/CAE to account for the lateral effects. The loads that were taken into consideration are the breaking, acceleration, and lateral loads. The breaking and acceleration load was calculated from equation (5-1). They act in the longitudinal direction of the bridge opposite of each other and are the same magnitude, see Figure 2.1. It's worth mentioning that the loads do not act the same time. Finally, the lateral load is equal to 25% of breaking or acceleration load (SS-EN 1991-2, 2003).

$$Q_{1k} = 0{,}6\alpha_{Q1}(2Q_{1k}) + 0{,}1\alpha_{q1}q_{1k}w_1L \tag{5-1}$$

$$180\alpha_{Q1}(kN) \leq Q_{1k} \leq 900(kN)$$

Where

L length of bridge

w_1 Width of the lane

In Abaqus/CAE the loads were modelled as a traction force and placed in Lane 1 with the lateral load being perpendicular to the breaking or acceleration load. To obtain the most critical load combination, the load directions were varied.

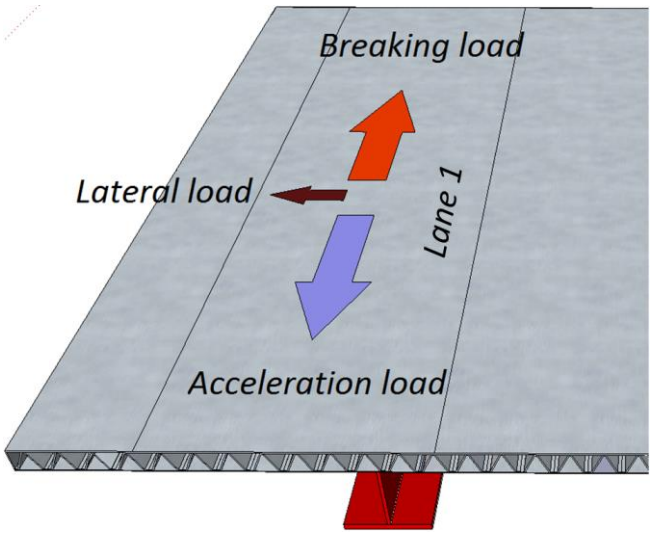

Figure 5.4 The direction of the horizontal loads that act on Lane 1 of the bridge.

Results obtained from the FEM-analysis indicated that the horizontal loads acting on the bridge did not contribute greatly to the stresses, deflection and buckling values. Therefore, it was chosen to neglect the effect of the horizontal loads in the calculations.

5.3 Effective width

The effective width has been calculated for the three different bridge models to account for the shear lag effect using equation (5-2) obtained from Zou et al. (2011). It is defined as the integral of the normal stress distribution within a given interval divided by the maximum stress σ_{max} at the deck-girder intersection.

$$b_{eff} = \frac{\int_0^b \sigma_{x\,dx}}{\sigma_{max}} \tag{5-2}$$

Where

σ_x Axial stresses in the x-direction, [MPa]

σ_{max} Maximum value of the axial stresses, [MPa]

b Length of half of the bridge width, [m]

b_{eff} Effective width, [m]

Load case one was used to obtain the normal stress distribution since it gave the highest stresses. The normal stresses were obtained in the interval b shown in Figure 5.5 which is equal to half the width of the bridge, 6532mm. The normal stress distribution was derived from all three models in Abaqus/CAE and the maximum stress was recorded. Thereafter the stress curve was integrated to obtain the total stresses per meter.

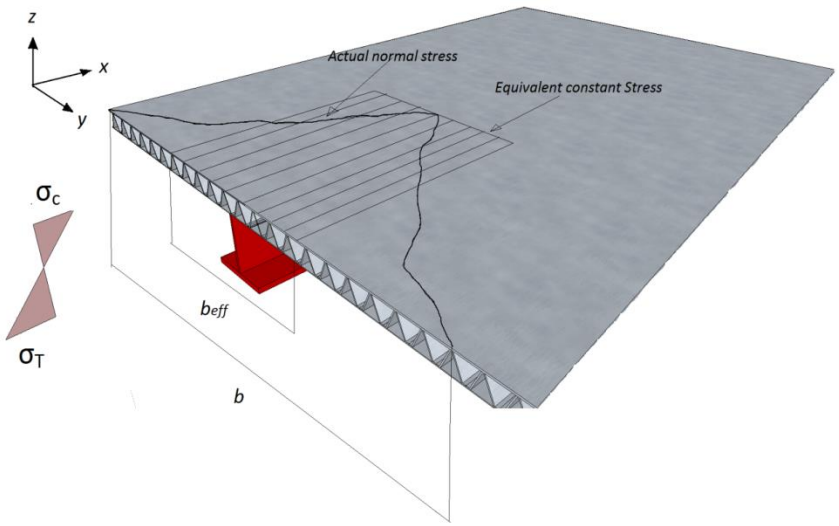

Figure 5.5 *Shear lag effect, showing the effective flange width and the normal stress distribution in the x-direction.*

The effective width for all three models and the utilization ratio is shown in Table 5.5. As it can be seen from the utilization ratio, model Max D_x utilizes most of the cross section of the deck as a top flange to the main girder at 66% utilization and Ortho utilizes the least at 37% utilization. If the utilization ratio is 100% then the bridge is working full compositely. The parameter that influences the distribution of the normal stresses is the horizontal shear stiffness G_{xy}, as the shear stiffness increases the normal stress distribution will be more uniform (Mara, 2014).

Table 5.5 *Effective flange width for the three bridge models, with utilization ratios*

Cross section	b_{eff} [mm]	Utilization ratio b_{eff}/b
Max D_x	4027	66%
Min A	3405	59%
Ortho	2427	37%

5.4 Ultimate limit state (ULS)

In this chapter stresses are checked in ULS for all bridge models to see how the models compare to each other. Stresses that were checked were the von Misses stresses and stresses in the x- and y-direction of different parts of the bridge.

Von Misses stress criteria considers all the principal stresses that act in all directions on a 3D-body when loaded and gives it as an equivalent stress. The von Misses stress is then compared with the yield stress of the material to see if the material will yield. The maximum von Misses stresses are recorded at the deck of all three bridge models and compared with the yield stress of the steel used. Von Misses stresses were also recorded locally for the core of each deck.

In the global analysis maximum stresses in the x- and y-direction were given for the main and transverse girder respectively. Stresses in the x-direction were taken for the main girder and for the section above it, to observe how the stress is distributed in this area see Figure 5.6. From this analysis, the neutral plane can be calculated where the stress is equal to zero. Parts of the bridge that are in compression and tension can also be seen from the neutral plane.

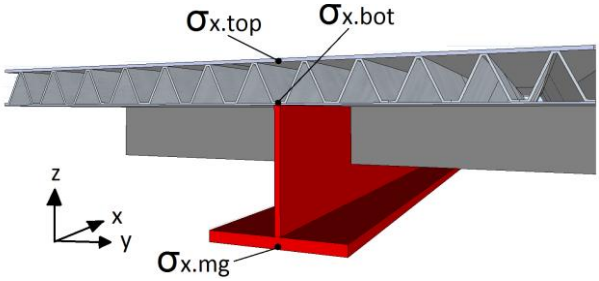

Figure 5.6 Illustration of the global stresses at the section where the main girder is located

In the local analysis the stresses in the x- and y-direction were studied at the area where the maximum wheel load was located, see Figure 5.7. The local stresses in this area can be studied to see the how the different parts of the bridge deck act when loaded in different directions so that appropriate adjustments can be made to the dimensions if needed.

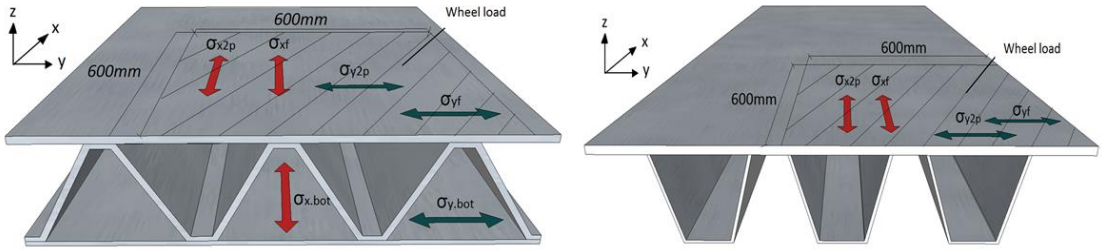

Figure 5.7 Illustration of the local stresses showing the area at which they were taken

The stresses were obtained from load case one and three since they gave the maximum stresses in the main and secondary girders respectively, see Table 5.6.

Table 5.6 *Maximum global and local stresses at the girders and the deck, taken for all three models. Yield stress of the steel is given as a reference, [MPa]*

Stresses	**Max D_x**	**Min A**	**Ortho**	
σ_{yield}	355	355	355	Maximum **von Misses** and yield stresses
$\sigma_{vM.deck}$	195	220	132	
$\sigma_{x.mg}$	175	195	396	Maximum **global** stresses in the x-direction in the main girder and the section above it
$\sigma_{x.top}$	-77	-85	-89	
$\sigma_{x.bot.global}$	-27	-39	-88	
σ_{yf}	222	191	83	Maximum **local** stresses in the x- and y-direction under the wheel load
σ_{xf}	142	65	69	
σ_{x2p}	14	164	121	
σ_{y2p}	178	179	108	
$\sigma_{y.bot}$	50	75		
$\sigma_{x.bot.local}$	22	63		
$\sigma_{y.tg}$	65	83	80	Maximum stresses in the **transverse girder**
$\sigma_{vM.core}$	81	107	104	Maximum **von Misses** stresses at the **core**

The maximum stresses for the optimization Max D_x and Min A are well below the yield stress of the steel grade used for the deck and the girders, therefore yielding conditions are not reached and the two bridge models have enough capacity to carry the loads. It can be observed from the global stresses obtained at the main girder of each bridge are higher for the orthotropic bridge than the other two. This depends on the effective flange width of each model and how the load is distributed to the main girders. Max D_x and Min A have larger effective flange widths than the orthotropic bridge, therefore decreasing the stresses. Furthermore, the bridges with the SSP decks distribute the load much more efficiently to the main girders than the orthotropic bridge deck. Illustrated below in Figure 5.8 is the stress distribution of the two SSP bridges and Max D_x has lower values of stresses as expected.

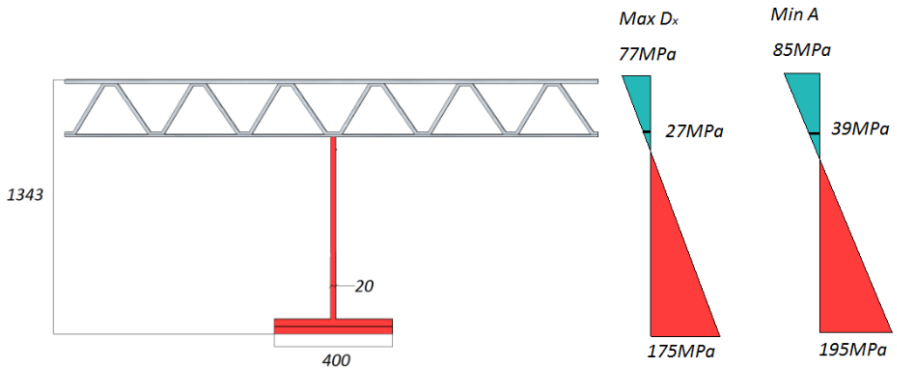

Figure 5.8 *Illustration of the global bending stresses in the longitudinal direction of the bridge*

It can be observed that the maximum stresses in the main girder for the orthotropic bridge exceed the yield stress of the steel used. The high stress can depend on the assumptions and simplifications that were taken for the orthotropic deck, described on the second paragraph of Section 4.2.

The overall local stresses on the top plate of the orthotropic deck are lower than the stresses of the top plates on the SSP models. This is due to the top plate of the orthotropic deck being more than double the thickness of the top plate of the SSP deck and hence it has more bending stiffness.

Maximum stresses on the transverse girders and the core of each deck are in similar magnitudes to each other and are quite low for all three models.

5.5 Serviceability limit state (SLS)

In the serviceability limit state the local and global deflection of the structure is the design criteria. The structure needs to fulfil the limit of $l/400$ where l is the length of the section being studied. Conditions in SLS are satisfied as long as the deflection is under the limit.

The local deflection of the top plate of the SSP decks was taken as a constraint in the optimization analysis, see APPENDIX A. The deflection was then verified with a FEM model in Abaqus/CAE for each optimization, see Figure 5.9. In the models the largest wheel load and all the distributed loads were given to give the worst case scenario. The boundary conditions were, clamped on one side and roller on the other. Rotation is allowed in the direction perpendicular to the corrugation. The results from the hand calculations, the FEM analysis and the limit allowed for the deflections are given in Table 5.7. The results are very similar and they satisfy the deflection limit.

Table 5.7 Local deflection for the top plate of the two SSP models from hand calculations and FEM analysis, [mm]

	Max D_x	**Min A**
MathCad	0.69	0.573
Abaqus/CAE	0.63	0.497
l/400	0.69	0.573

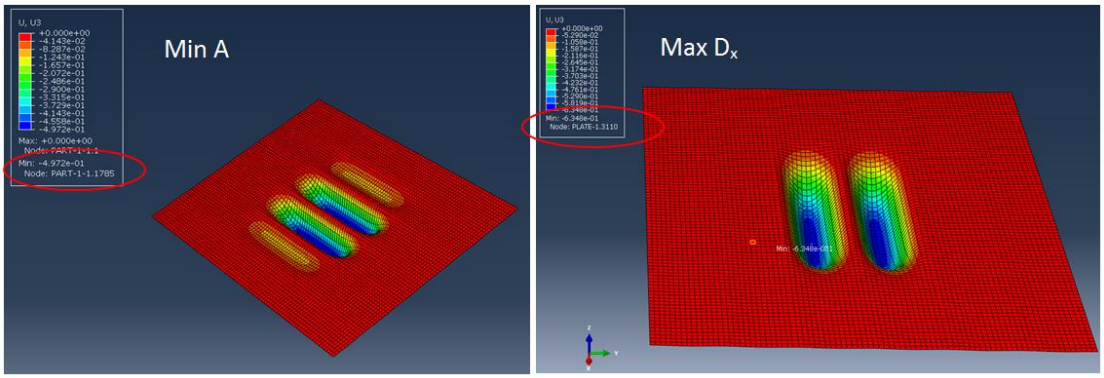

Figure 5.9 Local deflection in SLS for the top plate of the SSP decks.

The maximum global deflection and deflection in the main and transverse girders were obtained for the three bridge models, see Table 5.8. The values for each deflection are compared for each model and the allowed limit at that section. The maximum deflection was located on the console where the largest wheel load is located which is in lane one see Figure 5.10. Load case one gave the largest deflections for the whole bridge and the main girder while load case three gave the largest deflections on the secondary girders (not shown below).

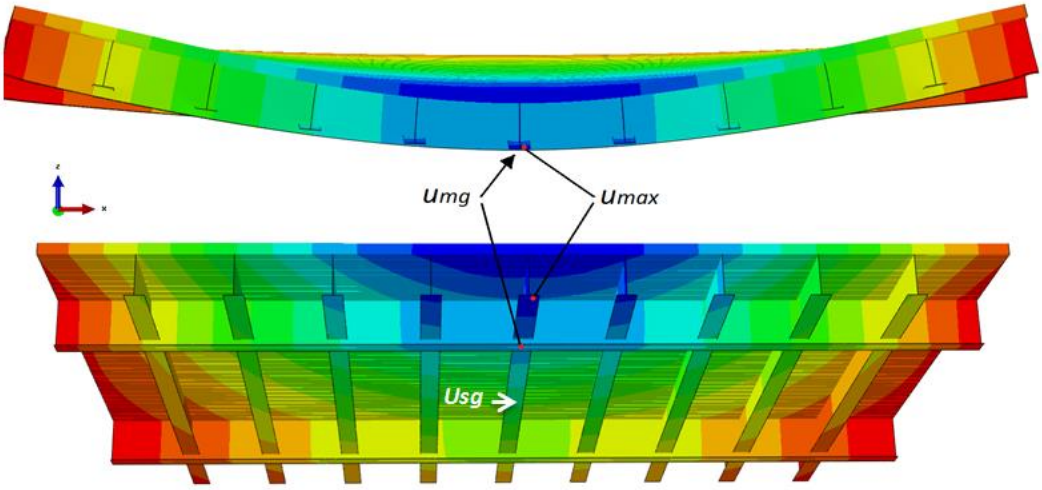

Figure 5.10 Illustration of the maximum deflection u_{max}, maximum deflection in the main girder u_{mg}. and maximum deflection in the transverse girder u_{sg}

The deflection of the orthotropic bridge is much larger than the other two models. This is due to the effective flange width of the two SSP models being larger than that of the orthotropic one. The stiffness is increased with increased effective width and in turn deflections are decreased. The deflection on the secondary girder of the orthotropic bridge is below the values of the other two bridges. This is due to the height of the transverse girders being larger in this model than the other two, hence having more stiffness.

The deflection of Max D_x and Min A are quite similar. Max D_x has a larger effective width than Min A so the difference in deflection is expected to be greater, however the weight of Min A is smaller which could compensate for the difference. Nevertheless the deflection of Max D_x at all sections is slightly smaller which is satisfactory.

Table 5.8 Global deflection for all bridge models and the limits allowed, [mm]

Deflection	**Max D_x**	**Min A**	**Ortho**	***l*/400**
u_{max} [mm]	23.5	31.1	45	45
u_{mg} [mm] (main girder)	19.2	26.1	36.7	45
u_{sg} [mm] (secondary girder)	2.1	2.4	1.3	20

5.6 Fatigue limit state (FLS)

For the fatigue loads acting on the bridge Load Model 3 (LM3) was used, see Figure 5.11. The model consists of four axles each of them having two identical wheels. The weight of each axel is equal to 120kN with a contact area of each wheel being 400mm and from the contribution of the asphalt cover the contact surface of the wheel on the deck becomes 600mm as described in figure Figure 5.2. The fatigue contribution was also taken under consideration in the optimization analysis where the stress calculated at the laser welded joints needed to be less than the stress value from that detail category given in EN 1993-1-9 (1993). Because there is no detail category for laser welded details in Eurocode, a reference detail category is used for the weld profile that is found in the connection of the stiffener-deck connection in an orthotropic steel deck. This detail category has a stress limit of 71MPa which is very conservative in regards to the strength of a laser welded detail. According to Bright & Smith (2004) a laser weld can withstand a stress capacity of up to 125MPa. This detail was chosen because it's where the fatigue cracking is more commonly caused in existing orthotropic decks as shown in Figure 2.2.

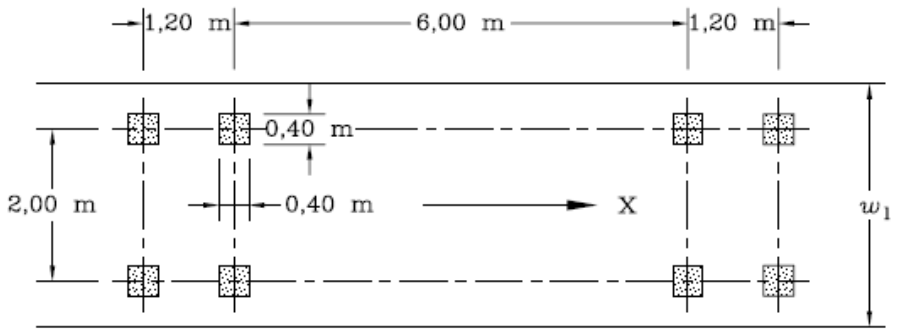

Figure 5.11 Fatigue Load Model 3, where w_1 is the lane width and X is the bridge longitudinal axis (SS-EN 1991-2, 2003)

The maximum local fatigue stresses were recorded for the top plate where the wheel load is acting for each bridge model, see Table 5.9. Results show that the stresses for all three models are under 71MPa which is sufficient to say that the bridge models have sufficient fatigue capacity at critical details. The stresses at the top plate of the SSP decks can be further decreased by increasing the thickness of the top plate and decreasing the thickness of the bottom plate and the core to compensate.

Table 5.9 Local fatigue stresses at the top plate for the orthotropic bridge and the limit allowed for that weld category [MPa]

Stresses	**Max D_x**	**Min A**	**Ortho**
σ_c	71	71	71
$\sigma_{vM.top.plate}$	62	54	29
σ_{yf}	71	54	23
σ_{xf}	31	9	13

The stresses for Min A are lower than Max Dx because the corrugation pitch is shorter for this configuration which causes the wheel load to touch on more corrugations.

5.7 Buckling Analysis

A linear buckling analysis was conducted for the bridges for load case 1 which was the most critical load position to determine the critical buckling modes and load factor λ. The buckling modes indicate where the bridges will buckle and the load factor will show the ratio of applied load that will cause buckling.

For all the three bridge models the first buckling mode was at the main girder over the support, see Figure 5.12. This is a shear buckling failure in the main girder. The bridge models Max D_x and Min A have similar load factors of 3.7 and 3.6 respectively, which are satisfactory results in a buckling point of view. The load factor for the orthotropic bridge model was 1.9. This result is sufficient, however not as good as the other two models.

Table 5.10 Load factor lambda for each bridge model

	Max D_x	**Min A**	**Ortho**
Load factor λ	3.7	3.6	1.9

A non-linear buckling analysis needs to be conducted to obtain the real behaviour of the bridge models, where the material and geometric nonlinearities can be recorded. Nevertheless, the results obtained from the linear buckling analysis were promising, with all the models having a buckling factor $\lambda > 1$. Therefore a non-linear buckling analysis was not conducted in this report.

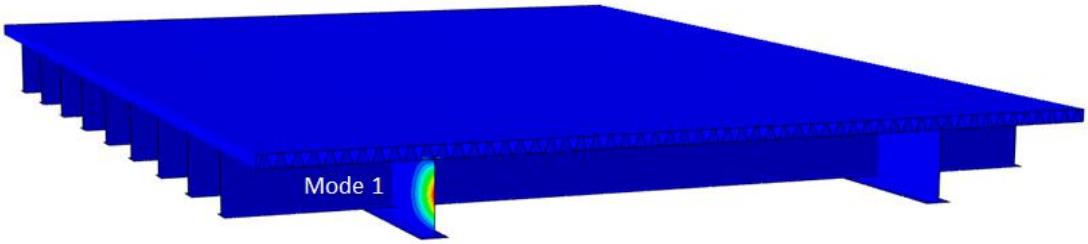

Figure 5.12 Illustration of the buckling mode 1 in the main girder

It is worth mentioning that in reality extra stiffeners are placed over the support of the main girders to avoid shear buckling at these positions. In the three bridge models no such stiffeners were placed and therefore resulting in the location of the first buckling mode at the end of one of the main girder. If stiffeners would have been placed at these locations another buckling mode would have been obtained somewhere in the bridge.

5.8 Further weight optimization

In this chapter an attempt to further optimize one of the two models with regards to decreasing the weight of the bridge is performed. This leads to an indication of the material savings that can be predicted which directly leads to cost savings for manufacturers.

The stresses for Max Dx and Min A are similar and quite low according to the stress data obtained in Table 5.6. In respect to the low stresses, improvements can be made to the dimensions of the two models so that the stresses are closer to the design values.

The model Min A was ideally chosen to further optimize because its total weight is already lighter than the orthotropic deck (10% lighter), local and global stresses are similar to Max D_x, and because it has lower fatigue stresses. It is worth mentioning that even though the deck of Min A was optimized with respect to weight which gave a weight reduction of 23% the total weight of the bridge will be higher. This is due to the area of the transverse girders for the orthotropic bridge being larger than the ones at Min A since they are directly welded to the top plate of the orthotropic deck.

A reduction in weight has already been achieved from decreasing the height of the main girders and the transverse girders of the models with the SSP deck to make sure that they are the same height as the orthotropic model as illustrated in Figure 5.1.

First the thickness of the bottom flange of the main girders was decreased from 60mm to 30mm, since the maximum stresses at the main girder were quite low for Min A. Secondly the dimensions of the cross section of the deck were changed so that the core and the two plates are utilized as much as possible while still keeping the same area of the deck cross-section. Thirdly, every other transverse girder was removed from the bridge since the stresses and the deflections of the transverse girders were quite low, see Figure 5.13.

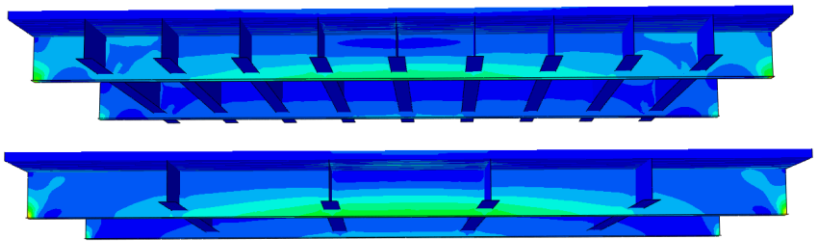

Figure 5.13 Illustration of Min A showing the girders that were removed for further optimization

The thickness of the top plate was increased to lower the local stresses while the thickness of the core and bottom plate was decreased to compensate for the change to the top plate. The new dimensions are given below in Table 5.11.

Table 5.11 Old and new thicknesses of the core and top and bottom plate of the deck for the optimization of Min A, [mm]

Thickness	**Min A**	**New Min A**
$t_{f.top}$	6.5	10.1
t_c	5.9	4
$t_{f.bot}$	5.7	4

The results from the new Min A were promising in that the stresses did not exceed the yield stress of the steel and the deflections were under their respective limits. The bridge was optimized until the maximum deflection of the secondary girders was close to the limit which was 44.5mm.

The distribution of the global stresses in the x-direction at the section where the main girder is located is given in Figure 5.14 for the two cases. It can be seen from the figure that the normal stresses in the main girder and the top plate are larger than the original and the stresses at the bottom plate have increased while the stresses at the top plate have decreased. This is expected since the thickness of the top plate is higher and the thickness of the bottom plate is lower. Local stresses at the top and bottom plate were slightly decreased and increased respectively, nevertheless they were still small to be of any concern.

Buckling of the new model was also checked and the results gave a buckling factor λ of 2.6 which is satisfactory.

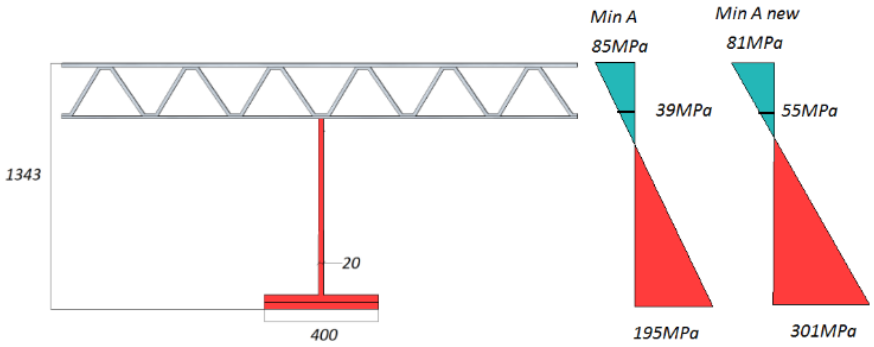

Figure 5.14 Illustration of the bending stresses at the main girder cross section of the bridge for Min A (left) and New Min A (right)

As a result of the changes to Min A the total weight of the final bridge structure is 44% lighter than the orthotropic one, that's an increase of 34% from the old Min A. This could be very attractive to manufacturers since the main interest is to reduce the overall weight of movable bridges without sacrificing bearing capacity.

6 Discussion

The optimization analysis of the SSP bridge deck enabled us to understand the bending stiffness and the weight reduction that was capable to be achieved. In order for the optimization to be improved other stiffness properties like shear and torsional stiffness could be optimized simultaneously to obtain a more optimal bridge deck.

In the FEM analysis the bridge Min A was chosen for the further study in regards to maximum utilization of the structural elements and further weight reduction. If the bridge model Max D_x was chosen, more weight reduction could have been achieved since it had better stiffness.

Furthermore a global fatigue analysis on the bridges was not performed because the most critical part of the bridge was at the connection of the top plate to the core for the SSP deck according to Bright & Smith (2004) and the top plate to the ribs for the orthotropic deck according to Ya et al., (2011). Therefore, the local effect of fatigue loads was studied instead.

7 Concluding remarks

In this thesis a thorough literature study was performed on the concept of the SSP deck for bridge design to understand its viability as a replacement for the orthotropic steel deck which is mostly used today. An optimization analysis was conducted on the structural performance of the SSP deck and compared with that of an existing orthotropic deck with the help of Abaqus/CAE.

Conclusions that were achieved from this thesis are:

- The results from the optimization analysis indicated that steel sandwich panels can be optimized to have increased stiffness relative to the weight or decreased weight relative to the stiffness of a conventional steel orthotropic panel.
- Results from FEM analysis provided the largest effective flange width for the bridge with the stiffer SSP deck and the smallest effective width for the orthotropic bridge. The larger the effective width the stiffer the bridge is, hence lowering overall stresses and deflections as shown in the FEM results for both SSP bridges. It can be concluded that the orthotropic deck was not utilized very efficiently.
- Local fatigue stresses were recorded under the wheel load to observe if stress values at the connection of core to top plate exceeded reference values according to that weld category class. Results showed that fatigue stresses were low in the stiffener to top plate connection in all three bridges models. The governing factor that influences the fatigue stresses at these details is the thickness of the plate and the length of the corrugation pitch.
- A significant weight reduction was achieved for the bridge with the steel sandwich deck. This is very attractive to manufacturers since the goal is to reduce the weight of movable bridges.

It can be concluded that a steel sandwich bridge deck can replace a conventional orthotropic deck in movable steel bridges. This is proven from the conclusions derived from the results which are given above also from the literature study and interviews conducted with manufactures.

7.1 Recommendations for future studies

In this report focus was kept mainly on optimizing the structural performance of the SSP bridge deck with relation to existing orthotropic steel deck, hence there is a great amount of research which can be conducted on other aspects of the structure.

One aspect worth studying that was not covered at all in this report is the energy efficiency of a steel sandwich panel. SSPs are known to have great shock absorbing capabilities from field tests performed on SSP walls for military purposes (Kenno Tech). This could be of interest to the structural engineering industry in studying how the structural integrity of a SSP deck bridge would be influenced during collision.

Another subject that could be further analysed is a detailed cost analysis of producing a steel sandwich panel deck from start to finish and a life cycle cost analysis. One example is savings can be achieved because the production of SSPs is often

automated, hence there is little need for manual work. In contrast equipment costs can be considerably higher than conventional equipment. Therefore a detailed cost analysis could be very useful to obtain an overall picture of the costs involved. A life cycle analysis should also be performed to understand how the influencing factors like corrosion, increasing traffic loads, influence the design life of the SSP deck.

Connections between panel to panel and panel to superstructure were mentioned briefly in this report. It is known that these details are crucial in making the structure work as a whole, so that the loads are efficiently distributed to the load bearing members. It was briefly mentioned in the report that these details can cause high stress concentration which would lead to a fail mechanism. An in depth study should be performed on the connections of panels in a SSP bridge to come to the best possible solution to this phenomenon.

In this thesis the deck was placed so that the corrugation of the core was parallel to the main girders. This was done because a comparison needed to be conducted between the concept of the SSP deck and an orthotropic steel deck. In the existing orthotropic bridge the main girders are also placed parallel to the longitudinal direction of the closed ribs. If the deck was placed in the direction where the main girders were perpendicular to the corrugation the structure would have a different behaviour. Further work could touch on this subject and study the weight reduction that can be achieved with this setup.

8 Bibliography

Abbott, S., Caccese, V., Thompson, L., Blomquist, P., & Hansen, E. (2007). *Automated Laser Welded High Performance Steel Sandwich Bridge Deck Development.* Maine: PLSystems.

Alwan, U., & Järve, D. (2012). *New Concept for Industrial Bridge Construction.* Göteborg: Chalmers University of Technology.

Aslanar, S. (2006). The effect of nucleus size on mechanical properties in electrical resistance spot welding of sheets used in automotive industry. *Materials and Design* , 125-131.

Backer, H. D., Outtier, A., & Bogaert, P. V. (2008). Analytical calculation of internal forces in orthotropic plated bridge decks based on the slope-deflection method. *Journal of Constructional Steel Research*, 1530-1539.

Biagi, R., & Bart-Smith, H. (2012). In-plane column response of metallic corrugated core sandwich panels. *International Journal of Solids and Structures*, 3901-3914.

Bright, S. R., & Smith, J. W. (2004). Fatigue performance of laser-welded steel bridge decks. *The Structural Engineer* , 31-39.

Caccese, V., & Yorulmaz, S. (2009). *Laser Welded Steel Sandwich Panel Bridge Deck Development: Finite Element Analysis and Stake Weld Strength Tests.* Maine: University of Maine.

Caccese, V., Blomquist, P., Berube, K., Webber, S., & Orozco, N. (2006). Effect of weld geometric profile on fatigue life of cruciform welds made by laser/GMAW processes. *Marine Structures*, 1-22.

Chang, W.-S., Ventsel, E., Krauthammer, T., & John, J. (2005). Bending behavior of corrugated-core sandwich plates. *Composite Structures* , 81-89.

Collin, P., & Lundmark, T. (2002). *Competitive Swedish composite bridges.* Zürich: International Association for Bridge and Structural Engineering.

Defalco, J. (2007). Practical Applications for Hybrid Laser Welding. *Welding* , 1-5.

DP, K. (2002). *Fatigue strength of HSLA-65 weldments.*

Egerland, S., Kammerhuber, C., & Staufer, H. (2013). *Applying the Solid State Laser-GMA Hybrid Process for Single- Sided Full Penetration Welding of Bulb Bar Profiles in Shipbuilding.* Austria: Fronius International GmBH.

EN 1993-1-9. (1993). *Eurocode 3: Design of steel structures - Part 1-9: Fatigue.*

ESAB . (2010). *Joint Specifications for Hybrid Laser Arc Welding Applications.*

European Standards. (2010). *EN 10029 Hot-rolled steel plates 3 mm thick or above - Tolerances on dimensions and shape.* Eurocode.

Everlast. (n.d.). *Arc Welding Pros and Cons*. Retrieved January 29, 2014, from Everlast web site: http://www.everlastgenerators.com/arc-welding-process.php

Finnås, A. (2014, February 10). Stainless Steel . (E. Beneus, & I. Koc, Interviewers)

Frank, D., Romanoff, J., & Remes, H. (2012). Fatigue strength assessment of laser stake-welded web-core steel sandwich panels. *Fatigue & Fracture of Engineering Materials & Structures* , 724-737.

Frauser, H. (2014, Marh 4). Hybrid Laser Arc Welding. (E. Beneus, & I. Koc, Interviewers)

Fryba, L., & Urushadze, S. (2011). Improvement of fatigue properties of orthotropic decks. *Engineering Structures* , 1166-1169.

Fung, T. C., Tan, K. H., & Lok, T. S. (1996). Shear Stiffness DQy For C-Core Sandwich Panels. *Journal of Structural Engineering*, 958-966.

Harris, D. K. (2007). *Lateral Load Distribution and Deck Design Recommendations for the Sandwich Plate System (SPS) in Bridge Applications* . Virginia: Virginia Polytechnic Institute and State University.

Hechler, O., & Collin, P. (2008). *On the use of duplex stainless steels in bridge construction.* European Commission .

Hoffman, D., Dahle, K., & Fiser, D. (2011). Gas Metal Arc Welding. *Welding*, 74-130.

Jelovica, J., Romanoff, J., Ehlers, S., & Remes, H. (2011). *Ultimate strength tests of corroded web-core and corrugated-core sandwich beams.* Espoo, Finland: School of Engineering.

Kaplan, A. (2014, March 4). Hybrid Laser Arc Welding. (E. Beneus, & I. Koc, Interviewers)

Kenno Tech. (n.d.). Retrieved May 29, 2014, from Kenno Tech Web Site: www.kennotech.fi

Kozak, J. (2005). Strength tests of steel sandwich panel. *Maritime Transportaton and Exploitation of Ocean and Coastal Resources* , 471-476.

Kozak, J. (2009). Selected problems on application of steel sandwich panels to marine structures. *Polish Maritime Research*, 9-15.

Kujala, P., & Klanac, A. (2002). Analytical and numerical analysis of non-symmetrical all steel sandwich panels under uniform pressure load. *International Design Conference* , 1205-1210.

Kujala, P., & Klanac, A. (2005). *Steel Sandwich Panels in Marine Applications.* Espoo, Finlad: Ship Laboratory, Helsinki University of Technology.

Libove, C., & Hubka, R. E. (1951). *Elastic constants for corrugated-core sandwich plates.* Virginia: National Technical Information Service .

Lok, T., & Cheng, Q. (1999). Elastic Deflection of Thin-Walled Sandwich Panel. *Journal of Sandwich Structures and Materials*, 1-279.

Mara, V. (2014). *Fiber reinforced polymer bridge decks: Sustainability and a novel panel – level connection.* Göteborg, Sweden: Chalmers University of Technology.

Mara, V. (2014). *Fibre reinforced polymer bridge decks: Sustainability and a novel panel-level connection* . Gothenburg: Chalmers University of Technology .

Mizuguchi, K. (2004). Rationalized Steel Deck Structure and Large Model Test for Developing New Type of Structure. *Proc., Int. Orthotropic Bridge Conf*, 675-688.

Munse WH, W. T. (1983). *Fatigue characterization of fabricated ship details for design.* Springfield: Ship Structure Committee.

Ono, S., Hirabayashi, Y., Shimozato, T., Inaba, N., Murano, M., & Miki, C. (2009). Fatigue Properties and Retrofitting of Existing Orthotropic Steel Bridge Decks. *Journal of JSCE*, 335-347.

Poirier, J. D., Vel, S. S., & Caccese, V. (2013). Multi-objective optimization of laser-welded steel sandwich panels for static loads using a genetic algorithm. *Engineering Structures*, 508-524.

Romanoff, J., & Varsta, P. (2006). Bending response of web-core sandwich beams. *Composite Structures*, 478-487.

SS-EN 1990/A1:2005. (2006). *Eurocode - Basis of structural design.*

SS-EN 1991-2. (2003). *Eurocode 1: Actions on structures - Part 2: Traffic loads on bridges.*

Standardization, European Committee for. (2005). *Eurocode 3: Design of steel structures - part 1-1: General rules and rules for buildings.* Brussels: CEN.

Stridh, L. E. (2014, March 04). On costs of hybrid laser-arc welding. (E. Beneus, & I. Koc, Interviewers)

Swedish Transport Agency. (n.d.). *Road: Swedish Transport Agency*. Retrieved March 4, 2014, from Swedish Transport Agency web site: http://www.transportstyrelsen.se/en/

Säynäjäkangas, J., & Taulavuori, T. (2004). *A review in design and manufacturing of stainless steel sandwich panels.* Finland: Outokumpu Stainless Oy.

TRVFS. (2011:12). *Trafikverkets författningssamling.*

TRVK Bro 11. (2011). *Trafikverkets tekniska krav Bro.*

U.S. Department of Transportation. (2012). Steel bridge design handbook: Bridge deck design. *Federal Highway Administration*, 1-52.

Wang, H.-X., & Chung, S. W. (2011). Equivalent Elastic Constants of Truss Core Sandwich Plates. *Journal of Pressure Vessel Technology*, 6.

Wolchuck, R. (1963). *Design manual for orthotropic steel plate deck bridges.* New York: American Institute of Steel Construction.

Xiao, Z. G., Yamada, K., Ya, S., & Zhao, X. L. (2008). Stress Analyses and Fatigue Evaluation of Rib-to-Deck Joints in Steel Orthotropic Decks. *International Journal of Fatigue* , 1387-1397.

Ya, S., & Yamada, K. (2008). Fatigue Durability Evaluation of Trough to Deck Plate Welded Joint of Orthotropic Steel Deck. *Journal of JSCE*, 603-616.

Ya, S., Kentaro, Y., & Toshiyuki, I. (2011). Fatigue Evaluation of Rib-to-Deck Welded Joints of Orthotropic Steel Bridge Deck. *Journal of Bridge Engineering*, 492-499.

Zou, B., Chen, A., F. Davalos, J., & A. Salim, H. (2011). Evaluation of effective flange width by shear lag model for orthotropic FRP bridge decks. *Compostie Structures*, 474-482.

APPENDIX A

Below are calculations of an orthotropic bridge deck for an existing bridge today. Calculations that are performed are the area per unit width of the cross section of the deck, the moment of inertia per unit width, bending stiffness, and the effective width of the flange. The bridge is considered to be simply supported on both ends.

Orthotropic Plate (Trafikverket)

Initial Data

Dimensions

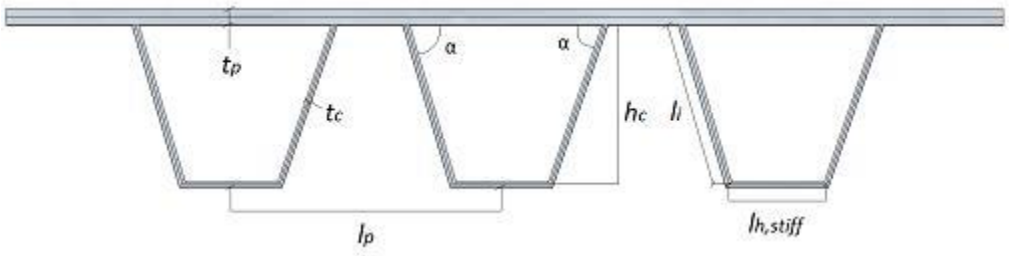

Length between stiffener legs at welded connection

$l_{leg.con} := 368mm$

Tickness of the top plate

$t_{p.ortho} := 16mm$

Thickness of the stiffener

$t_{c.ortho} := 12mm$

Angle for the incline stiffener

$$\alpha_{stiff} := \operatorname{atan}\left(\frac{2}{1}\right) = 63.435 \cdot deg$$

Length of the top plate

$$l_p := 0.5m$$

Distance between stiffeners

$$l_{spac} := 132mm$$

Length for the horizontal stiffener

$$l_{h.stiff} := 188mm - 16.97mm = 0.171\,m$$

Height of the girders

$$h_{c.ortho} := 179mm$$

Length of the incline stiffener

$$l_{i.stiff} := \frac{h_{c.ortho}}{\sin(\alpha_{stiff})} = 0.2\,m$$

Height of the deck

$$h_{ortho} := h_{c.ortho} + t_{p.ortho} + \frac{t_{c.ortho}}{2} = 0.201\,m$$

Material Properties

$$\nu := 0.3$$

Poisson's ratio

$$\rho_{S355N} := 7850\,\frac{kg}{m^3}$$

Density of steel

$$E_{S355N} := 210GPa$$

Modulus of elasticity

$$G_c := \frac{E_{S355N}}{2\cdot(1+\nu)} = 80.769\cdot GPa$$

Shear modulus of elasticity

$$f_y := 355MPa$$

Yielding strength

Areas

Area of the top plate

$$A_{top} := l_p \cdot t_{p.ortho} = 8\times 10^{-3}\,m^2$$

Area of the incline stiffener element

$$A_{i.stiff} := 2\cdot\left(t_{c.ortho}\cdot l_{i.stiff}\right) = 4.803\times 10^{-3}\,m^2$$

Area of bottom part of the stiffener

$$A_{h.stiff} := \left(t_{c.ortho}\cdot l_{h.stiff}\right) = 2.052\times 10^{-3}\,m^2$$

Total area of the orthotropic plate

$$A_{tot.ortho} := A_{top} + A_{i.stiff} + A_{h.stiff} = 0.015\,m^2$$

Area of the core

$$A_{c.ortho} := A_{i.stiff} + A_{h.stiff} = 6.855 \times 10^{-3}\,m^2$$

Total weight of the section

$$A_{ortho} := \frac{A_{tot.ortho}}{l_p} = 0.03\,\frac{1}{m}\cdot m^2$$

$$G_{ortho} := A_{ortho}\cdot \rho_{S355N} = 233.23\,\frac{kg}{m^2}$$

Calculating the neutral axis

$$z_{na.ortho} := \frac{A_{top}\cdot\frac{t_{p.ortho}}{2} + A_{i.stiff}\cdot\left(\frac{h_{c.ortho}}{2} + t_{p.ortho}\right) + A_{h.stiff}\cdot\left(h_{c.ortho} + t_{p.ortho}\right)}{A_{tot.ortho}} = 0.065\,m$$

Moment of Inertia

Moment of Inertia for bottom part of stiffeners

X direction

$$I_{h.stiff.x} := \frac{l_{h.stiff}\cdot t_{c.ortho}^{3}}{12} + A_{h.stiff}\cdot\left(t_{p.ortho} + h_{c.ortho} - z_{na.ortho}\right)^2 = 3.452 \times 10^{-5}\,m^4$$

Moment of Inertia for inclined part of stiffeners

$$I_{i.stiff.x} := \frac{2 \cdot t_{c.ortho} \cdot l_{i.stiff}^{3}}{12} \cdot \sin(\alpha_{stiff})^2 \ldots = 2.305 \times 10^{-5}\,m^4$$

$$+ A_{i.stiff} \cdot \left(\frac{h_{c.ortho}}{2} + t_{p.ortho} + \frac{t_{c.ortho}}{2} - z_{na.ortho} \right)^2$$

Moment of Inertia of the top plate

$$I_{top.x} := \frac{l_p \cdot t_{p.ortho}^{3}}{12} + A_{top} \cdot \left(z_{na.ortho} - \frac{t_{p.ortho}}{2} \right)^2 = 2.649 \times 10^{-5}\,m^4$$

Total Moment of Inertia

$$I_{tot.ortho.x} := I_{h.stiff.x} + I_{i.stiff.x} + I_{top.x} = 8.406 \times 10^{-5}\,m^4$$

$$I_{ortho.x} := \frac{I_{tot.ortho.x}}{l_p} = 1.681 \times 10^{-4} \cdot m^3$$

Y direction

$$I_{tot.ortho.y} := \frac{l_p \cdot t_{p.ortho}^{3}}{12} + A_{top} \cdot \left(z_{na.ortho} - \frac{t_{p.ortho}}{2} \right)^2 = 2.649 \times 10^{-5}\,m^4$$

$$I_{ortho.y} := \frac{I_{tot.ortho.y}}{l_p} = 5.298 \times 10^{-5} \cdot m^3$$

Bending Stiffness per unit width [Nm]

X direction

$$D_{x.ortho} := I_{ortho.x} \cdot E_{S355N} = 3.531 \times 10^{7} \cdot N \cdot m$$

Y direction

$$D_{y.ortho} := \frac{I_{ortho.y} \cdot E_{S355N}}{1 - \nu^{2}\left(1 - \frac{I_{ortho.y} \cdot E_{S355N}}{D_{x.ortho}}\right)} = 1.186 \times 10^{7} \cdot N \cdot m$$

Torsional Rigidity per unit width [Nm]

$$D_{xy.ortho} := \sqrt{D_{x.ortho} \cdot D_{y.ortho}} = 2.046 \times 10^{7} \cdot N \cdot m$$

Axial Stiffness per unit width [N/m]

X direction

$$E_{x.ortho} := E_{S355N} \cdot A_{ortho} = 6.239 \times 10^{9} \cdot \frac{N}{m}$$

Y direction

$$E_{y.ortho} := \frac{E_{S355N} \cdot t_{p.ortho}}{1 - \nu^{2}\left(1 - \frac{E_{S355N} \cdot t_{p.ortho}}{E_{x.ortho}}\right)} = 3.506 \times 10^{9} \cdot \frac{N}{m}$$

Steel Sandwich Panel

Initial Data

Dimensional constants

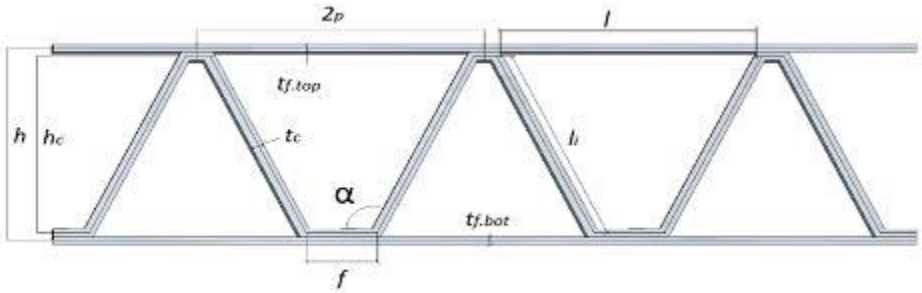

height of the cross-section

$$h_{ssp}\left(h_{c.ssp}, t_{f.top}, t_{f.bot}, t_{c.ssp}\right) := h_{c.ssp} + t_{f.top} + t_{f.bot} + t_{c.ssp}$$

length of the inclined leg of the core

$$l_{i.ssp}\left(h_{c.ssp}, \alpha_{ssp}\right) := \frac{h_{c.ssp}}{\sin\left(\alpha_{ssp}\right)}$$

length of corrugation opening

$$l_{buck}\left(h_{c.ssp}, \alpha_{ssp}, f_{ssp}\right) := 2 l_{i.ssp}\left(h_{c.ssp}, \alpha_{ssp}\right) \cdot \cos\left(\alpha_{ssp}\right) + f_{ssp}$$

half of the corrugation pitch

$$p_{ssp}\left(h_{c.ssp}, \alpha_{ssp}, f_{ssp}\right) := \frac{f_{ssp}}{2} + \frac{l_{buck}\left(h_{c.ssp}, \alpha_{ssp}, f_{ssp}\right)}{2}$$

length of cross-section

$$l_{ssp}(h_{c.ssp}, \alpha_{ssp}, f_{ssp}) := 2 \cdot p_{ssp}(h_{c.ssp}, \alpha_{ssp}, f_{ssp})$$

configurations ratios

$$hc\_tc(h_{c.ssp}, t_{c.ssp}) := \frac{h_{c.ssp}}{t_{c.ssp}}$$

$$p\_hc(h_{c.ssp}, \alpha_{ssp}, f_{ssp}) := \frac{p_{ssp}(h_{c.ssp}, \alpha_{ssp}, f_{ssp})}{h_{c.ssp}}$$

Areas

Area of top flanges

$$A_{f.top}(t_{f.top}, h_{c.ssp}, \alpha_{ssp}, f_{ssp}) := t_{f.top} \cdot l_{ssp}(h_{c.ssp}, \alpha_{ssp}, f_{ssp})$$

Area of bottom flange

$$A_{f.bot}(t_{f.bot}, h_{c.ssp}, \alpha_{ssp}, f_{ssp}) := t_{f.bot} \cdot l_{ssp}(h_{c.ssp}, \alpha_{ssp}, f_{ssp})$$

Area of the core

$$A_{c.ssp}(t_{c.ssp}, h_{c.ssp}, \alpha_{ssp}, f_{ssp}) := 2 \cdot f_{ssp} \cdot t_{c.ssp} + 2 \cdot t_{c.ssp} \cdot l_{i.ssp}(h_{c.ssp}, \alpha_{ssp})$$

Total Area

$$A_{tot.ssp}(h_{c.ssp}, t_{f.top}, t_{f.bot}, t_{c.ssp}, \alpha_{ssp}, f_{ssp}) := A_{f.top}(t_{f.top}, h_{c.ssp}, \alpha_{ssp}, f_{ssp}) \ldots + A_{f.bot}(t_{f.bot}, h_{c.ssp}, \alpha_{ssp}, f_{ssp}) \ldots + A_{c.ssp}(t_{c.ssp}, h_{c.ssp}, \alpha_{ssp}, f_{ssp})$$

Total area per unit width [m]

$$A_{ssp}(h_{c.ssp}, t_{f.top}, t_{f.bot}, t_{c.ssp}, \alpha_{ssp}, f_{ssp}) := \frac{A_{tot.ssp}(h_{c.ssp}, t_{f.top}, t_{f.bot}, t_{c.ssp}, \alpha_{ssp}, f_{ssp})}{l_{ssp}(h_{c.ssp}, \alpha_{ssp}, f_{ssp})}$$

Total weight of the section

$$G_{ssp}(h_{c.ssp}, t_{f.top}, t_{f.bot}, t_{c.ssp}, \alpha_{ssp}, f_{ssp}) := A_{ssp}(h_{c.ssp}, t_{f.top}, t_{f.bot}, t_{c.ssp}, \alpha_{ssp}, f_{ssp}) \cdot \rho_{S355N}$$

Neutral Axis

$$z_{na.ssp}(h_{c.ssp}, t_{f.top}, t_{f.bot}, t_{c.ssp}, \alpha_{ssp}, f_{ssp}) := \frac{\left[\begin{array}{l} A_{f.top}(t_{f.top}, h_{c.ssp}, \alpha_{ssp}, f_{ssp}) \cdot \frac{t_{f.top}}{2} + t_{c.ssp} \cdot f_{ssp} \cdot \left(t_{f.top} + \frac{t_{c.ssp}}{2}\right) \dots \\ + 2 \cdot t_{c.ssp} \cdot l_{i.ssp}(h_{c.ssp}, \alpha_{ssp}) \cdot \left(\frac{h_{c.ssp}}{2} + t_{f.top} + \frac{t_{c.ssp}}{2}\right) \dots \\ + t_{c.ssp} \cdot f_{ssp} \cdot \left(t_{f.top} + \frac{t_{c.ssp}}{2} + h_{c.ssp}\right) \dots \\ + A_{f.bot}(t_{f.bot}, h_{c.ssp}, \alpha_{ssp}, f_{ssp}) \cdot \left(\frac{t_{f.top}}{2} + h_{ssp}(h_{c.ssp}, t_{f.top}, t_{f.bot}, t_{c.ssp})\right) \end{array}\right]}{A_{tot.ssp}(h_{c.ssp}, t_{f.top}, t_{f.bot}, t_{c.ssp}, \alpha_{ssp}, f_{ssp})}$$

Moment of Inertia

X direction

moment of Inertia for the top flange

$$I_{f.top.ssp.x}(h_{c.ssp}, t_{f.top}, t_{f.bot}, t_{c.ssp}, \alpha_{ssp}, f_{ssp}) := \frac{l_{ssp}(h_{c.ssp}, \alpha_{ssp}, f_{ssp}) \cdot t_{f.top}^{3}}{12} \dots + l_{ssp}(h_{c.ssp}, \alpha_{ssp}, f_{ssp}) \cdot t_{f.top} \cdot \left(z_{na.ssp}(h_{c.ssp}, t_{f.top}, t_{f.bot}, t_{c.ssp}, \alpha_{ssp}, f_{ssp}) - \frac{t_{f.top}}{2}\right)^{2}$$

moment of inertia for the top horisontal part of the core

$$I_{c.top.ssp.x}\left(h_{c.ssp}, t_{f.top}, t_{f.bot}, t_{c.ssp}, \alpha_{ssp}, f_{ssp}\right) := \frac{f_{ssp} \cdot t_{c.ssp}^{3}}{12} \ldots + f_{ssp} \cdot t_{c.ssp} \cdot \left(z_{na.ssp}\left(h_{c.ssp}, t_{f.top}, t_{f.bot}, t_{c.ssp}, \alpha_{ssp}, f_{ssp}\right) - t_{f.top} - \frac{t_{c.ssp}}{2} \right)^{2}$$

moment of inertia for the inclined part of the core

$$I_{inc.ssp.x}\left(h_{c.ssp}, t_{f.top}, t_{f.bot}, t_{c.ssp}, \alpha_{ssp}, f_{ssp}\right) := 2 \cdot \frac{t_{c.ssp} \cdot l_{i.ssp}\left(h_{c.ssp}, \alpha_{ssp}\right)^{3}}{12} \cdot \sin\left(\alpha_{ssp}\right)^{2} \ldots + 2 t_{c.ssp} \cdot l_{i.ssp}\left(h_{c.ssp}, \alpha_{ssp}\right) \cdot \left(\begin{array}{l} t_{f.top} + \frac{t_{c.ssp}}{2} + \frac{h_{c.ssp}}{2} \ldots \\ + -z_{na.ssp}\left(h_{c.ssp}, t_{f.top}, t_{f.bot}, t_{c.ssp}, \alpha_{ssp}, f_{ssp}\right) \end{array} \right)^{2}$$

moment of inertia for the bottom part of the core

$$I_{c.bot.ssp.x}\left(h_{c.ssp}, t_{f.top}, t_{f.bot}, t_{c.ssp}, \alpha_{ssp}, f_{ssp}\right) := \frac{f_{ssp} \cdot t_{c.ssp}^{3}}{12} \ldots + f_{ssp} \cdot t_{c.ssp} \cdot \left(t_{f.top} + \frac{t_{c.ssp}}{2} + h_{c.ssp} - z_{na.ssp}\left(h_{c.ssp}, t_{f.top}, t_{f.bot}, t_{c.ssp}, \alpha_{ssp}, f_{ssp}\right) \right)^{2}$$

moment of inertia for the bottom flange

$$I_{f.bot.ssp.x}\left(h_{c.ssp}, t_{f.top}, t_{f.bot}, t_{c.ssp}, \alpha_{ssp}, f_{ssp}\right) := \frac{l_{ssp}\left(h_{c.ssp}, \alpha_{ssp}, f_{ssp}\right) \cdot t_{f.bot}^{3}}{12} \ldots + l_{ssp}\left(h_{c.ssp}, \alpha_{ssp}, f_{ssp}\right) \cdot t_{f.bot} \cdot \left(\begin{array}{l} \frac{t_{f.top}}{2} + h_{ssp}\left(h_{c.ssp}, t_{f.top}, t_{f.bot}, t_{c.ssp}\right) \ldots \\ + -z_{na.ssp}\left(h_{c.ssp}, t_{f.top}, t_{f.bot}, t_{c.ssp}, \alpha_{ssp}, f_{ssp}\right) \end{array} \right)^{2}$$

Total moment of inertia for SSP in x direction

$$I_{tot.ssp.x}(h_{c.ssp}, t_{f.top}, t_{f.bot}, t_{c.ssp}, \alpha_{ssp}, f_{ssp}) := I_{f.top.ssp.x}(h_{c.ssp}, t_{f.top}, t_{f.bot}, t_{c.ssp}, \alpha_{ssp}, f_{ssp}) \ldots + I_{c.top.ssp.x}(h_{c.ssp}, t_{f.top}, t_{f.bot}, t_{c.ssp}, \alpha_{ssp}, f_{ssp}) \ldots + I_{inc.ssp.x}(h_{c.ssp}, t_{f.top}, t_{f.bot}, t_{c.ssp}, \alpha_{ssp}, f_{ssp}) \ldots + I_{c.bot.ssp.x}(h_{c.ssp}, t_{f.top}, t_{f.bot}, t_{c.ssp}, \alpha_{ssp}, f_{ssp}) \ldots + I_{f.bot.ssp.x}(h_{c.ssp}, t_{f.top}, t_{f.bot}, t_{c.ssp}, \alpha_{ssp}, f_{ssp})$$

Y direction

moment of inertia for the top flange in y direction

$$I_{f.top.ssp.y}(h_{c.ssp}, t_{f.top}, t_{f.bot}, t_{c.ssp}, \alpha_{ssp}, f_{ssp}) := \frac{1_{ssp}(h_{c.ssp}, \alpha_{ssp}, f_{ssp}) \cdot t_{f.top}^{3}}{12} \ldots + 1_{ssp}(h_{c.ssp}, \alpha_{ssp}, f_{ssp}) \cdot t_{f.top} \cdot \left(z_{na.ssp}(h_{c.ssp}, t_{f.top}, t_{f.bot}, t_{c.ssp}, \alpha_{ssp}, f_{ssp}) - \frac{t_{f.top}}{2} \right)^{2}$$

moment of inertia for the bottom flange in y direction

$$I_{f.bot.ssp.y}(h_{c.ssp}, t_{f.top}, t_{f.bot}, t_{c.ssp}, \alpha_{ssp}, f_{ssp}) := \frac{1_{ssp}(h_{c.ssp}, \alpha_{ssp}, f_{ssp}) \cdot t_{f.bot}^{3}}{12} \ldots + 1_{ssp}(h_{c.ssp}, \alpha_{ssp}, f_{ssp}) \cdot t_{f.bot} \cdot \left(\frac{t_{f.top}}{2} + h_{ssp}(h_{c.ssp}, t_{f.top}, t_{f.bot}, t_{c.ssp}) \ldots + -z_{na.ssp}(h_{c.ssp}, t_{f.top}, t_{f.bot}, t_{c.ssp}, \alpha_{ssp}, f_{ssp}) \right)^{2}$$

Total moment of inertia for SSP in y direction

$$I_{tot.ssp.y}(h_{c.ssp}, t_{f.top}, t_{f.bot}, t_{c.ssp}, \alpha_{ssp}, f_{ssp}) := I_{f.top.ssp.y}(h_{c.ssp}, t_{f.top}, t_{f.bot}, t_{c.ssp}, \alpha_{ssp}, f_{ssp}) \ldots + I_{f.bot.ssp.y}(h_{c.ssp}, t_{f.top}, t_{f.bot}, t_{c.ssp}, \alpha_{ssp}, f_{ssp})$$

Moment of inertia in X and Y direction **per unit width** [m^3]

$$I_{ssp.x}(h_{c.ssp}, t_{f.top}, t_{f.bot}, t_{c.ssp}, \alpha_{ssp}, f_{ssp}) := \frac{I_{tot.ssp.x}(h_{c.ssp}, t_{f.top}, t_{f.bot}, t_{c.ssp}, \alpha_{ssp}, f_{ssp})}{1_{ssp}(h_{c.ssp}, \alpha_{ssp}, f_{ssp})}$$

$$I_{ssp.y}(h_{c.ssp}, t_{f.top}, t_{f.bot}, t_{c.ssp}, \alpha_{ssp}, f_{ssp}) := \frac{I_{tot.ssp.y}(h_{c.ssp}, t_{f.top}, t_{f.bot}, t_{c.ssp}, \alpha_{ssp}, f_{ssp})}{1_{ssp}(h_{c.ssp}, \alpha_{ssp}, f_{ssp})}$$

Bending Stiffness per unit width

Bending stiffness in the stiff direction per unit width

$$D_{x.ssp}(h_{c.ssp}, t_{f.top}, t_{f.bot}, t_{c.ssp}, \alpha_{ssp}, f_{ssp}) := E_{S355N} \cdot I_{ssp.x}(h_{c.ssp}, t_{f.top}, t_{f.bot}, t_{c.ssp}, \alpha_{ssp}, f_{ssp})$$

Bending stiffness in the weak direction per unit width

$$D_{y.ssp}(h_{c.ssp}, t_{f.top}, t_{f.bot}, t_{c.ssp}, \alpha_{ssp}, f_{ssp}) := \frac{E_{S355N} \cdot I_{ssp.y}(h_{c.ssp}, t_{f.top}, t_{f.bot}, t_{c.ssp}, \alpha_{ssp}, f_{ssp})}{1 - \nu^2 \left(1 - \frac{E_{S355N} \cdot I_{ssp.y}(h_{c.ssp}, t_{f.top}, t_{f.bot}, t_{c.ssp}, \alpha_{ssp}, f_{ssp})}{D_{x.ssp}(h_{c.ssp}, t_{f.top}, t_{f.bot}, t_{c.ssp}, \alpha_{ssp}, f_{ssp})}\right)}$$

Torsional Stiffness per unit width

$$D_{xy.ssp}(h_{c.ssp}, t_{f.top}, t_{f.bot}, t_{c.ssp}, \alpha_{ssp}, f_{ssp}) := 2 \cdot G_c \cdot I_{ssp.y}(h_{c.ssp}, t_{f.top}, t_{f.bot}, t_{c.ssp}, \alpha_{ssp}, f_{ssp})$$

Axial Stiffness per unit width

Axial stiffness in the stiff direction per unit width

$$E_{x.ssp}(h_{c.ssp}, t_{f.top}, t_{f.bot}, t_{c.ssp}, \alpha_{ssp}, f_{ssp}) := E_{S355N} \cdot A_{ssp}(h_{c.ssp}, t_{f.top}, t_{f.bot}, t_{c.ssp}, \alpha_{ssp}, f_{ssp})$$

Axial stiffness in the weak direction per unit width

$$E_{y.ssp}(h_{c.ssp}, t_{f.top}, t_{f.bot}, t_{c.ssp}, \alpha_{ssp}, f_{ssp}) := \frac{E_{S355N} \cdot (t_{f.top} + t_{f.bot})}{1 - \nu^2 \left[1 - \frac{E_{S355N} \cdot (t_{f.top} + t_{f.bot})}{E_{x.ssp}(h_{c.ssp}, t_{f.top}, t_{f.bot}, t_{c.ssp}, \alpha_{ssp}, f_{ssp})}\right]}$$

Horizontal shear stiffness <u>per unit width</u>

$$G_{xy}(h_{c.ssp}, t_{f.top}, t_{f.bot}, t_{c.ssp}, \alpha_{ssp}, f_{ssp}) := \frac{G_c \cdot t_{c.ssp}^2}{\frac{A_{c.ssp}(t_{c.ssp}, h_{c.ssp}, \alpha_{ssp}, f_{ssp})}{l_{ssp}(h_{c.ssp}, \alpha_{ssp}, f_{ssp})}} + G_c \cdot (t_{f.top} + t_{f.bot})$$

Transverse shear stiffness <u>per unit width</u>

transverse shear stiffness **parallel** to the corrugation

$$D_{Qx} = \frac{G_c \cdot t_{c.ssp}^2}{A_{c.ssp.x}} \cdot \left(\frac{h_{ssp}}{p_{ssp}}\right)^2$$

area, per unit width, of the corrugation cross-sectio, [m]

$$A_{c.ssp.x}(h_{c.ssp}, t_{c.ssp}, \alpha_{ssp}, f_{ssp}) := \frac{l_{i.ssp}(h_{c.ssp}, \alpha_{ssp}) \cdot t_{c.ssp}}{p_{ssp}(h_{c.ssp}, \alpha_{ssp}, f_{ssp})}$$

$$D_{Qx}(h_{c.ssp}, t_{f.top}, t_{f.bot}, t_{c.ssp}, \alpha_{ssp}, f_{ssp}) := \frac{G_c \cdot t_{c.ssp}^2}{A_{c.ssp.x}(h_{c.ssp}, t_{c.ssp}, \alpha_{ssp}, f_{ssp})} \cdot \left(\frac{h_{ssp}(h_{c.ssp}, t_{f.top}, t_{f.bot}, t_{c.ssp})}{p_{ssp}(h_{c.ssp}, \alpha_{ssp}, f_{ssp})}\right)^2$$

transverse shear stiffnes **perpendicular** to the corrugation

$$D_{Qy} = S \cdot h_{ssp} \left(\frac{E_{S355N}}{1 - \nu_c^{\,2}} \right) \left(\frac{t_c}{h_c} \right)^3$$

Nondimensional coefficient (S)

The expression for S is simplified to reflect our core shape. These simplifications are that we have a symmetrical cross section and that the the radius between the contact area of face sheets and the core is assumed to be zero. The formula was obtained from the report "Elastic Constants for Corrugated-core Sandwich Plates".

Note: It is worth mentioning that even though the cross section is not really symmterical, the value of S would not deviate much from the original value as long as the neutral axis is close to the middle of the height of the cross section.

$$S = \frac{6 \cdot \frac{h_{c.ssp}}{p_{ssp}} B_1 \cdot B_4 + \left(\frac{p_{ssp}}{h_{c.ssp}} \right)^2}{12 \left[-2 \left(\frac{p_{ssp}}{h_{c.ssp}} \right)^2 \cdot B_2 + \frac{h_{c.ssp}}{h_{ssp}} \left[6 \cdot B_4 \cdot \left(B_1 \cdot B_3 - B_2^{\,2} \right) + \left(\frac{p_{ssp}}{h_{c.ssp}} \right)^3 \cdot B_3 \right] + \frac{h_{ssp}}{h_{c.ssp}} \cdot \frac{p_{ssp}}{h_{c.ssp}} \cdot B_1 \right]}$$

where

$$B_1 = K_{Iz} + \frac{1}{12} \left(\frac{t_{c.ssp}}{h_{c.ssp}} \right)^2 \cdot K_{Lz}$$

$$B_2 = K_{Iyz} - \frac{1}{12} \left(\frac{t_{c.ssp}}{h_{c.ssp}} \right)^2 \cdot K_{Lyz}$$

$$B_3 = K_{Iy} + \frac{1}{12}\left(\frac{t_{c.ssp}}{h_{c.ssp}}\right)^2 \cdot K_{Ly}$$

$$B_4 = \left(\frac{t_{f.ssp}}{t_{c.ssp}}\right)^3$$

where

$$K_{Iz} = \frac{2}{3}\left(\frac{k_1}{h_{c.ssp}}\right)^2 \cdot \frac{d_1}{h_{c.ssp}} + \frac{2}{3}\left[\frac{1}{8}\left(\frac{p_{ssp}}{h_{c.ssp}}\right)^3 - \left(\frac{b_1}{h_{c.ssp}}\right)^3\right]$$

$$K_{Iyz} = \frac{2}{3} \cdot \frac{j_1}{h_{c.ssp}} \cdot \frac{k_1}{h_{c.ssp}} \cdot \frac{d_1}{h_{c.ssp}} + \frac{1}{2}\left[\frac{1}{4}\left(\frac{p_{ssp}}{h_{c.ssp}}\right)^2 - \left(\frac{b_1}{h_{c.ssp}}\right)^2\right]$$

$$K_{Iy} = \frac{2}{3}\left(\frac{j_1}{h_{c.ssp}}\right)^2 \cdot \frac{d_1}{h_c} + \frac{1}{4} \cdot \frac{f_{ssp}}{h_{c.ssp}}$$

$$K_{Lz} = 2 \cdot \frac{d_1}{h_{c.ssp} \cdot \sin(\alpha_{ssp})^2}$$

$$K_{Lyz} = 2 \cdot \frac{d_1}{h_{c.ssp}} \cdot \sin(\alpha_{ssp}) \cdot \cos(\alpha_{ssp})$$

$$K_{Ly} = \frac{f_{ssp}}{h_{c.ssp}} + 2 \cdot \frac{d_1}{h_{c.ssp}} \cdot \cos(\alpha)^2$$

where

$$d_1(h_{c.ssp},\alpha_{ssp}) := \frac{l_{i.ssp}(h_{c.ssp},\alpha_{ssp})}{2}$$

$$k_1(h_{c.ssp},\alpha_{ssp}) := d_1(h_{c.ssp},\alpha_{ssp})\cdot\cos(\alpha_{ssp})$$

$$b_1(h_{c.ssp},\alpha_{ssp}) := k_1(h_{c.ssp},\alpha_{ssp})$$

$$j_1(h_{c.ssp}) := \frac{h_{c.ssp}}{2}$$

$$a_1(h_{c.ssp}) := j_1(h_{c.ssp})$$

thus

$$K_{Iz}(h_{c.ssp},\alpha_{ssp},f_{ssp}) := \frac{2}{3}\left(\frac{k_1(h_{c.ssp},\alpha_{ssp})}{h_{c.ssp}}\right)^2\cdot\frac{d_1(h_{c.ssp},\alpha_{ssp})}{h_{c.ssp}} + \frac{2}{3}\left[\frac{1}{8}\left(\frac{p_{ssp}(h_{c.ssp},\alpha_{ssp},f_{ssp})}{h_{c.ssp}}\right)^3 - \left(\frac{b_1(h_{c.ssp},\alpha_{ssp})}{h_{c.ssp}}\right)^3\right]$$

$$K_{Iyz}(h_{c.ssp},\alpha_{ssp},f_{ssp}) := \frac{2}{3}\cdot\frac{j_1(h_{c.ssp})}{h_{c.ssp}}\cdot\frac{k_1(h_{c.ssp},\alpha_{ssp})}{h_{c.ssp}}\cdot\frac{d_1(h_{c.ssp},\alpha_{ssp})}{h_{c.ssp}} + \frac{1}{2}\left[\frac{1}{4}\left(\frac{p_{ssp}(h_{c.ssp},\alpha_{ssp},f_{ssp})}{h_{c.ssp}}\right)^2 - \left(\frac{b_1(h_{c.ssp},\alpha_{ssp})}{h_{c.ssp}}\right)^2\right]$$

$$K_{Iy}(h_{c.ssp},\alpha_{ssp},f_{ssp}) := \frac{2}{3}\left(\frac{j_1(h_{c.ssp})}{h_{c.ssp}}\right)^2\cdot\frac{d_1(h_{c.ssp},\alpha_{ssp})}{h_{c.ssp}} + \frac{1}{4}\cdot\frac{f_{ssp}}{h_{c.ssp}}$$

$$K_{Lz}(h_{c.ssp},\alpha_{ssp}) := 2\cdot\frac{d_1(h_{c.ssp},\alpha_{ssp})}{h_{c.ssp}\cdot\sin(\alpha_{ssp})^2}$$

$$K_{Lyz}(h_{c.ssp},\alpha_{ssp}) := 2\cdot\frac{d_1(h_{c.ssp},\alpha_{ssp})}{h_{c.ssp}}\cdot\sin(\alpha_{ssp})\cdot\cos(\alpha_{ssp})$$

$$K_{Ly}(h_{c.ssp},\alpha_{ssp},f_{ssp}) := \frac{f_{ssp}}{h_{c.ssp}} + 2\cdot\frac{d_1(h_{c.ssp},\alpha_{ssp})}{h_{c.ssp}}\cdot\cos(\alpha_{ssp})^2$$

thus

$$B_1(h_{c.ssp},t_{c.ssp},\alpha_{ssp},f_{ssp}) := K_{Iz}(h_{c.ssp},\alpha_{ssp},f_{ssp}) + \frac{1}{12}\left(\frac{t_{c.ssp}}{h_{c.ssp}}\right)^2\cdot K_{Lz}(h_{c.ssp},\alpha_{ssp})$$

$$B_2(h_{c.ssp},t_{c.ssp},\alpha_{ssp},f_{ssp}) := K_{Iyz}(h_{c.ssp},\alpha_{ssp},f_{ssp}) - \frac{1}{12}\left(\frac{t_{c.ssp}}{h_{c.ssp}}\right)^2\cdot K_{Lyz}(h_{c.ssp},\alpha_{ssp})$$

$$B_3(h_{c.ssp},t_{c.ssp},\alpha_{ssp},f_{ssp}) := K_{Iy}(h_{c.ssp},\alpha_{ssp},f_{ssp}) + \frac{1}{12}\left(\frac{t_{c.ssp}}{h_{c.ssp}}\right)^2\cdot K_{Ly}(h_{c.ssp},\alpha_{ssp},f_{ssp})$$

$$B_4(t_{f.bot},t_{c.ssp}) := \left(\frac{t_{f.bot}}{t_{c.ssp}}\right)^3$$

thus

$$S(h_{c.ssp},t_{f.top},t_{f.bot},t_{c.ssp},\alpha_{ssp},f_{ssp}) := \frac{6\cdot\frac{h_{c.ssp}}{p_{ssp}(h_{c.ssp},\alpha_{ssp},f_{ssp})}\cdot B_1(h_{c.ssp},t_{c.ssp},\alpha_{ssp},f_{ssp})\cdot B_4(t_{f.bot},t_{c.ssp}) + \left(\frac{p_{ssp}(h_{c.ssp},\alpha_{ssp},f_{ssp})}{h_{c.ssp}}\right)^2}{12\left[-2\left(\frac{p_{ssp}(h_{c.ssp},\alpha_{ssp},f_{ssp})}{h_{c.ssp}}\right)^2\cdot B_2(h_{c.ssp},t_{c.ssp},\alpha_{ssp},f_{ssp}) + \frac{h_{c.ssp}}{h_{ssp}(h_{c.ssp},t_{f.top},t_{f.bot},t_{c.ssp})}\left[6\cdot B_4(t_{f.bot},t_{c.ssp})\cdot\left(B_1(h_{c.ssp},t_{c.ssp},\alpha_{ssp},f_{ssp})\cdot B_3(h_{c.ssp},t_{c.ssp},\alpha_{ssp},f_{ssp}) - B_2(h_{c.ssp},t_{c.ssp},\alpha_{ssp},f_{ssp})^2\right) + \left(\frac{p_{ssp}(h_{c.ssp},\alpha_{ssp},f_{ssp})}{h_{c.ssp}}\right)^3\cdot B_3(h_{c.ssp},t_{c.ssp},\alpha_{ssp},f_{ssp})\right] + \frac{h_{ssp}(h_{c.ssp},t_{f.top},t_{f.bot},t_{c.ssp})}{h_{c.ssp}}\cdot\frac{p_{ssp}(h_{c.ssp},\alpha_{ssp},f_{ssp})}{h_{c.ssp}}\cdot B_1(h_{c.ssp},t_{c.ssp},\alpha_{ssp},f_{ssp})\right]}$$

thus the transverse shear stiffness perpendicular to the corrugation is obtained below

$$D_{Qy}(h_{c.ssp},t_{f.top},t_{f.bot},t_{c.ssp},\alpha_{ssp},f_{ssp}) := S(h_{c.ssp},t_{f.top},t_{f.bot},t_{c.ssp},\alpha_{ssp},f_{ssp})\cdot h_{ssp}(h_{c.ssp},t_{f.top},t_{f.bot},t_{c.ssp})\cdot\left(\frac{E_{S355N}}{1-\nu^2}\right)\left(\frac{t_{c.ssp}}{h_{c.ssp}}\right)^3$$

LOADS

Reduction factors

$\alpha_{Q1} := 0.9$

$\alpha_{q1} := 0.7$

$\psi_{0.UDL} := 0.4$

$\psi_{0.TS} := 0.75$

Permanent loads

Thickness of the asphalt cover

$t_{cover} := 100mm$

Contact area of the wheel taking the asphalt cover into consideration

$a_c := 600mm$

Asphalt density in [kN/m^3], trvk_bro_2011, pg. 45

$a_d := 23 \frac{kN}{m^3}$

Asphalt load

$q_{asp} := a_d \cdot t_{cover} \cdot a_c = 1.38 \cdot \frac{kN}{m}$

Self load per unit width

$q_{self}(h_{c.ssp}, t_{f.top}, t_{f.bot}, t_{c.ssp}, \alpha_{ssp}, f_{ssp}) := G_{ssp}(h_{c.ssp}, t_{f.top}, t_{f.bot}, t_{c.ssp}, \alpha_{ssp}, f_{ssp}) \cdot g \cdot a_c$

total permanent load

$q(h_{c.ssp}, t_{f.top}, t_{f.bot}, t_{c.ssp}, \alpha_{ssp}, f_{ssp}) := q_{self}(h_{c.ssp}, t_{f.top}, t_{f.bot}, t_{c.ssp}, \alpha_{ssp}, f_{ssp}) + q_{asp}$

LM1

$$Q_{w.LM1} := \frac{300kN \cdot \alpha_{Q1}}{2 \cdot a_c} = 225 \cdot \frac{kN}{m}$$

Point load

$$q_{LM1} := 9\frac{kN}{m^2} \cdot \alpha_{q1} \cdot a_c = 3.78 \cdot \frac{kN}{m}$$

Distributed Load

$$q_{l1}(h_{c.ssp}, t_{f.top}, t_{f.bot}, t_{c.ssp}, \alpha_{ssp}, f_{ssp}) := q(h_{c.ssp}, t_{f.top}, t_{f.bot}, t_{c.ssp}, \alpha_{ssp}, f_{ssp}) + Q_{w.LM1} + q_{LM1} \cdot \psi_{0.UDL}$$

$$q_{l2}(h_{c.ssp}, t_{f.top}, t_{f.bot}, t_{c.ssp}, \alpha_{ssp}, f_{ssp}) := q(h_{c.ssp}, t_{f.top}, t_{f.bot}, t_{c.ssp}, \alpha_{ssp}, f_{ssp}) + q_{LM1} + Q_{w.LM1} \cdot \psi_{0.TS}$$

$$q_{load}(h_{c.ssp}, t_{f.top}, t_{f.bot}, t_{c.ssp}, \alpha_{ssp}, f_{ssp}) := \max(q_{l1}(h_{c.ssp}, t_{f.top}, t_{f.bot}, t_{c.ssp}, \alpha_{ssp}, f_{ssp}), q_{l2}(h_{c.ssp}, t_{f.top}, t_{f.bot}, t_{c.ssp}, \alpha_{ssp}, f_{ssp}))$$

Fatigue LM3

$$q_{w.LM3} := \frac{120kN}{2 \cdot a_c} = 100 \cdot \frac{kN}{m}$$

$$q_{tot}(h_{c.ssp}, t_{f.top}, t_{f.bot}, t_{c.ssp}, \alpha_{ssp}, f_{ssp}) := q_{w.LM3} + q(h_{c.ssp}, t_{f.top}, t_{f.bot}, t_{c.ssp}, \alpha_{ssp}, f_{ssp})$$

Deflection

$$I_{top}(t_{f.top}) := \frac{0.6 \cdot m \cdot t_{f.top}^{3}}{12}$$

$$\delta_I(h_{c.ssp}, t_{f.top}, t_{f.bot}, t_{c.ssp}, \alpha_{ssp}, f_{ssp}) := \frac{q_{load}(h_{c.ssp}, t_{f.top}, t_{f.bot}, t_{c.ssp}, \alpha_{ssp}, f_{ssp}) \cdot l_{ssp}(h_{c.ssp}, \alpha_{ssp}, f_{ssp})^4}{384 \cdot E_{S355N} \cdot I_{top}(t_{f.top})}$$

OPTIMIZATION ANALYSIS

In the optimization analysis the steel sandwich panel (SSP) cross section is optimized with regards to moment of inertia and area of the cross section. In the first step the moment of inertia for the SSP is maximized to give the most optimal dimensions within the given constraints. In the second optimization the total area per unit width of the cross section of the SSP is minimized with regards to the given constraints.

$$\varepsilon_3 := \sqrt{\frac{235\text{MPa}}{f_y}} = 0.814$$

Strength ratio for cross-section class 3

Definition of constraints

Maximum width to thickness ratios for compression parts must be in cross-section class 3

$$\frac{l_{i.ssp}}{t_{c.ssp}} \le 42 \cdot \varepsilon_3$$

$$\frac{l_{buck}}{t_{f.top}} \le 42 \cdot \varepsilon_3$$

.

$$\frac{l_{buck}}{t_{f.bot}} \le 42 \varepsilon_3$$

The total area of the cross-section for the SSP has to be smaller or equal to the total area of the orthotropic plate.

$$A_{ssp} \le A_{ortho}$$

The total moment of inertia in the stiffer direction for the sandwich panel must be larger or equal to the total moment of inertia for the orthotropic plate.

$$I_{ssp.x} \ge I_{ortho.x}$$

The angle of corrugation should be between 45deg and 70deg according to a study conducted in the optimization of a corrugated sandwich panel. It was conlcuded that with an increasing corrugation angle the shear stiffness decreases drastically.

$$45\text{deg} \le \alpha_{ssp} \le 70\text{deg}$$

The length of the horizontal corrugated segment has to be a small as possible to minimize the resulting moments which cause local buckling in the face plate.

$$f_{ssp}$$

The local deflection of the top plate needs to fulfill the required control l.ssp/400. Taken from TRVFS 2011:12, pg. 64.

$$\delta_I \le \frac{l_{ssp}}{400}$$

To check the fatigue strength of the weld joints the stress in the joints needs to be less than the stress value from the detail category given in EN_1993-1-9. There is no detail category in Eurocode for the laser weld detail connection that is used in a SSP so 71MPa is taken as a reference since it's a reasonable stress value used for toe cracking of weld. Load Model 3 was used for the fatigue loads acting on the deck.

$$71\text{MPa} \ge \frac{q_{w.LM3} \cdot l_{ssp}^{\,2}}{1\text{m} \cdot 2 \cdot t_{f.top}^{\,2}}$$

Function that needs to be maximized

$$I_{ssp.x}\left(h_{c.ssp}, t_{f.top}, t_{f.bot}, t_{c.ssp}, \alpha_{ssp}, f_{ssp}\right) := \frac{I_{tot.ssp.x}\left(h_{c.ssp}, t_{f.top}, t_{f.bot}, t_{c.ssp}, \alpha_{ssp}, f_{ssp}\right)}{l_{ssp}\left(h_{c.ssp}, \alpha_{ssp}, f_{ssp}\right)}$$

Function that nees to be minimized

$$A_{ssp}\left(h_{c.ssp}, t_{f.top}, t_{f.bot}, t_{c.ssp}, \alpha_{ssp}, f_{ssp}\right) := \frac{A_{tot.ssp}\left(h_{c.ssp}, t_{f.top}, t_{f.bot}, t_{c.ssp}, \alpha_{ssp}, f_{ssp}\right)}{l_{ssp}\left(h_{c.ssp}, \alpha_{ssp}, f_{ssp}\right)}$$

Predefined values

$h_{c.ssp} := 180mm$

$t_{f.top} := 7mm$

$\alpha_{ssp} := 65 \cdot deg$

$t_{c.ssp} := 7mm$

$t_{f.bot} := 7mm$

$f_{ssp} := 20mm$

Constraints

Given

$$0 \le \frac{l_{buck}(h_{c.ssp}, \alpha_{ssp}, f_{ssp})}{t_{f.bot}} \le 42 \cdot \epsilon_3$$

$$0 \le \frac{l_{buck}(h_{c.ssp}, \alpha_{ssp}, f_{ssp})}{t_{f.top}} \le 42 \cdot \epsilon_3$$

$$I_{ssp.x}(h_{c.ssp}, t_{f.top}, t_{f.bot}, t_{c.ssp}, \alpha_{ssp}, f_{ssp}) > I_{ortho.x}$$

$$0 \le \frac{l_{i.ssp}(h_{c.ssp}, \alpha_{ssp})}{t_{c.ssp}} \le 42 \cdot \epsilon_3$$

$$0 \le A_{ssp}(h_{c.ssp}, t_{f.top}, t_{f.bot}, t_{c.ssp}, \alpha_{ssp}, f_{ssp}) \le A_{ortho}$$

$$45deg \le \alpha_{ssp} \le 70deg$$

$$71\text{MPa} \geq \frac{q_{w.LM3} \cdot l_{ssp}\left(h_{c.ssp}, \alpha_{ssp}, f_{ssp}\right)^2}{\left(1\text{m}\, t_{f.top}^{\ 2} \cdot 2\right)}$$

$$f_{ssp} \leq 35\text{mm}$$

$$\frac{l_{ssp}\left(h_{c.ssp}, \alpha_{ssp}, f_{ssp}\right)}{400} \geq \delta_I\left(h_{c.ssp}, t_{f.top}, t_{f.bot}, t_{c.ssp}, \alpha_{ssp}, f_{ssp}\right)$$

In this section the moment of inertia is maximized while the area of the cross section of the SSP is kept the same as orthtropic steel deck (OSD). The purpose is to see how much more stiffness can be achieved by the SSP if the weight of the deck of SSP is kept the same as the deck from OSD.

Maximization of the moment of inertia

$$\begin{pmatrix} h_{c.sspI} \\ t_{f.topI} \\ t_{f.botI} \\ t_{c.sspI} \\ \alpha_{sspI} \\ f_{sspI} \end{pmatrix} := \text{Maximize}\left(I_{ssp.x}, h_{c.ssp}, t_{f.top}, t_{f.bot}, t_{c.ssp}, \alpha_{ssp}, f_{ssp}\right)$$

New dimensional values obtained

$$\begin{pmatrix} \frac{h_{c.sspI}}{mm} \\ \frac{t_{f.topI}}{mm} \\ \frac{t_{f.botI}}{mm} \\ \frac{t_{c.sspI}}{mm} \\ \alpha_{sspI}\cdot\frac{180}{\pi} \\ \frac{f_{sspI}}{mm} \end{pmatrix} = \begin{pmatrix} 225 \\ 7.8 \\ 7.1 \\ 7.2 \\ 65.3 \\ 35 \end{pmatrix}$$

Fatigue stress

$$\frac{q_{w.LM3}\cdot l_{ssp}\left(h_{c.sspI},\alpha_{sspI},f_{sspI}\right)^2}{\left(1m\, t_{f.topI}{}^2\cdot 2\right)} = 62.285\cdot MPa$$

Dimensions

length of the corrugation

$$l_{ssp}\left(h_{c.sspI},\alpha_{sspI},f_{sspI}\right) = 0.277\,m$$

length of the corrugation opening

$$l_{buck}\left(h_{c.sspI},\alpha_{sspI},f_{sspI}\right) = 0.242\,m$$

height of the cross section

$$h_{ssp}\left(h_{c.sspI}, t_{f.topI}, t_{f.botI}, t_{c.sspI}\right) = 0.247\,m$$

neutral zone

$$z_{na.ssp}\left(h_{c.sspI}, t_{f.topI}, t_{f.botI}, t_{c.sspI}, \alpha_{sspI}, f_{sspI}\right) = 0.123\,m$$

Deflection in LM1

$$\frac{l_{ssp}\left(h_{c.sspI}, \alpha_{sspI}, f_{sspI}\right)}{400} = 0.692 \cdot mm$$

$$\delta_I\left(h_{c.sspI}, t_{f.topI}, t_{f.botI}, t_{c.sspI}, \alpha_{sspI}, f_{sspI}\right) = 0.692 \cdot mm$$

Moment of Inertia

in the stiff direction

$$I_{ssp.x}\left(h_{c.sspI}, t_{f.topI}, t_{f.botI}, t_{c.sspI}, \alpha_{sspI}, f_{sspI}\right) = 3.051 \times 10^{-4} \cdot \frac{m^4}{m}$$

$$I_{ortho.x} = 1.681 \times 10^{-4} \cdot \frac{m^4}{m}$$

$$u_{IIx} := \frac{I_{ssp.x}\left(h_{c.sspI}, t_{f.topI}, t_{f.botI}, t_{c.sspI}, \alpha_{sspI}, f_{sspI}\right)}{I_{ortho.x}} = 1.815$$

in the weak direction

$$I_{ssp.y}\left(h_{c.sspI}, t_{f.topI}, t_{f.botI}, t_{c.sspI}, \alpha_{sspI}, f_{sspI}\right) = 2.272 \times 10^{-4} \cdot \frac{m^4}{m}$$

$$I_{ortho.y} = 5.298 \times 10^{-5} \cdot \frac{m^4}{m}$$

$$u_{IIy} := \frac{I_{ssp.y}\left(h_{c.sspI}, t_{f.topI}, t_{f.botI}, t_{c.sspI}, \alpha_{sspI}, f_{sspI}\right)}{I_{ortho.y}} = 4.289$$

Area

$$A_{ssp}\left(h_{c.sspI}, t_{f.topI}, t_{f.botI}, t_{c.sspI}, \alpha_{sspI}, f_{sspI}\right) = 0.03\,m$$

$$A_{ortho} = 0.03\,m$$

$$u_{IA} := \frac{A_{ortho}}{A_{ssp}\left(h_{c.sspI}, t_{f.topI}, t_{f.botI}, t_{c.sspI}, \alpha_{sspI}, f_{sspI}\right)} = 1$$

---

configurations relationships

$$hc\_tc\left(h_{c.sspI}, t_{c.sspI}\right) = 31.05$$

$$p\_hc\left(h_{c.sspI}, \alpha_{sspI}, f_{sspI}\right) = 0.615$$

In the section below a minimization of the total area per unit width of the sandwich panel cross section is performed. The moment of inertia in the stiff direction is kept the same as the orthotropic deck. The purpose is to see how much weight reduction can be achieved with a steel sandwich panel deck while still having the same stiffness.

Constraints are kept the same as with the previous evaluation

Given

$$0 \le \frac{l_{buck}\left(h_{c.ssp}, \alpha_{ssp}, f_{ssp}\right)}{t_{f.bot}} \le 42\varepsilon_3$$

$$0 \le \frac{l_{buck}\left(h_{c.ssp}, \alpha_{ssp}, f_{ssp}\right)}{t_{f.top}} \le 42\varepsilon_3$$

$$0 \le \frac{l_{i.ssp}(h_{c.ssp}, \alpha_{ssp})}{t_{c.ssp}} \le 42 \cdot \varepsilon_3$$

$$A_{ssp}(h_{c.ssp}, t_{f.top}, t_{f.bot}, t_{c.ssp}, \alpha_{ssp}, f_{ssp}) \le A_{ortho}$$

$$40deg \le \alpha_{ssp} \le 80deg$$

$$I_{ssp.x}(h_{c.ssp}, t_{f.top}, t_{f.bot}, t_{c.ssp}, \alpha_{ssp}, f_{ssp}) \ge I_{ortho.x}$$

$$f_{ssp} \le 35mm$$

$$71MPa \ge \frac{q_{w.LM3} \cdot l_{ssp}(h_{c.ssp}, \alpha_{ssp}, f_{ssp})^2}{\left(1m\, t_{f.top}{}^2 \cdot 2\right)}$$

$$\frac{l_{ssp}(h_{c.ssp}, \alpha_{ssp}, f_{ssp})}{400} \ge \delta_l(h_{c.ssp}, t_{f.top}, t_{f.bot}, t_{c.ssp}, \alpha_{ssp}, f_{ssp})$$

Minimization of the the total area

$$\begin{pmatrix} h_{c.sspA} \\ t_{f.topA} \\ t_{f.botA} \\ t_{c.sspA} \\ \alpha_{sspA} \\ f_{sspA} \end{pmatrix} := \text{Minimize}(A_{ssp}, h_{c.ssp}, t_{f.top}, t_{f.bot}, t_{c.ssp}, \alpha_{ssp}, f_{ssp})$$

New dimensional values obtained

$$\begin{pmatrix} \frac{h_{c.sspA}}{mm} \\ \frac{t_{f.topA}}{mm} \\ \frac{t_{f.botA}}{mm} \\ \frac{t_{c.sspA}}{mm} \\ \alpha_{sspA} \cdot \frac{180}{\pi} \\ \frac{f_{sspA}}{mm} \end{pmatrix} = \begin{pmatrix} 184.1 \\ 6.5 \\ 5.7 \\ 5.9 \\ 66.6 \\ 35 \end{pmatrix}$$

Fatigue stress

$$\frac{q_{w.LM3} \cdot l_{ssp}\left(h_{c.sspA}, \alpha_{sspA}, f_{sspA}\right)^2}{\left(1m\, t_{f.topA}{}^2 \cdot 2\right)} = 62.331 \cdot MPa$$

length of the corrugation

$$l_{ssp}\left(h_{c.sspA}, \alpha_{sspA}, f_{sspA}\right) = 0.229\,m$$

length of the corrugation opening

$$l_{buck}\left(h_{c.sspA}, \alpha_{sspA}, f_{sspA}\right) = 0.194\,m$$

height of the cross section

$$h_{ssp}\left(h_{c.sspA}, t_{f.topA}, t_{f.botA}, t_{c.sspA}\right) = 0.202\,m$$

neutral zone

$$z_{na.ssp}\left(h_{c.sspA}, t_{f.topA}, t_{f.botA}, t_{c.sspA}, \alpha_{sspA}, f_{sspA}\right) = 0.1\,m$$

Deflection in LM1

$$\frac{l_{ssp}\left(h_{c.sspA}, \alpha_{sspA}, f_{sspA}\right)}{400} = 0.573 \cdot mm$$

$$\delta_I\left(h_{c.sspA}, t_{f.topA}, t_{f.botA}, t_{c.sspA}, \alpha_{sspA}, f_{sspA}\right) = 0.573 \cdot mm$$

New minimized area

$$A_{ssp}\left(h_{c.sspA}, t_{f.topA}, t_{f.botA}, t_{c.sspA}, \alpha_{sspA}, f_{sspA}\right) = 0.024\,m$$

$$A_{ortho} = 0.03\,m$$

$$u_{AA} := \frac{A_{ortho}}{A_{ssp}\left(h_{c.sspA}, t_{f.topA}, t_{f.botA}, t_{c.sspA}, \alpha_{sspA}, f_{sspA}\right)} = 1.226$$

Moment of Inertia

in the stiff direction

$$I_{ssp.x}\left(h_{c.sspA}, t_{f.topA}, t_{f.botA}, t_{c.sspA}, \alpha_{sspA}, f_{sspA}\right) = 1.681 \times 10^{-4} \cdot \frac{m^4}{m}$$

$$I_{ortho.x} = 1.681 \times 10^{-4} \cdot \frac{m^4}{m}$$

$$u_{IAx} := \frac{I_{ssp.x}\left(h_{c.sspA}, t_{f.topA}, t_{f.botA}, t_{c.sspA}, \alpha_{sspA}, f_{sspA}\right)}{I_{ortho.x}} = 1$$

in the weak direction

$$I_{ssp.y}\left(h_{c.sspA}, t_{f.topA}, t_{f.botA}, t_{c.sspA}, \alpha_{sspA}, f_{sspA}\right) = 1.238 \times 10^{-4} \cdot \frac{m^4}{m}$$

$$I_{ortho.y} = 5.298 \times 10^{-5} \cdot \frac{m^4}{m}$$

$$u_{IAy} := \frac{I_{ssp.y}\left(h_{c.sspA}, t_{f.topA}, t_{f.botA}, t_{c.sspA}, \alpha_{sspA}, f_{sspA}\right)}{I_{ortho.y}} = 2.337$$

---

configurations relationships

$$hc\_tc\left(h_{c.sspA}, t_{c.sspA}\right) = 31.37$$

$$p\_hc\left(h_{c.sspA}, \alpha_{sspA}, f_{sspA}\right) = 0.622$$

BENDING AND SHEAR STIFFNESS ANALYSIS

For the case of maximizing the moment of inertia while keeping the area constant

Bending Stiffness

<u>stiff direction</u>

$$D_{x.ssp}\left(h_{c.sspI}, t_{f.topI}, t_{f.botI}, t_{c.sspI}, \alpha_{sspI}, f_{sspI}\right) = 6.407 \times 10^{7} \cdot N \cdot m$$

$$D_{x.ortho} = 3.531 \times 10^{7} \cdot N \cdot m$$

Stifness comparison of the SSP with the OSD

$$D_{x.ortho} \le D_{x.ssp}\left(h_{c.sspI}, t_{f.topI}, t_{f.botI}, t_{c.sspI}, \alpha_{sspI}, f_{sspI}\right) = 1$$

$$u_x := \frac{D_{x.ssp}\left(h_{c.sspI}, t_{f.topI}, t_{f.botI}, t_{c.sspI}, \alpha_{sspI}, f_{sspI}\right)}{D_{x.ortho}} = 1.815$$

82% more stiffness of the SSP

weak direction

$$D_{y.ssp}\left(h_{c.sspI}, t_{f.topI}, t_{f.botI}, t_{c.sspI}, \alpha_{sspI}, f_{sspI}\right) = 4.884 \times 10^{7} \cdot N \cdot m$$

$$D_{y.ortho} = 1.186 \times 10^{7} \cdot N \cdot m$$

Stifness comparison of the SSP with the OSD

$$D_{y.ortho} \le D_{y.ssp}\left(h_{c.sspI}, t_{f.topI}, t_{f.botI}, t_{c.sspI}, \alpha_{sspI}, f_{sspI}\right) = 1$$

$$u_y := \frac{D_{y.ssp}\left(h_{c.sspI}, t_{f.topI}, t_{f.botI}, t_{c.sspI}, \alpha_{sspI}, f_{sspI}\right)}{D_{y.ortho}} = 4.119$$

Weight

Since in this case the area of the SSP is kept almost the same as to the area of the ortho, then the weight will be similar as well.

$$G_{ortho} = 233.23 \frac{kg}{m^2}$$

$$G_{ssp}\left(h_{c.sspI}, t_{f.topI}, t_{f.botI}, t_{c.sspI}, \alpha_{sspI}, f_{sspI}\right) = 233.23 \frac{kg}{m^2}$$

$$u_{GI} := \frac{G_{ssp}\left(h_{c.sspI}, t_{f.topI}, t_{f.botI}, t_{c.sspI}, \alpha_{sspI}, f_{sspI}\right)}{G_{ortho}} = 1$$

0% more weight of SSP

Torsional stiffness

$$D_{xy.ssp}\left(h_{c.sspI}, t_{f.topI}, t_{f.botI}, t_{c.sspI}, \alpha_{sspI}, f_{sspI}\right) = 3.671 \times 10^{7} \cdot N \cdot m$$

$$D_{xy.ortho} = 2.046 \times 10^{7} \cdot N \cdot m$$

$$u_{xyII} := \frac{D_{xy.ssp}\left(h_{c.sspI}, t_{f.topI}, t_{f.botI}, t_{c.sspI}, \alpha_{sspI}, f_{sspI}\right)}{D_{xy.ortho}} = 1.794$$

79% more torsional stiffness for SSP

Axial stiffness

$$E_{x.ssp}\left(h_{c.sspI}, t_{f.topI}, t_{f.botI}, t_{c.sspI}, \alpha_{sspI}, f_{sspI}\right) = 6.239 \times 10^{9} \cdot \frac{N}{m}$$

$$E_{x.ortho} = 6.239 \times 10^{9} \cdot \frac{N}{m}$$

$$u_{EI} := \frac{E_{x.ssp}\left(h_{c.sspI}, t_{f.topI}, t_{f.botI}, t_{c.sspI}, \alpha_{sspI}, f_{sspI}\right)}{E_{x.ortho}} = 1$$

Shear stiffness for SSP

transverse shear stiffness **parallel** to the corrugation

$$D_{Qx}\left(h_{c.sspI}, t_{f.topI}, t_{f.botI}, t_{c.sspI}, \alpha_{sspI}, f_{sspI}\right) = 1.043 \times 10^{9} \cdot \frac{N}{m}$$

transverse shear stiffnes **perpendicular** to the corrugation

$$D_{Qy}\left(h_{c.sspI}, t_{f.topI}, t_{f.botI}, t_{c.sspI}, \alpha_{sspI}, f_{sspI}\right) = 9.772 \times 10^{7} \cdot \frac{N}{m}$$

Horizontal shear stiffness

$$G_{xy}\left(h_{c.sspI}, t_{f.topI}, t_{f.botI}, t_{c.sspI}, \alpha_{sspI}, f_{sspI}\right) = 1.491 \times 10^{9} \cdot \frac{N}{m}$$

For the case of minimizing the the area while keeping the moment of inertia constant.

Bending Stiffness

stiff direction

Since in this case the moment of inertia in the stiff direction of the SSP is kept the same as that of ortho, then the bending stiffness will be the same as well.

$$D_{x.ssp}\left(h_{c.sspA}, t_{f.topA}, t_{f.botA}, t_{c.sspA}, \alpha_{sspA}, f_{sspA}\right) = 3.531 \times 10^{7} \cdot N \cdot m$$

$$D_{x.ortho} = 3.531 \times 10^{7} \cdot N \cdot m$$

Stifness comparison of the SSP with the OSD

$$D_{x.ortho} \leq D_{x.ssp}\left(h_{c.sspA}, t_{f.topA}, t_{f.botA}, t_{c.sspA}, \alpha_{sspA}, f_{sspA}\right) = 1$$

$$u_{xA} := \frac{D_{x.ssp}\left(h_{c.sspA}, t_{f.topA}, t_{f.botA}, t_{c.sspA}, \alpha_{sspA}, f_{sspA}\right)}{D_{x.ortho}} = 1$$

weak direction

$$D_{y.ssp}\left(h_{c.sspA}, t_{f.topA}, t_{f.botA}, t_{c.sspA}, \alpha_{sspA}, f_{sspA}\right) = 2.664 \times 10^{7} \cdot N \cdot m$$

$$D_{y.ortho} = 1.186 \times 10^{7} \cdot N \cdot m$$

Stifness comparison of the SSP with the OSD

$$D_{y.ortho} \leq D_{y.ssp}(h_{c.sspA}, t_{f.topA}, t_{f.botA}, t_{c.sspA}, \alpha_{sspA}, f_{sspA}) = 1$$

$$u_{yA} := \frac{D_{y.ssp}(h_{c.sspA}, t_{f.topA}, t_{f.botA}, t_{c.sspA}, \alpha_{sspA}, f_{sspA})}{D_{y.ortho}} = 2.246$$

Weight

$$G_{ortho} = 233.23 \frac{kg}{m^2}$$

$$G_{ssp}(h_{c.sspA}, t_{f.topA}, t_{f.botA}, t_{c.sspA}, \alpha_{sspA}, f_{sspA}) = 190.268 \frac{kg}{m^2}$$

$$u_{GA} := \frac{G_{ortho}}{G_{ssp}(h_{c.sspA}, t_{f.topA}, t_{f.botA}, t_{c.sspA}, \alpha_{sspA}, f_{sspA})} = 1.226$$

23% larger weight of the ortho

Torsional Stiffness

$$D_{xy.ssp}(h_{c.sspA}, t_{f.topA}, t_{f.botA}, t_{c.sspA}, \alpha_{sspA}, f_{sspA}) = 2 \times 10^{7} \cdot N \cdot m$$

$$D_{xy.ortho} = 2.046 \times 10^{7} \cdot N \cdot m$$

$$u_{xyIA} := \frac{D_{xy.ssp}(h_{c.sspA}, t_{f.topA}, t_{f.botA}, t_{c.sspA}, \alpha_{sspA}, f_{sspA})}{D_{xy.ortho}} = 0.978$$

Axial stiffness

$$E_{x.ssp}\left(h_{c.sspA}, t_{f.topA}, t_{f.botA}, t_{c.sspA}, \alpha_{sspA}, f_{sspA}\right) = 5.09 \times 10^{9} \cdot \frac{N}{m}$$

$$E_{x.ortho} = 6.239 \times 10^{9} \cdot \frac{N}{m}$$

$$u_{EA} := \frac{E_{x.ortho}}{E_{x.ssp}\left(h_{c.sspA}, t_{f.topA}, t_{f.botA}, t_{c.sspA}, \alpha_{sspA}, f_{sspA}\right)} = 1.226$$

Shear stiffness for SSP

transverse shear stiffness **parallel** to the corrugation

$$D_{Qx}\left(h_{c.sspA}, t_{f.topA}, t_{f.botA}, t_{c.sspA}, \alpha_{sspA}, f_{sspA}\right) = 8.434 \times 10^{8} \cdot \frac{N}{m}$$

transverse shear stiffnes **perpendicular** to the corrugation

$$D_{Qy}\left(h_{c.sspA}, t_{f.topA}, t_{f.botA}, t_{c.sspA}, \alpha_{sspA}, f_{sspA}\right) = 4.639 \times 10^{7} \cdot \frac{N}{m}$$

Horizontal shear stiffness

$$G_{xy}\left(h_{c.sspA}, t_{f.topA}, t_{f.botA}, t_{c.sspA}, \alpha_{sspA}, f_{sspA}\right) = 1.213 \times 10^{9} \cdot \frac{N}{m}$$

APPENDIX B

Load calculations

Division of the carriageway into notional lanes

Table 4.1 - Number and width of notional lanes

Carriageway width w	Number of notional lanes	Width of a notional lane w_l	Width of the remaining area
$w < 5{,}4$ m	$n_l = 1$	3 m	$w - 3$ m
$5{,}4$ m $\leq w < 6$ m	$n_l = 2$	$\frac{w}{2}$	0
6 m $\leq w$	$n_l = Int\left(\frac{w}{3}\right)$	3 m	$w - 3 \times n_l$
NOTE For example, for a carriageway width equal to 11m, $n_l = Int\left(\frac{w}{3}\right) = 3$, and the width of the remaining area is $11 - 3 \times 3 = 2$m.			

Geometric data

$l_{bridge} := 18m$

$l_{axle.long} := 1.2m$

$l_{axle.trans} := 2m$

Carriagway width

$w := 13.080m$

Number of notional lanes

$$n_1 := \begin{cases} 1 \text{ if } w < 5.4m \\ 2 \text{ if } 5.4m \le w < 6m \\ \text{floor}\left(\frac{w}{3m}\right) \text{ if } 6m \le w \end{cases} = 4$$

4 lanes

Width of a notional lane

$$w_1 := \begin{cases} 3 \cdot m \text{ if } w < 5.4m \\ \frac{w}{2} \text{ if } 5.4m \le w < 6m \\ 3 \cdot m \text{ if } 6m \le w \end{cases} = 3\,m$$

3 meters per notional lane

Width of the remaining area

$$w_{ra} := \begin{cases} (w - 3m) \text{ if } w < 5.4m \\ 0 \text{ if } 5.4m \le w < 6m \\ \left(w - 3m \cdot n_1\right) \text{ if } 6m \le w \end{cases} = 1.08\,m$$

Remaining area

$$w_p := \frac{w_{ra}}{2} = 0.54\,m$$

remaining area per side

Load Combinations LM1

Table 4.2 - Load model 1 : characteristic values

Location	Tandem system *TS*	*UDL* system
	Axle loads Q_{ik} (kN)	q_{ik} (or q_{ik}) (kN/m^2)
Lane Number 1	300	9
Lane Number 2	200	2,5
Lane Number 3	100	2,5
Other lanes	0	2,5
Remaining area (q_{rk})	0	2,5

Adjustments factors according to TRVFS 2001_12

$\alpha_{Q1} := 0.9$

$\alpha_{Q2} := 0.9$

$\alpha_{Q3} := 0$

$\alpha_{q1} := 0.7$

$\alpha_{q2} := 1.0$

Distributed loads

$q_{1k} := 9 \frac{kN}{m^2}$

$q_{2k} := 2.5 \frac{kN}{m^2}$

$q_{rk} := 2.5 \frac{kN}{m^2}$

$q_{3k} = q_{4k} = q_{2k}$

Area per wheel load (covers the contribution of the asphalt)

$A_Q := 600mm^2$

Point Loads

$Q_{1k} := 300kN$

$Q_{2k} := 200kN$

$Q_{3k} := 100kN$

$Q_{1d} := \frac{Q_{1k}}{2 \cdot A_Q} = 250 \cdot MPa$

$Q_{2d} := \frac{Q_{2k}}{2 \cdot A_Q} = 166.667 \cdot MPa$

$Q_{3d} := \frac{Q_{3k}}{2 \cdot A_Q} = 83.333 \cdot MPa$

Permanent loads

Self weight of the deck

$G_w := 5 \frac{kN}{m^2}$

Asphalt weight

$h_a := 100mm$

height of asphalt

$b := 23 \frac{kN}{m^3}$

$B := b \cdot h_a = 2.3 \cdot \frac{kN}{m^2}$

Self weight of asphalt

ULS

Varaktiga och tillfälliga d. s	Permanenta laster		Variabel huvudlast	Samverkande variabla laster	
	Ogynnsamma	Gynnsam-ma		Största last	Övriga laster
(Uttryck 6.10a)	γ_d 1,35 $G_{kj,sup}$ γ_d 1,35 P_k	1,00 $G_{kj,inf}$ 1,00 P_k		*När lasten är ogynnsam:* γ_d 1,5 $\psi_{0,1}Q_{k,1}$ *När lasten är gynnsam: 0*	*När lasten är ogynnsam:* γ_d 1,5 $\psi_{0,i}Q_{k,i}$ *När lasten är gynnsam: 0*
(Uttryck 6.10b)	γ_d 0,89·1,35 $G_{kj,sup}$ γ_d 1,35 P_k	1,00 $G_{kj,inf}$ 1,00 P_k	*När lasten är ogynnsam:* γ_d 1,5 $Q_{k,1}$ *När lasten är gynnsam: 0*		*När lasten är ogynnsam:* γ_d 1,5 $\psi_{0,i}$ $Q_{k,i}$ *När lasten är gynnsam: 0*

(VVFS 2007:197)

Load combinations in ULS are conducted according to the table above obtained from TRVFS 2011:12

Partial safety factors from National Annex

$\gamma_{G.sup} := 1.35$

$\gamma_{G.inf} := 1.0$

$\xi := 0.89$

$\gamma_{q.ULS} := 1.5$

$\psi_{TS} := 0.75$

$\psi_{UDL} := 0.4$

Load case 1

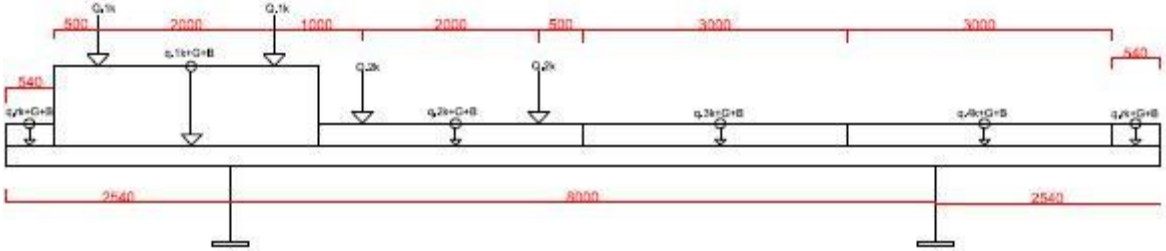

6.10a

all loads are unfavorable

$$\gamma_{G.sup}\cdot\left(G_w + B\right) + \gamma_{q.ULS}\cdot\psi_{TS}\cdot\left(Q_{1d} + Q_{2d}\right) + \gamma_{q.ULS}\cdot\psi_{UDL}\cdot\left(q_{1k} + q_{2k}\right) + \gamma_{q.ULS}\cdot\psi_{UDL}\cdot q_{rk}$$

loads with unfavorable axle loads and other loads are favorable

$$\left(\gamma_{G.sup} + \gamma_{G.inf}\right)\cdot G_w + \left(\gamma_{G.sup} + \gamma_{G.inf}\right)\cdot B + \gamma_{q.ULS}\cdot\psi_{TS}\cdot\left(Q_{1d} + Q_{2d}\right) \ldots$$
$$+ \gamma_{q.ULS}\cdot\psi_{UDL}\cdot\left(q_{1k} + q_{2k}\right) + \gamma_{q.ULS}\cdot\psi_{UDL}\cdot q_{rk}$$

loads on the span where the largest point and the distributed load is located are unfavorable. The rest of the loads are favorable

$$\left(\gamma_{G.sup} + \gamma_{G.inf}\right)\cdot G_w + \left(\gamma_{G.sup} + \gamma_{G.inf}\right)\cdot B + \gamma_{q.ULS}\cdot\psi_{TS}\cdot\left(Q_{1d}\right) \ldots$$
$$+ \gamma_{q.ULS}\cdot\psi_{UDL}\cdot q_{1k} + \gamma_{q.ULS}\cdot\psi_{UDL}\cdot q_{rk}$$

6.10b

all loads are unfavorable

$$\xi\cdot\gamma_{G.sup}\cdot\left(G_w + B\right) + \gamma_{q.ULS}\cdot\left(Q_{1d} + Q_{2d}\right) + \gamma_{q.ULS}\cdot\psi_{UDL}\cdot\left(q_{1k} + q_{2k}\right) + \gamma_{q.ULS}\cdot\psi_{UDL}\cdot q_{rk}$$

or

$$\xi\cdot\gamma_{G.sup}\cdot\left(G_w + B\right) + \gamma_{q.ULS}\cdot\psi_{TS}\cdot\left(Q_{1d} + Q_{2d}\right) + \gamma_{q.ULS}\cdot\left(q_{1k} + q_{2k}\right) + \gamma_{q.ULS}\cdot q_{rk}$$

loads with axle loads are unfavorable and other loads are favorable

$$\xi \cdot \gamma_{G.sup} \cdot (G_w + B) + \gamma_{G.inf} \cdot (G_w + B) + \gamma_{q.ULS} \cdot (Q_{1d} + Q_{2d}) \cdots$$
$$+ \gamma_{q.ULS} \cdot \psi_{UDL} \cdot (q_{1k} + q_{2k}) + \gamma_{q.ULS} \cdot \psi_{UDL} \cdot q_{rk}$$

or

$$\xi \cdot \gamma_{G.sup} \cdot (G_w + B) + \gamma_{G.inf} \cdot (G_w + B) + \gamma_{q.ULS} \cdot (q_{1k} + q_{2k}) + \gamma_{q.ULS} \cdot q_{rk} \cdots$$
$$+ \gamma_{q.ULS} \cdot \psi_{TS} \cdot (Q_{1d} + Q_{2d})$$

loads on the span where the largest point and the distributed load is located are unfavorable. The rest of the loads are favorable

$$\xi \cdot \gamma_{G.sup} \cdot (G_w + B) + \gamma_{G.inf} \cdot (G_w + B) + \gamma_{q.ULS} \cdot (Q_{1d}) \cdots$$
$$+ \gamma_{q.ULS} \cdot \psi_{UDL} \cdot (q_{1k}) + \gamma_{q.ULS} \cdot \psi_{UDL} \cdot q_{rk}$$

or

$$\xi \cdot \gamma_{G.sup} \cdot (G_w + B) + \gamma_{G.inf} \cdot (G_w + B) + \gamma_{q.ULS} \cdot (q_{1k}) + \gamma_{q.ULS} \cdot q_{rk} \cdots$$
$$+ \gamma_{q.ULS} \cdot \psi_{TS} \cdot (Q_{1d})$$

Load case 2

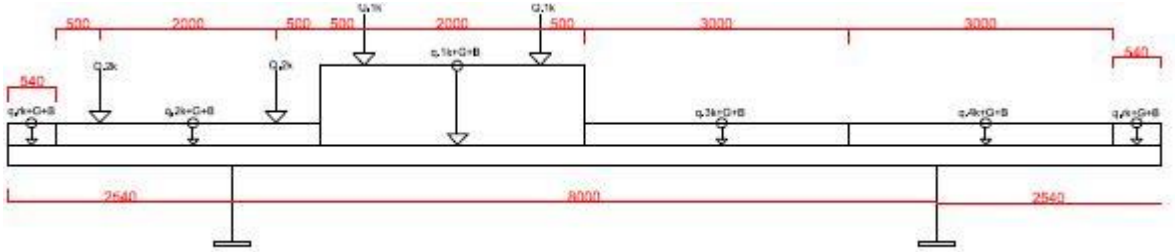

6.10a

all loads are unfavorable

$$\gamma_{G.sup}\cdot\left(G_w + B\right) + \gamma_{q.ULS}\cdot\psi_{TS}\cdot\left(Q_{1d} + Q_{2d}\right) + \gamma_{q.ULS}\cdot\psi_{UDL}\cdot\left(q_{1k} + q_{2k}\right) + \gamma_{q.ULS}\cdot\psi_{UDL}\cdot q_{rk}$$

Only the loads in the mid-span are unfavorable

$$\left(\gamma_{G.sup} + \gamma_{G.inf}\right)\cdot G_w + \left(\gamma_{G.sup} + \gamma_{G.inf}\right)\cdot B + \gamma_{q.ULS}\cdot\psi_{TS}\cdot\left(Q_{1d}\right) + \gamma_{q.ULS}\cdot\psi_{UDL}\cdot\left(q_{1k} + q_{2k}\right)$$

The loads on the left and mit span are unfavorable

$$\left(\gamma_{G.sup} + \gamma_{G.inf}\right)\cdot G_w + \left(\gamma_{G.sup} + \gamma_{G.inf}\right)\cdot B + \gamma_{q.ULS}\cdot\psi_{TS}\cdot\left(Q_{1d}\right) \cdots$$
$$+\gamma_{q.ULS}\cdot\psi_{UDL}\cdot\left(q_{1k} + q_{2k}\right) + \gamma_{q.ULS}\cdot\psi_{UDL}\cdot q_{rk}$$

6.10b

all loads are unfavorable

$$\xi\cdot\gamma_{G.sup}\cdot\left(G_w + B\right) + \gamma_{q.ULS}\cdot\left(Q_{1d} + Q_{2d}\right) + \gamma_{q.ULS}\cdot\psi_{UDL}\cdot\left(q_{1k} + q_{2k}\right) + \gamma_{q.ULS}\cdot\psi_{UDL}\cdot q_{rk}$$

or

$$\xi\cdot\gamma_{G.sup}\cdot\left(G_w + B\right) + \gamma_{q.ULS}\cdot\psi_{TS}\cdot\left(Q_{1d} + Q_{2d}\right) + \gamma_{q.ULS}\cdot\left(q_{1k} + q_{2k}\right) + \gamma_{q.ULS}\cdot q_{rk}$$

loads on left and mid-span are unfavorable

$$\xi\cdot\gamma_{G.sup}\cdot\left(G_w + B\right) + \gamma_{G.inf}\cdot\left(G_w + B\right) + \gamma_{q.ULS}\cdot\left(Q_{1d} + Q_{2d}\right) \cdots$$
$$+\gamma_{q.ULS}\cdot\psi_{UDL}\cdot\left(q_{1k} + q_{2k}\right) + \gamma_{q.ULS}\cdot\psi_{UDL}\cdot q_{rk}$$

or

$$\xi\cdot\gamma_{G.sup}\cdot\left(G_w + B\right) + \gamma_{G.inf}\cdot\left(G_w + B\right) + \gamma_{q.ULS}\cdot\left(q_{1k} + q_{2k}\right) + \gamma_{q.ULS}\cdot q_{rk} \cdots$$
$$+\gamma_{q.ULS}\cdot\psi_{TS}\cdot\left(Q_{1d} + Q_{2d}\right)$$

loads on the span where the largest point and the distributed load is located are unfavorable. The rest of the loads are favorable

$$\xi \cdot \gamma_{G.sup} \cdot (G_w + B) + \gamma_{G.inf} \cdot (G_w + B) + \gamma_{q.ULS} \cdot (Q_{1d}) + \gamma_{q.ULS} \cdot \psi_{UDL} \cdot (q_{1k} + q_{2k})$$

or

$$\xi \cdot \gamma_{G.sup} \cdot (G_w + B) + \gamma_{G.inf} \cdot (G_w + B) + \gamma_{q.ULS} \cdot (q_{1k} + q_{2k}) + \gamma_{q.ULS} \cdot \psi_{TS} \cdot (Q_{1d})$$

Load case 3

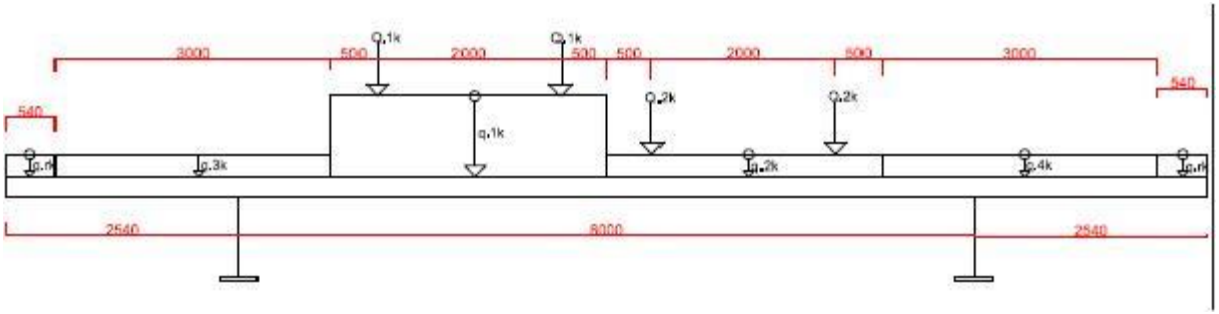

6.10a

all loads are unfavorable

$$\gamma_{G.sup}\cdot\left(G_w + B\right) + \gamma_{q.ULS}\cdot\psi_{TS}\cdot\left(Q_{1d} + Q_{2d}\right) + \gamma_{q.ULS}\cdot\psi_{UDL}\cdot\left(q_{1k} + q_{2k}\right) + \gamma_{q.ULS}\cdot\psi_{UDL}\cdot q_{rk}$$

loads are favorable and unfavorable

$$\left(\gamma_{G.sup} + \gamma_{G.inf}\right)\cdot G_w + \left(\gamma_{G.sup} + \gamma_{G.inf}\right)\cdot B + \gamma_{q.ULS}\cdot\psi_{TS}\cdot\left(Q_{1d} + Q_{2d}\right) + \gamma_{q.ULS}\cdot\psi_{UDL}\cdot\left(q_{1k} + q_{2k}\right)$$

6.10b

all loads are unfavorable

$$\xi\cdot\gamma_{G.sup}\cdot\left(G_w + B\right) + \gamma_{q.ULS}\cdot\left(Q_{1d} + Q_{2d}\right) + \gamma_{q.ULS}\cdot\psi_{UDL}\cdot\left(q_{1k} + q_{2k}\right) + \gamma_{q.ULS}\cdot\psi_{UDL}\cdot q_{rk}$$

or

$$\xi\cdot\gamma_{G.sup}\cdot\left(G_w + B\right) + \gamma_{q.ULS}\cdot\psi_{TS}\cdot\left(Q_{1d} + Q_{2d}\right) + \gamma_{q.ULS}\cdot\left(q_{1k} + q_{2k}\right) + \gamma_{q.ULS}\cdot q_{rk}$$

loads are favorable and unfavorable

$$\xi\cdot\gamma_{G.sup}\cdot\left(G_w + B\right) + \gamma_{G.inf}\cdot\left(G_w + B\right) + \gamma_{q.ULS}\cdot\left(Q_{1d} + Q_{2d}\right) + \gamma_{q.ULS}\cdot\psi_{UDL}\cdot\left(q_{1k} + q_{2k}\right)$$

or

$$\xi\cdot\gamma_{G.sup}\cdot\left(G_w + B\right) + \gamma_{G.inf}\cdot\left(G_w + B\right) + \gamma_{q.ULS}\cdot\left(q_{1k} + q_{2k}\right) + \gamma_{q.ULS}\cdot\psi_{TS}\cdot\left(Q_{1d} + Q_{2d}\right)$$

SLS

Combination	Permanent actions G_d		Prestress	Variable actions Q_d	
	Unfavourable	Favourable		Leading	Others
Characteristic	$G_{kj,sup}$	$G_{kj,inf}$	P	$Q_{k,1}$	$\psi_{0,i}Q_{ki}$
Frequent	$G_{kj,sup}$	$G_{kj,inf}$	P	$\psi_{1,1}Q_{k,1}$	$\psi_{2,i}Q_{ki}$
Quasi-permanent	$G_{kj,sup}$	$G_{kj,inf}$	P	$\psi_{2,1}Q_{k,1}$	$\psi_{2,i}Q_{ki}$

In the serviceability limit state the factor gamma (γ) is equal to 1 and is not dependent on wether the load is favorable or unfavorable. The loads are calculated according to the table above (SS-EN 1990/A1:2005)